

Alma Mater Studiorum – Università di Bologna

DOTTORATO DI RICERCA IN

Meccanica e Scienze Avanzate dell'Ingegneria

Ciclo XXX

Settore Concorsuale: 09/C2

Settore Scientifico Disciplinare: ING-IND/18

**DEVELOPMENT AND CHARACTERIZATION OF A PLASMA
GUN SOURCE FOR BIOMEDICAL APPLICATIONS**

Presentata da: Emanuele Simoncelli

Coordinatore Dottorato

Prof. Marco Carricato

Supervisore

Prof. Vittorio Colombo

Esame finale anno 2018

*... Be the **change** you want to see in the world...*

Mahatma Ghandi

*... See that the **imagination of nature** is far, far greater than
the imagination of man...*

Richard P. Feynman

Sentences you will probably never read in a published paper:

*“To be honest, we came up with the hypothesis
after doing the experiments.”*

www.PHDCOMINCS.com

Index

INTRODUCTION.....	5
1. PLASMA GUN FOR DENTAL APPLICATIONS.....	11
1.1. LITERATURE OVERVIEW AND ROADMAP OF EXPERIMENTAL ACTIVITIES	11
1.1.1. <i>Context</i>	11
1.1.2. <i>Bacterial related oral diseases and CAP treatment potentialities</i>	13
1.1.3. <i>CAP treatment potentialities in endodontic treatments</i>	15
1.1.3.1. Cleaning phase.....	15
1.1.3.2. Restoration phase.....	18
1.1.4. <i>CAP treatment potentialities in other dental applications</i>	22
1.1.4.1. Polymerization.....	22
1.1.4.2. Improvement of osseointegration, implants biocompatibility, coagulation, cell migration.....	22
1.1.4.3. Tooth bleaching, whitening	22
1.1.5. <i>CAP sources for dentistry</i>	23
1.1.6. <i>Perspectives for CAP treatment in dentistry</i>	24
1.1.7. <i>Road map of experimental activities</i>	25
1.2. PG TREATMENT TO ASSIST THE DECONTAMINATION OF ROOT CANAL IN ENDODONTIC PROCEDURE.....	28
1.2.1. <i>Materials & Methods</i>	28
1.2.1.1. Plasma Gun architecture and operating conditions	28
1.2.1.2. Screening of PG operating conditions by means of qualitative analysis of bacterial growth inhibition areas on agar plates	29
1.2.1.3. Evaluation of the bacterial load reduction in liquid suspensions	30
1.2.1.4. Decontamination tests on realistic tooth models.....	30
1.2.1.4.1. Standardization of realistic tooth models	31
1.2.1.4.2. PG Activated Water for the indirect treatment of contaminated tooth models.....	31
1.2.1.4.3. Direct PG treatment of contaminated tooth models	33
1.2.1.5. Peroxides, nitrates, nitrites and pH measurements	33
1.2.1.6. Decontamination tests on realistic monocal premandibular tooth.....	34
1.2.1.6.1. Standardization of extracted tooth	34
1.2.1.6.2. Contamination of extracted tooth.....	34
1.2.1.6.3. Treatments of contaminated tooth.....	35
1.2.1.6.4. Staining LIVE/DEAD analysis through Confocal Laser Scanning Microscopy (CLSM)	36
1.2.2. <i>Results</i>	37
1.2.2.1. Analysis of the growth inhibition area on contaminated TSA plates	37
1.2.2.2. Quantitative evaluation of bacterial load reduction in bacterial suspensions.....	38
1.2.2.3. Decontamination of root canal models	38
1.2.2.3.1. Indirect plasma treatment: wet and dry environment.....	38
1.2.2.3.2. Direct plasma treatment: wet and dry environment	40
1.2.2.3.3. Positive controls with 0,2% CHX and 0,6% NaClO	41
1.2.2.3.4. Chemical analysis of pH and reactive species produced in sterile water treated by Plasma Gun	42
1.2.2.4. Decontamination of ex-vivo extracted teeth through CLSM analysis.....	43
1.2.3. <i>Discussion of results</i>	45
1.3. PG TREATMENT TO ASSIST THE RESTORATION OF ROOT CANAL IN ENDODONTIC PROCEDURE	49
1.3.1. <i>Preliminary results on coronal-medial canal restoration and overview on guttapercha obturation of apical region</i>	49
1.3.2. <i>Materials & Methods</i>	50
1.3.2.1. Tooth sample preparation	50
1.3.2.2. Pushout test.....	54
1.3.2.3. CLSM analysis.....	55
1.3.3. <i>Results</i>	56
1.3.3.1. Pushout tests	56
1.3.3.2. CLSM analysis.....	57
1.3.4. <i>Discussion of results</i>	58

1.4.	CONCLUSIONS	63
1.5.	BIBLIOGRAPHY	65
2.	PLASMA GUN FOR CANCER APPLICATIONS	75
2.1.	LITERATURE OVERVIEW AND ROADMAP OF EXPERIMENTAL ACTIVITIES	75
2.1.1.	<i>Cancer therapy: induction of apoptosis</i>	75
2.1.2.	<i>Plasma & Oncology</i>	77
2.1.3.	<i>RONs in Plasma Activated Medium (PAM): selectivity and self-perturbation of apoptosis induction</i> ...	78
2.1.4.	<i>Roadmap of experimental activities</i>	84
2.2.	MATERIALS & METHODS	86
2.2.1.	<i>Cell culture</i>	86
2.3.1.	<i>Cytotoxicity analysis</i>	87
2.3.1.1.	Discrimination of cell death mechanisms	87
2.3.1.2.	Analysis of the perturbation of mitochondrial membrane potential.....	88
2.3.1.3.	Cell cycle analysis.....	88
2.3.1.4.	Analysis of histones phosphorylation H2A.X	89
2.3.2.	<i>Detection of Hydrogen Peroxides and Nitrites in Plasma-treated Medium</i>	89
2.4.	RESULTS	90
2.4.1.	<i>Cell viability</i>	90
2.4.2.	<i>Analysis of cell cycle</i>	91
2.4.3.	<i>Analysis of mitochondrial membrane potential</i>	91
2.4.4.	<i>Analysis of γ-H2AX phosphorylation</i>	92
2.4.5.	<i>Measurement of RONS density in PAM</i>	93
2.5.	DISCUSSION OF RESULTS	95
2.6.	CONCLUSIONS	96
2.7.	BIBLIOGRAPHY	97
3.	SPECTROSCOPY TECHNIQUES FOR PLASMA PROCESSES CHARACTERIZATION	103
3.1.	LITERATURE OVERVIEW AND ROADMAP OF EXPERIMENTAL ACTIVITIES	103
3.1.1.	<i>Optical spectroscopy techniques for the characterization of plasma-assisted processes</i>	103
3.1.2.	<i>Roadmap of experimental activities</i>	106
3.2.	MATERIAL & METHODS	108
3.2.1.	<i>Surface DBD plasma source</i>	108
3.2.2.	<i>Setup for optical absorption spectroscopy (OAS)</i>	109
3.2.3.	<i>Setup for optical emission spectroscopy (OES)</i>	110
3.2.4.	<i>Data processing for OAS experiments</i>	110
3.2.5.	<i>Data processing for OES experiments</i>	112
3.3.	RESULTS	114
3.3.1.	<i>Electrical characterization</i>	114
3.3.2.	<i>O₃ kinetics</i>	115
3.3.3.	<i>NO₃ kinetics</i>	116
3.3.4.	<i>NO₂ kinetics</i>	117
3.3.5.	<i>Measurements of vibrational temperature of N₂</i>	118
3.4.	DISCUSSION OF RESULTS	119
3.5.	CONCLUSIONS	124
3.6.	BIBLIOGRAPHY	125
4.	DEVELOPMENT OF PLASMA GUN SOURCE	129
4.1.	INTRODUCTION	129
4.2.	DEVELOPMENT OF A MEDICAL DEVICE PROTOTYPE BASED ON PLASMA GUN CONFIGURATION	131
4.3.	BIBLIOGRAPHY	138

Introduction

Cold atmospheric pressure plasma (CAP) technologies are permeating many fields of industrial and biomedical applications. In particular, since CAPs have shown attractive properties in the production of an enhanced gas and liquid chemistry, exploitable in different fields such as inactivation of prokaryotic cells, modification/activation of material surfaces, and interaction with biological tissue, the scientific community in the last decades has been addressing a great effort in the field of medical applications, also known as Plasma Medicine.

Although an increasing number of research groups is working in this scientific field, CAP sources are still under investigation and the road toward the development of established medical devices based on CAP technology is still long and complicate. A young international scientific community, several plasma sources with different configurations, few reference devices with limited experimental data, are the causes of this hard-growth. On the other hand, the beauty and the strength that feed this world of research are deeply enclosed in the multidisciplinary approach that leads to a cooperation between scientists: medical doctors, physicists, biologists, dentists, and engineers, all inspired by a unique common challenge: CAPs as an innovative, pervasive, environmentally friendly, promising and effective technology applied to the medicine field.

Wishing to do a step toward this aim, my PhD project has been focused on the development and testing of a CAP device based on the Plasma Gun configuration for medical applications.

In order to evaluate the Plasma Gun source performances in different fields of application, I have run several experimental activities with the Research Group for Industrial Application of Plasmas (IAP group) at Alma Mater Studiorum - Università di Bologna, mainly in the field of dental and oncological applications. During the last three years I had the opportunity to contribute to the widening of the IAP group multidisciplinary network of collaborations within Università di Bologna and also outside, in the framework of international projects such as the European COST action MP1101 “Biomedical applications of atmospheric pressure plasma technology” and COST action TD1208: “Electrical discharges with liquids for future applications”. In particular, with the valuable support and effort of a team of endodontics driven by Dr. R. Tonini the efficacy of a Plasma Gun treatment in the disinfection of contaminated root canal systems and in the increase of adhesion performances during the obturation of a restored root canal has been proved. On the other hand, in collaboration with the research group of Pharmacology and Toxicology (Alma Mater Studiorum - Università di Bologna) driven by Prof. C. Fimognari and Dr. E. Turrini and partially supported by a National SIR grant (RBSI14DBMB “*Non-thermal plasma as an innovative anticancer strategy: in vitro and ex vivo studies in leukaemia models*”), fundamental studies on the potentialities of Plasma Gun treatment to induce apoptosis in leukaemia cells have been carried out. In the light of the promising results, with

the precious support of the spin-off company AlmaPlasma srl, great effort has been addressed to the development of a new plasma system for biomedical applications based on Plasma Gun configuration. Thus, the device's design has been made according to the most important ISO for medical instrumentations (eg. ISO 14971, ISO 13485, ISO 10993, DIN-SPE 91315). Finally, I focused my studies on the spectroscopy techniques for the characterization of plasma processes that allow to obtain quantitative information about the composition and temperatures of plasma. With the purpose of getting deeper inside in the knowledge of optical absorption and emission spectroscopy, I spent two months at Department of Applied Physics at Ghent University, Belgium with the supervision of Prof. Nikiforov aimed at investigating the kinetics of reactive species produced during and after a plasma treatment. These diagnostic techniques, leading to directly control plasma processes, can gain rising interest in industrial and biomedical perspectives as monitoring systems.

The achieved results have been reported in the following papers published or submitted to international journals:

1. Simoncelli E, Barbieri D, Laurita R, Liguori A, Stancampiano A, Viola L, Tonini R, Gherardi M, Colombo V, *Preliminary investigation of the antibacterial efficacy of a handheld Plasma Gun source for endodontic procedures*. Clinical Plasma Medicine 2015; 3:77–86.
2. Boselli M, Colombo V, Gherardi M, Laurita R, Liguori A, Sanibondi P, Simoncelli E, Stancampiano A, *Characterization of a Cold Atmospheric Pressure Plasma Jet Device Driven by Nanosecond Voltage Pulses*. IEEE Transactions on Plasma Science 2014:1–13.
3. Stancampiano A, Simoncelli E, Gherardi M, Boselli M, Laurita R, Colombo V, *Plasma-liquid interaction of a plasma jet impinging on a water surface*, submitted to Plasma Sources Science and Technology.
4. Stancampiano A, Forgione D, Simoncelli E, Laurita R, Gherardi M, Tonini R, Colombo V, *Cold Atmospheric Plasma (CAP) treatment to improve the bonding strength of dentin-adhesive system interface in dental composite restoration*, submitted to Dental Materials.
5. Simoncelli E, Nikiforov A, Schulpen J, Laurita R, Gherardi M, Colombo V, *UV-VIS optical spectroscopy investigation on the kinetics of long-lived RONS produced by SDBD plasma source*, submitted to Plasma Sources Science and Technology.

Furthermore, I took part into other research activities, mainly involved in the field of the diagnostics of plasma discharges, which led to the following scientific works:

1. Obrusnik A, Boselli M, Stancampiano A, Simoncelli E, Gherardi M, Colombo V, Zajickova L, *On the origin of plasma-induced acoustic waves in kilohertz atmospheric-pressure plasma jets*, submitted to Applied Physics Letter.
2. Boselli M, Gherardi M, Simoncelli E, Stancampiano A, Traldi E, Colombo V, Settles G S, *Schlieren imaging: a powerful tool for atmospheric plasma diagnostic*, invited submission to EPJ Techniques and Instrumentations.

The results have been also presented at international conferences (the underline contributions were presented by myself):

1. *Characterization of a non-equilibrium atmospheric pressure plasma jet driven by nanosecond voltage pulses*, 20th Symposium on Application of Plasma Processes (SAPP XX) - COST TD1208 Workshop on Application of Gaseous Plasma with Liquids, Tatranská Lomnica, Slovakia, 17-22 January 2015.
2. *Plasma Gun decontamination of bacteria in liquid suspensions*, 20th Symposium on Application of Plasma Processes (SAPP XX) - COST TD1208 Workshop on Application of Gaseous Plasma with Liquids, Tatranská Lomnica, Slovakia, 17-22 January 2015.
3. *Advanced investigation of the interaction between a plasma jet and a liquid surface: influence of electrical and fluid dynamic parameters*, 1th Frontiers in Low Temperature Plasma Diagnostics (FLTPD IX), IGESA, Porquerolles Island, Hyères, Var, France, 24-28 May 2015.
4. *Advanced study of the interaction between a plasma jet and a liquid surface: influence of atmosphere and substrate composition*, 1th Frontiers in Low Temperature Plasma Diagnostics (FLTPD IX), IGESA, Porquerolles Island, Hyères, Var, France, 24-28 May 2015.
5. *Characterization of a cold nanopulsed plasma jet in free-flow configuration and imping on different substrates*, 22nd International Symposium on Plasma Chemistry (ISPC 22), Antwerp, Belgium, 5-10 July 2015.
6. *Advanced investigation of electrical and fluid-dynamic parameters on a nanopulsed plasma jet impinging on a liquid substrate*, 22nd International Symposium on Plasma Chemistry (ISPC 22), Antwerp, Belgium, 5-10 July 2015.
7. *Investigation of antibacterial efficacy of a plasma gun source for endodontic applications*, 22nd International Symposium on Plasma Chemistry (ISPC 22), Antwerp, Belgium, 5-10 July 2015.
8. *Investigation of antibacterial efficacy of a Plasma Gun source for endodontic applications*, Joint meeting of COST Actions CMST TD1208 and MPNS MP1101, Bertinoro, Italy, 13-16 September 2015.
9. *Advanced investigation of electrical and fluid-dynamic parameters on a nanopulsed plasma jet impinging on a liquid substrate*, Joint meeting of COST Actions CMST TD1208 and MPNS MP1101, Bertinoro, Italy, 13-16 September 2015.
10. *Treatment of infected ex-vivo skin tissue with a low power atmospheric inductively coupled plasma source optimized through design oriented simulations*, Joint meeting of COST Actions CMST TD1208 and MPNS MP1101, Bertinoro, Italy, 13-16 September 2015.
11. *Characterization of a cold nanopulsed plasma jet in free-flow configuration and imping on different substrates*, Joint meeting of COST Actions CMST TD1208 and MPNS MP1101, Bertinoro, Italy, 13-16 September 2015.
12. *Plasma treatment in dentistry*, 6th International Conference on Plasma Medicine (ICPM 6), Bratislava, Slovakia, 4-9 September 2016.
13. *Study of potential cytotoxicity on eukaryotic cells associated with the use of plasma activated liquids in dental applications*, 6th International Conference on Plasma Medicine (ICPM 6), Bratislava, Slovakia, 4-9 September 2016.
14. *Cold atmospheric plasma (CAP) treatment to improve the bonding strength of adhesive-dentin interface in dental composite restoration*, 6th International Conference on Plasma Medicine (ICPM 6), Bratislava, Slovakia, 4-9 September 2016.
15. *Treatment of infected ex-vivo human skin tissue with a low power atmospheric inductively coupled plasma source optimized through design oriented simulations*, 6th International Conference on Plasma Medicine (ICPM 6), Bratislava, Slovakia, 4-9 September 2016.

16. *Advanced investigation on the plasma-liquid interaction in a plasma jet impinging on a water surface*, 6th International Conference on Plasma Medicine (ICPM 6), Bratislava, Slovakia, 4-9 September 2016.
17. *Qualitative live/dead confocal laser analysis on the decontamination efficacy of Cap treatment on ex-vivo tooth root canals*, 6th International Conference on Plasma Medicine (ICPM 6), Bratislava, Slovakia, 4-9 September 2016.
18. *A novel cold atmospheric plasma device for dental applications*, 6th International Conference on Plasma Medicine (ICPM 6), Bratislava, Slovakia, 4-9 September 2016.
19. *New perspectives for adhesion improvement: Chances and hopes*, 19th International Congress of Accademia Italiana di Odontoiatria Conservativa e Restaurativa (AIC IXX) and CONSEURO, Bologna, Italy, 11–13 May 2017.
20. *Bactericidal effect of atmospheric pressure plasma treatment of synthetic sea water*, International Conference on Plasmas with Liquids (ICPL 2017), Prague, Czech Republic, 5-9 March 2017.
21. *Cold Atmospheric Plasma (CAP) treatment to improve the bonding strength of adhesive-dentin interface in dental composite restoration*, Gordon Research Conference “Plasma Processing Science”, Andover (NH), USA, 24-29 July 2016.
22. *Plasma treatment of tooth root canal for enhancement of bond strength of dental adhesive system*, 43rd IEEE International Conference on Plasma Sciences (ICOPS 43), Banff, AB, Canada, 19-23 June 2016.
23. *Investigation of the efficacy of plasma gun decontamination of realistic root canal models for endodontic applications*, 6th Central European Symposium on Plasma Chemistry (CESPC – 6), Bressanone, Italy, 6-10 September 2015.
24. *Multi-diagnostic investigation of a non-equilibrium atmospheric pressure plasma jet driven by nanosecond voltage pulses in free-flow configuration and while imping on different substrates*, 6th Central European Symposium on Plasma Chemistry (CESPC – 6), Bressanone, Italy, 6-10 September 2015.
25. *Plasma gun decontamination of bacteria in liquid suspension*, 2nd Annual Meeting on COST Action TD1208 “Electrical Discharges with liquids for Future Application”, Barcelona, Spain, 23-26 February 2015.
26. *Investigation of antibacterial efficacy of a plasma gun source for endodontic applications*, 42nd IEEE International Conference on Plasma Sciences (ICOPS 42), Belek, Antalya, Turkey, 24- 28 May 2015.
27. *Characterization of a cold atmospheric pressure plasma jet driven by nanosecond high-voltage pulses*, 42nd IEEE International Conference on Plasma Sciences (ICOPS 42), Belek, Antalya, Turkey, 24- 28 May 2015.
28. *Effect of nanosecond-pulsed dielectric barrier discharge on human T-lymphoblastoid leukemia cells*, International Symposium on Plasma Chemistry (ISPC 23), Montreal, Canada, 30 July-4 August 2017.
29. *Cold atmospheric pressure plasma treatment to improve the bonding strength of dentin-adhesive system interface in dental composite restoration*, Convegno nazionale della Società Italiana dei Biomateriali (SIB 2017), Milano, Italy, 24-26 May 2017.
30. *New research tools for the field of cold atmospheric plasma applications*, Convegno nazionale della Società Italiana dei Biomateriali (SIB 2017), Milano, Italy, 24-26 May 2017.

31. *Atmospheric non-equilibrium plasma sources and processes with a focus on plasma medicine & antibacterial applications*, 68th Annual Gaseous Electronics Conference (GEC-68)/9th Annual International Conference on Reactive Plasma (ICRP-9)/33rd Symposium on Plasma Processing (SPP-33), Honolulu, USA, 12-16 October 2015.
32. *Surface modification of biological materials with atmospheric non-equilibrium plasma sources and processes for plasma medicine & antibacterial applications*, MRS Spring Meeting & Exhibit, Phoenix, USA, 28 March-1 April 2016.
33. *Atmospheric pressure non-equilibrium plasmas for material treatment: surface modification and thin film deposition*, MRS Spring Meeting & Exhibit, Phoenix, USA, 28 March-1 April 2016.
34. *Atmospheric pressure non-equilibrium plasmas for material treatment and nanofabrication*, EMN Meeting on Biomaterials 2016, Phuket, Thailand, 4-7 April 2016.

Finally, I have been co-supervisor for the following MA and BA thesis:

1. Luca Viola, *Valutazione sperimentale dell'efficacia di una sorgente Plasma Gun per applicazioni biomedicali in ambito endodontico e coagulativo*, MA.
2. Alberto Migliorelli, *Caratterizzazione di una sorgente di plasma di non equilibrio a pressione atmosferica per applicazioni dentali: analisi di rischio e efficacia antibatterica*, MA.
3. Martina Santucci, *Installation, diagnostics and testing of the COST Reference microplasma jet for biomedical applications of atmospheric pressure plasmas*, MA.
4. Simona Antoci, *Diagnostica in spettroscopia ottica di emissione (OES) di una sorgente plasma jet in condizioni di free flow e incidente su substrato liquido*, BA.
5. Luca Fontanili, *Studio dell'interazione tra un plasma jet nanopulsato con substrati metallici, dielettrici e liquidi*, BA.
6. Francesco Manghi, *Realizzazione e caratterizzazione funzionale di una sorgente di plasma atmosferico di non equilibrio per l'abbattimento di inquinanti organici in soluzione acquosa*, BA.
7. Marco Lanconelli, *Trattamenti di inattivazione batterica in liquido tramite plasma di non equilibrio per applicazioni in campo energetico*, BA.
8. Francesco Marastoni, *Analisi chimica delle specie reattive prodotte in mezzi di coltura cellulare a seguito di trattamenti con sorgenti di plasma di non equilibrio a pressione atmosferica*, BA.
9. Giacomo Marcelli, *Caratterizzazione e progettazione di una sorgente Plasma Gun per applicazioni endoscopiche*, BA.
10. Alessia Paci, *Caratterizzazione e ottimizzazione prestazionale di una sorgente plasma DBD-jet per applicazioni biomedicali*, BA.
11. Federico Rampa, *Trattamento plasma assistito di acqua con una sorgente Dielectric Barrier Discharge (DBD): analisi delle specie reattive prodotte e potere battericida*, BA.
12. Alessio Tacito, *Sviluppo e caratterizzazione di sorgenti plasma per la decontaminazione batterica di soluzioni acquose*, BA.
13. Paolo Tancioni, *Ottimizzazione sperimentale del processo plasma con sorgente DBD per decontaminazione di acqua*, BA.
14. Marta Diolaiti, *Trattamento di soluzioni acquose tramite sorgenti di plasma di non equilibrio: analisi quantitativa e qualitativa delle specie reattive prodotte e potere battericida*, BA.

1. Plasma Gun for dental applications

1.1. Overview of literature and of experimental activities

1.1.1. Context

From the fact sheet n.318 [1] drawn up by the World Health Organization (WHO) regarding the oral health, that is recognized to be essential to general health and quality of life, it is highlighted that:

- a) worldwide, 60–90% of school children and nearly 100% of adults have dental cavities, often leading to pain and discomfort;
- b) severe periodontal (gum) disease, which may result in tooth loss, is found in 15–20% of middle-aged (35-44 years) adults;
- c) globally, about 30% of people aged 65–74 have no natural teeth mainly due to dental cavities and periodontal disease that are considered the major causes of tooth loss.

Oral diseases not only impact the individual through pain and discomfort, but also the wider community, through the health system and associated economic costs [2]. The current European spending is close to €79 billion, and if the trends continue, this figure could be as high as €93 billion in 2020. Studies have also shown that the mouth care's expenditure is likely to exceed that for cancer, heart disease, stroke or dementia [2].

The WHO Programme priority is to address the so-called 10/90 gap – only 10% of funding allocated for oral and dental research being used to support programs designed to address the everyday problems (caries, periodontal disease, and tooth wear) which adversely thus obtaining a 90% savings on the world population costs for health and well-being [3]. This, together with further research to heal oral cancer, major malformations, notably cleft lip and palate, chronic pain and oral and dental problems, it is suggested to be a top priority [4]. Thus, the attention for dental treatments and health care increases every year.

In dental clinics, the most common diseases are dental caries and periodontal disease. Generally, oral infections can evolve in dental caries, gingivitis, periodontitis and peri-mucositis, that are biofilm triggered diseases, and may result in the tooth death [5–7]. Although teeth brushing, fluoride uptake, antibiotics and vaccines have been used as treatment modalities for oral diseases, the conventional chairside treatments are characterized by pain, long-time treatment and only partial effectiveness of therapies [8,9]. Therefore, novel and efficient microbial inactivation methods are sought by the dental field of both research and business [6].

Moreover, the restoration of the infected tooth plays an important role in conventional dental procedures; recently, dental restoration has been adopting ceramic-based composite materials as their standards are biologically safer and aesthetically higher. However, the success of adhesive

restoration, considered as an alternative to dental amalgams, is often limited by short clinical lifetime. That, in turn, depends upon complex interactions among the patient, the restorative material, and the clinician [10]. Innovations in materials science can open opportunities for the development of materials effective in the adhesive restoration.

Finally, it is worth mentioning that also dental aesthetics such as tooth whitening is going to be one of the most economically important parts of dental clinics [6].

Nairn HF Wilson, President of the British Dental Association, has just claimed how “*with many questions emanating from current research, changing patterns of disease, ever-increasing patient expectations, innovations in research methodologies and the need to investigate the possible application of new technologies in dentistry, setting priorities for future oral and dental research is increasingly challenging*”, underlining the great and necessary effort requested to the scientific community in order to achieve clinical outcomes exploitable in clinical practice [4].

Atmospheric pressure non-thermal plasmas, also known as Cold Atmospheric Plasmas (CAP), thanks to the production at low operating temperature of charged particles, reactive species, radiation and electro-magnetic fields [6], have shown great potential as innovative and multifunctional technology for dental applications. A highly reactive chemistry is produced by CAP at low temperature, and this feature leads to the application of a CAP treatment directly on living tissues. As a gaseous medium, CAP has the capability to penetrate irregular cavities/fissures such as in dentinal tubules or apical regions and inactivate bacteria, actively fighting bacterial infections [11]. Moreover, CAP can activate (bio-)surfaces such as enamel/dentin for the enhancement of the adhesive restoration or zirconia/titanium for a higher biocompatibility of dental implants.

Plasma medicine has evolved rapidly in the past two decades, and investments in research and development by national governments and national and international research institutions have been supporting increasingly the basic research. Clinic-associated research centers have been systematically trying to apply CAP treatment to real medical procedures [5].

In dentistry, the first investigations regarding the feasibility of plasma technology started at the beginning of the century with Eva Stoffels and Raymond Sladek’s research [5,12]. CAP have been shown to be highly efficient at killing planktonic bacteria without damaging human tissues [6,13]. CAP treatment did not change the viability of mesenchymal cells, not induce morphologic alteration to mucosa and periodontal tissues [11,14–16].

Potential dental applications of CAP, that may become important in the near future, include: dental caries, healing of microbial infections, inactivation of biofilms, root canal disinfection, activation of dental surfaces in tooth restoration, polymerization of dental materials, promotion of coagulation and osteointegration, and teeth bleaching [8].

Thus, great emphasis has been being addressed to the design and development of CAP-based technology exploitable in real-life dental procedures, in accordance with the standards requirements regarding biological and electromagnetic safety for both users and patients.

1.1.2. Bacterial related oral diseases and CAP treatment potentialities

Most common oral diseases caused by bacterial infections are dental caries and periodontal disease [6,17].

Dental caries is a disease of hard tissues of teeth (enamel and dentin) caused by organic acids formed by bacteria in dental plaque through an anaerobic metabolism of carbohydrates derived from the diet. The resulting environment with acid pH increases the solubility and demineralization of the dental hard tissues. Dental decay is entirely preventable, but is one of the most common chronic diseases. Progressive dental caries may result in cavities, pain and loss of teeth [1,2]. The most common cariogenic pathogens are *Streptococcus mutans*, *S. anginosus*, *S. constellatus*, *S. gordonii*, *S. intermedius*, *S. mitis*, *S. oralis*, *S. salivarius*, and *S. sanguis* [18]. The standard treatment is to remove the decayed tissues and to fill the cavity with fillings, usually composed of dental amalgam, or composite resin [19]. The lack of a prompt healing of dental caries leads to infection of the dental pulp and consequentially to the death of the tooth, resulting in the need of an endodontic treatment aimed at the tooth and root canal restoration.

In the absence of treatment, gingivitis may progress to periodontitis, which is a destructive periodontal disease [20]. Periodontal (or gum) diseases are bacterial infections and destroy one or more of the periodontal tissues, including the gingiva, periodontal ligament, cementum, and bone that support and anchor teeth [6]. *Porphyromonas gingivalis*, *Prevotella intermedia*, *Fusobacterium nucleatum*, *Treponema denticola*, *Bacteroides forsythus*, *Campylobacter rectus*, and *Actinobacillus actinomycetemcomitans* are well-known pathogens causing periodontal diseases [21]. When severe, the bony support for teeth is extensively compromised causing otherwise healthy teeth to be lost. Chronic periodontitis can cause bleeding gums, loss of fibers and bone, recession of gums, periodontal abscesses, drifting of teeth, tooth mobility and ultimately tooth loss [2]. Successful treatments for dental caries and periodontitis requires the removal of the bacterial plaque and then the healing of the compromised hard or soft tissue. In the specific case of periodontal diseases, initial therapy involves non-surgical cleaning below the gum line by using a procedure called scaling and debridement, while surgical approaches include open flap debridement, osseous surgery, and bone grafting [22].

However, the effectiveness of disinfectant treatments is challenging and affected by the practitioners' ability and the quality/characteristics of irrigants used for the disinfection. Generally, irrigants with

high antibacterial properties result cytotoxic for biological tissues and may cause severe and hazardous post-treatment complications [23].

Since plasmas present antibacterial properties and allow to reach irregular structures and narrow channels within the diseased tooth to be cleaned [6,8], CAP has been investigated as innovative treatment for oral bacterial-related diseases. CAP produce abundant components, which have strong interactions with microorganisms, such as charged particles, radiation, and reactive oxygen and nitrogen species at room temperature, thus avoiding any thermal damage to the tissues [6,24].

The idea of using plasma as innovative antibacterial treatment in dental field was pioneered by Eva Stoffels, who proved the ability of plasmas to inactivate *Escherichia coli* [12], considered as a target microorganism for root canal infections [25].

Nowadays, it is well recognized that a broad spectrum of bacteria in planktonic state can be inactivated by CAP, including Gram-negative *Pseudomonas aeruginosa* and *Escherichia coli* and Gram-positive *Staphylococcus aureus*, *Bacillus subtilis*, *S. mutans* and *Micrococcus luteus* [11,16,26–29]. Fundamental studies have highlighted how the CAP's antibacterial activity was not due to UV emission [16] but rather to oxygen, nitrogen or nitrogen oxide radicals [30,31], which led to oxidative damages to cell membrane, DNA, and proteinaceous enzymes [28,32] and to the etching effect of plasma on the bacterial layer during the chemical process of oxidation [33,34].

In the real oral environment, microorganisms exist in the form of a biofilm. The matured oral biofilm is a three-dimensionally-structured community of many microbial species [33,35]. For example, dental plaque, a biofilm on the tooth surface, consists of complex communities of oral bacteria with hundreds of species present [36]. Furthermore, biofilms are also present on artificial surfaces in the oral cavity such as dentures or implants [33,37,38]. Biofilms developed on tooth and oral mucosa cause caries, periodontal diseases, and oral mucositis, which can also lead to inflammation around dental implants [6].

Therefore, there was a shift in research interest from planktonic to biofilm, and different research groups begun to evaluate the effects of CAP on biofilm models. Many studies exhibited imperfect, but highly promising results [33,39,40] although treatments by means of high antiseptic irrigants, such as solution with 6% of sodium hypochlorite, guarantee higher bacterial load reduction [8].

The limitations of CAP with regard to inhibiting biofilm were discussed in a few studies [40,41], which showed incomplete removal or recovery of *S. mutans* biofilms after CAP treatment. It was hypothesized that biofilm thickness might have prevented plasma from exerting a bactericidal effect to bacteria at the bottom and/or that cell debris from killed bacteria on the surface blocked further penetration of plasma [11]. On the other hand, Rupf et al. [24] demonstrated that combinatorial treatment with plasma and a non-abrasive air/water spray is suitable for the inactivation of oral

biofilms from microstructured titanium used in dental implants. Furthermore, Koban et al. [42] reported that the treatment of dental biofilms composed of *S. mutans* with CAP was more efficient than the treatment with chlorhexidine *in vitro*, though saliva multi-species biofilm revealed to be more resistant to CAP treatment (Fig.1.1).

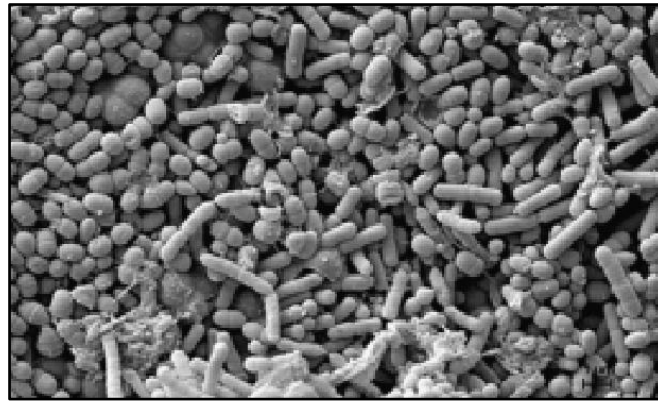


Fig. 1.1. SEM micrographs of saliva multi-species biofilms grown on titanium discs [42].

Clearly, additional work is warranted to optimize CAP's use for biofilm reduction in oral environment [11]. Although few groups showed a relevant inactivation of the pathogens in the root canal, better results can be expected in the future with improvements in CAP devices [6].

1.1.3. CAP treatment potentialities in endodontic treatments

1.1.3.1. Cleaning phase

Endodontic therapy, also known as root canal treatment, is required when the pulp of a tooth becomes infected (Fig.1.2), frequently caused by *E. faecalis* [43–45]. The root canal system has a complex and unpredictable morphology with complicate structures, such as isthmuses, ramifications, deltas, irregularities, and in particular dentinal tubules [46] that can be covered by biofilm. Moreover, bacteria can enter dentinal tubules as deep as 500–1000 μm [47].

Conventional endodontic treatments consist of: a first phase where, after tooth opening, the root canal is shaped by means of stainless steel and nichel titanium instruments, to create a standardized conical geometry, to more easily and more efficiently perform the following parts of the endodontic procedure, a second phase of cleaning of the root canal to significantly reduce the bacterial load, typically performed rinsing with irrigants, and a final phase of obturation to seal the root canal (Fig. 1.3).

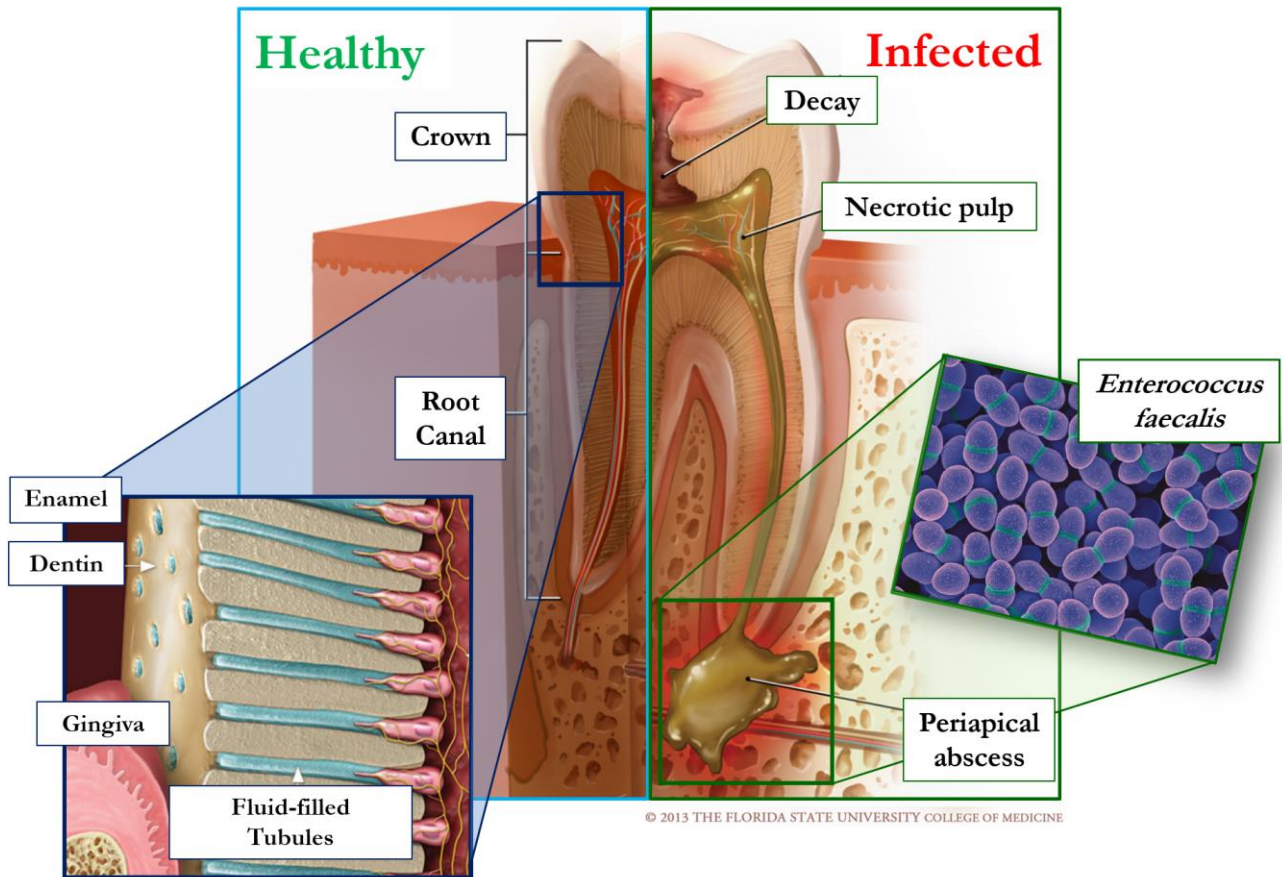


Fig. 1.2. Comparison between healthy and infected root canal. © 2013 THE FLORIDA STATE UNIVERSITY – COLLAGE OF MEDICINE.



Fig. 1.3. RX images of a tooth before and after endodontic treatment.

The decontamination of infected tooth root canal, especially in its apical region, is a crucial phase of endodontic therapy, aimed at preventing post treatment re-infection [48]. In fact, one of the most recognized causes of failure in endodontic treatments procedures is the persistence of microorganism in the treated canal, that may lead to dental granulomas with severe infections [48–50].

Although, a variety of methods have been tested for the disinfection of root canals such as mechanic cleaning, laser irradiation, ultrasound [51–55], the root canal cleaning is conventionally performed with chemical irrigants [33,56]. Concerning the cleaning phase, several clinical studies have

demonstrated that the conventional irrigation with sodium hypochlorite (NaClO) 1-6% (disinfectant solution) and EDTA 17% (chelant solutions) ensures good decontamination results [57–59]. In particular, in order to obtain an almost complete disinfection of the root canals, the cleaning phase requires a disinfectant solution with high concentrations of NaClO (>5.25%) as irrigant [57]; on the other hand, NaClO is a strong oxidizer and cause severe chemical burns to soft tissue, which can lead to necrosis, upon incorrect handling; indeed, NaClO accidents are common hazardous post-treatment complications for endodontic treatment patients [23]. Moreover, common tests to assess the efficacy in decontaminating the root canal are not representative of the efficacy of the treatment inside the whole of the root canal; in particular, bacteria confined in areas such as lateral tubules (Fig. 1.4) and apical regions cannot be completely recovered with the conventional microbiological techniques.

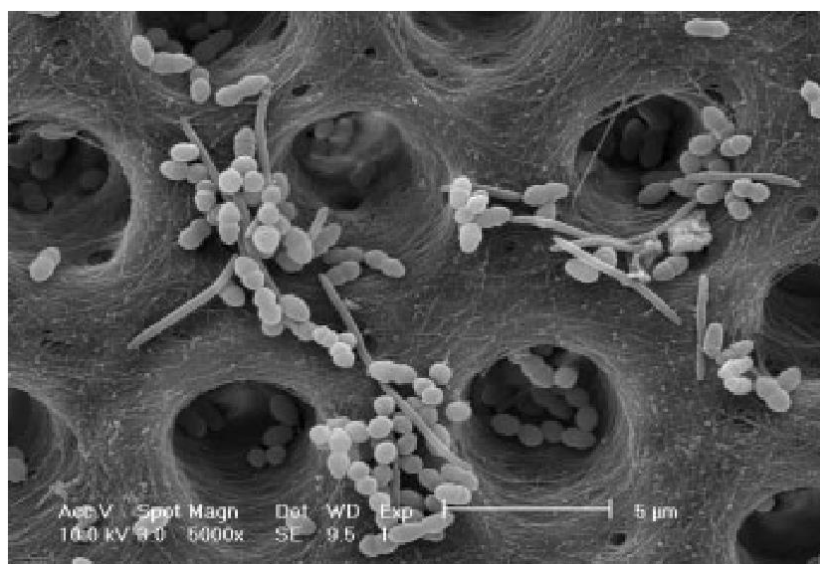


Fig. 1.4. SEM image of *F. nucleatum* and *E. faecalis* contaminated dentinal tubules [60].

Unfortunately, due to the complex morphology and the unpredictable anatomy of the root canal in real teeth, these confined areas cannot be accessed also by mechanical instrumentation and cleaning solutions [48], resulting in a reduction of the effectiveness of conventional methods and hindering the success of endodontic therapies. Clinical procedure is driven by the search of a difficult balance between lowering the risk of incomplete disinfection and the safety concerns raised by the toxicity of the chemical agents used and by the reduction of tooth structural resistance [56]. These limitations, resulting in a lack of a universally recognized clinical procedure, prompt the development of innovative tools and therapies to enhance the current success rate of the endodontic treatments. This procedure strongly dependent on the practitioner's ability and the eliminating of the residual micro-organisms especially within the biofilm is still a challenging task [33,56]. Moreover, clinical investigations showed that there are around 10% of treatment failures when conventional disinfections were performed [61,62] and, thus, innovative solutions are currently demanding.

In numerous *in-vitro* and *ex-vivo* experiments have been reported that a CAP treatment can efficiently inactivate *E. faecalis*, one of the main bacterial species that cause failure of root-canal treatment [6,32,33,63–68]. These promising results after using CAP have pointed out that the CAP has a capability of reaching deep into the complex canal down to the apical region [33]. Interestingly, CAP was seen not only as an alternative to conventional therapies but also as an opportunity for synergistic treatments; the combination of CAP and NaClO washing (3% concentration, a compromise between antibacterial efficacy and patient safety) was found to be more effective than the two treatments performed alone in the inactivation of *E. faecalis* biofilms in extracted teeth [56]. On the other hand, only few studies were performed on root canals contaminated with *E. faecalis* biofilm and the efficacy of a CAP treatment in disinfecting multi-species biofilms, closer to the real-life situation, has not yet been proved.

1.1.3.2. Restoration phase

The final step of endodontic treatment consists in the restoration phase. The disinfected root canal must be sealed in the apical region and then filled with a luting material able to guarantee a solid cohesion between the filler and the dentin substrate. Finally, the dental crown is restored upon the obturated canal system. Occasionally, a fiber post can be inserted in the canal during its filling to ensure a stronger anchor of the restored crown with the root canal. Currently, the conventional restoration involves ceramic-based composite materials for aesthetic and biocompatible reasons, since it has been found that the historical dental amalgams present the uncontrol release of hazardous mercury [10,69,70].

The introduction of these materials for the dental restoration has paved the way for a new field of restorative dentistry: the adhesive dentistry, that has greatly advanced since being first discovered by Buonocore [71–74]. The bonding strength between the filling material and enamel/dentin substrates is obtained by a chemical and micro-mechanical interaction among them.

By the way, the achievement of an efficient and stable bond between tooth substrate and resin materials remains a challenge in composite restorative dentistry. The debonding is the main reason for failure of composite restorations due to their imperfect adhesion of ceramic-based materials with tooth enamel/dentin [56]. Matrix and/or filler deterioration in dental composites, due to mechanical and/or environmental loads, interfacial debonding, microcracking, and/or filler particle fracture lead to a progressive degradation and crack initiation and growth, resulting in catastrophic failure of dental restorations [75–77]. Dental adhesive systems are designed to bond composite resins to enamel or dentin providing retention to composite fillings. A good adhesive system should be able to withstand mechanical forces and shrinkage stress in addition to preventing leakage along the restoration's margins [78,79].

As far as the restoration of tooth root canal is concerned [80], bonding to dentin results a complex task because of dentin composition (approximately 50% inorganic mineral, (hydroxyapatite), 30% organic components (collagen) and 20% fluid) [81,82] and morphology (presence of tubules) [83–85]. The conditioning of dentin surface before application of adhesive systems plays an important role in the achievement of durable dental restorations. For example, the shaping phase of the root canal leaves a layer of debris (smear layer) over the dentine surface, that needs to be removed by means of a chelating agent, such as citric acid or EDTA, in order to improve the performances of the following phases of cleaning and restoration [86].

Multicomponent adhesive systems are used at the dentin–composite interface to promote their adhesion by conditioning the collagen fibers of dentine substrate. [56]. Common dental adhesive systems utilize an acid component (“etchant”) as the first step of the bonding process to remove the residual smear layer and demineralize the dentin surface and expose collagen fibrils. Afterward, a “primer” component is applied to prepare the dentin surface to withhold composite material, favouring a micromechanical interlocking between them. Primers are usually water- and HEMA-rich solutions that ensure complete expansion of the collagen fibril meshwork and wet the collagen with hydrophilic monomers [73]. In particular, self-etch adhesive systems, containing acidic monomers that simultaneously “etch” and “prime” the dental substrate in a single step, have steadily growing popularity in today’s dental practices [74]. After the primer application, a hydrophobic resin monomer (“adhesive resin”) is then applied. Finally, the root canal is sealed with a ceramic-based luting material. After the polymerization of applied materials by means of self-, dual- or light-curing [87], a hybrid layer consisting of resin, collagen and hydroxyapatite crystals, that bonds the hydrophobic restorative materials to the underlying hydrophilic dentin, is formed and this layer is recognized as the weakest part in dental composite restorations [80,88].

From a physicochemical point of view, dental bonding is weak because it is a process in which dental substrate and resin - 2 highly heterogeneous materials - are joined together via hybridization [11]. Furthermore, adhesion failures may have extra different causes including: incomplete adhesive system infiltration, water sorption and hydrolysis of the adhesive resin, inadequate monomer/polymer conversion, incomplete solvent evaporation, degradation of the collagen component of the hybrid layer by proteolytic enzymes [89].

Optimal adhesion could be achieved when the adhesive system is well spread across the entire adherend surface, with high degree of wettability [33,90]. However, it is worth mentioning that high hydrophilicity brings about the risk of adhesive-phase separation due to preferential penetration of its hydrophilic components. Moreover, increased hydrophilicity of dentin/enamel may result in a higher

degradation rate by facilitating penetration of water and hydrolytic enzymes at the interface, which may lead to a rapid and dramatic decrease in bond strength in the long term [11].

The resin polymerization is another crucial step for the formation of a thick and strong hybrid layer [11]. Suboptimal polymerization is common in current dentin bonding procedures due to the mutual presence of hydrophobic photo-initiator and hydrophilic components in common adhesive systems [89,91]. Compromised polymerization not only leads to an unstable resin phase but also leaves demineralized dentin collagen exposed to the degenerative oral environment, leading to an unstable collagen phase as well [73,74]. Thus, resin polymerization is fundamental for the resin-collagen microinterlocking mechanism, whose stability underlies dentin bonding durability [11,88,92]. Clinically, the failure of the dentine/adhesive system bond leads to an increase of bacteria load in the perimeter of composite material, promoting a premature failure of moderate-to-large composite restorations [78,89]. Under these perspectives, in the apical regions different filling materials, such as guttapercha, coupled with endodontic cements are generally used to completely seal the root apex with the aim of entombing the residual bacteria and preventing any contacts with the peri-apical tissues and nerves [93–95]. By the way, these materials are recognized to have lower adhesive properties in respect to the restorative materials used in coronal region of root canal [93,96,97].

The need for better adhesive performances for dental restoration systems has prompted the research of innovative tools and therapies [89]. Innovation in materials science beyond the confines of dentistry has created new classes of materials, delivered ever-improving physical properties with meso-, nano-, and even smaller fillers, that may will be applied and enhance the composite restoration [10]. By the way, the scientific community is still encouraging the research posing important questions; Dr. Watson, from the Department of Biomaterials of King's College London Dental Institute, in his considerations about "Priorities for Future Innovation, Research, and Advocacy in Dental Restorative Materials, [10]" asks: "*Should simple material(s) be created that require only one operative placement stage vs. multiple materials with multiple steps like etch, line, seal, fill? Or should an over-engineered material be developed that can be exceptionally forgiving of operator skill? Innovations beyond the traditional borders of dentistry need to be explored and may offer interesting alternatives for the future [98]. But how long will it take to modify, test, and introduce these new materials – and what will it cost to do so?*"

Transitioning the ability of CAP to increase the surface energy of a treated material from plastics to dentin [56], CAP treatment can be considered as an alternative and attractive solution to the open questions regarding adhesive restoration. By means of CAP exposure, dentine surface can be activated before sealing procedure improving the dental bonding strength. CAP can improve the

hydrophilicity of dentin surface and enhance adhesion through 2 mechanisms: etching/ablation and modification of dentin surface.

Preliminary data has shown that plasma treatment increases bonding strength at the dentin/ composite interface [8]; Ritts and colleagues showed how CAP treatment of dentin before the application of the adhesive system could significantly enhance the adhesion performances [99]. Different studies have shown that, after the chelant/etching phase for the opening of dentinal tubules from smear layer and the CAP treatment aimed increase dentin wettability respectively, a facilitated adhesive penetration into dentin collagen is resulted, which led in thicker hybrid layer and, consequently, better bonding performance [11,56]. The increase of surface energy favours the penetration of the adhesive system, particularly its hydrophilic components, into the dentinal tubules, creating more and longer resin tags and thus improving the bonding strength [56,100]. By means of scanning electron microscope images resin tags longer and more tortuous with lateral projections were observed in the case of plasma pre-treatment of dentin [100,101], as also shown in Fig.1.5. EDX/XPS studies affirmed significant increase in oxygen content on CAP treated dental surfaces, reflecting the introduction of oxygen-containing groups to the substrates which increase the dentin wettability [55,64,102–104].

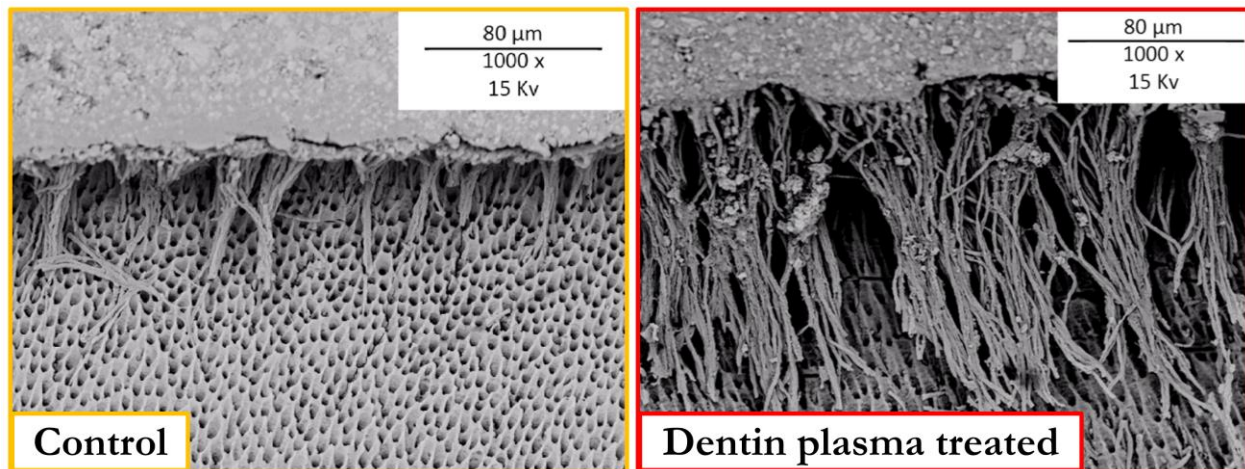


Fig. 1.5. SEM images of formation of resin tags in dentinal substrates in the case of conventional conditioning (control) and plasma treatment of dentin surface.

The prerequisites for an excellent dentin-adhesive hybridization include not only an optimal adhesive penetration, but also a stable dentin adhesive physicochemical interaction. Hirata and co-workers reported that following 1 year of aging in water, the improvement in bonding strength provided by CAP treatment of dentin was lost and there was no appreciable difference compared with untreated samples [56,105]. Thus, the long-term stability of plasma-assisted restorations remains an open question, with a limited number of papers dealing with this subject [56] and experimental studies are necessary to evaluate the ageing effect of plasma treatment.

1.1.4. CAP treatment potentialities in other dental applications

1.1.4.1. Polymerization

Another common reason for composite restoration failure is insufficient conversion from monomer to polymer of the adhesive system, making it more prone to degradation, especially in presence of water infiltration [56]. It has been long documented that plasma can induce polymerization by direct energy transfer (i.e., bombarding reactive species, including radicals, ions, and metastable species, to monomer) and indirect energy transfer (e.g., absorption of UV-visible emission by monomer [106–108]). Polymers synthesized by plasma exposure demonstrated high cross-linking and high degrees of polymerization [33,109]. In this context, CAP was shown to be a promising tool for conversion of the adhesive monomer more efficiently and with lower sensitivity to the water entrapped in the adhesive than conventional photopolymerization lamps [56,110]. Recently, the efficacy of CAP in terms of polymerization was tested and verified on self-etch adhesive systems with no negative effects of water on the degree of conversion of plasma-cured samples [110].

1.1.4.2. Improvement of osseointegration, implants biocompatibility, coagulation, cell migration

Although titanium and titanium alloys are widely used for fabrication of dental implants, zirconia implants were introduced into dental implantology as an alternative to titanium implants because of its toothlike colour, mechanical properties, biocompatibility, and low plaque affinity [111]. The possibility to modify implant surface hydrophilicity or wettability has recently received considerable attention [112] for enhancing implant biocompatibility. Earlier studies of the effect of CAP on titanium surfaces pointed out an improved cell adhesion by changing surface roughness and wettability, which decreases after plasma exposure [113,114]. CAP treatment can occur both during the manufacturing process and immediately prior to implant placement [115,116], with the aim of increasing the spread of osteoblastic cells and enhancing the osseointegration.

CAP stimulates the cell migration not only increasing the hydrophilicity of surfaces but also direct treating living tissue. A study demonstrated that direct application of CAP to gingival fibroblasts stimulates their migration without affecting cell viability or damaging cell membranes, with promising implications for gingival wound healing (e.g., after implant surgery) where fibroblasts are responsible for the important step of producing new extracellular matrix [56,117].

Moreover, plasmas can assist and stimulate a rapid blood coagulation [13,118]. Because many vessels are located around the oral cavity, when repairing an oral wound, bleeding control can ensure a good healing [6].

1.1.4.3. Tooth bleaching, whitening

Tooth bleaching has become a popular aesthetic service in dentistry [33]. Beautiful white teeth make people confident and attractive; therefore, many people seek cosmetic whitening of discoloured teeth. Methods used for tooth bleaching include bleaching strips, bleaching gel, and laser bleaching [6]. Currently available bleaching agents are based primarily on oxidizing agents such as hydrogen peroxide (H_2O_2) or carbamide peroxide [119]. Oxidizing agents effectively remove chromogens from tooth enamel and dentin. In-office bleaching methods use a high concentration (30–44%) of H_2O_2 and involve irradiation of the teeth with light to enhance bleaching efficacy. The light source may enhance bleaching by heating the H_2O_2 and consequently accelerating bleaching, but this mechanism has yet to be confirmed. The application of light may [120] or may not [121] significantly improve the efficacy of the bleaching system.

Plasma can be a good tool for tooth whitening because it is a good source of reactive oxygen species [6,122,123]. Lee et al. also showed that in combination with hydrogen peroxide, CAP removed stains from extracted teeth stained by either coffee or wine [124]. Claiborne D et al. used a plasma plume on extracted human teeth and observed a statistically significant increase in the whitening of the teeth after exposure to CAP + 36% hydrogen peroxide gel [125]. CAP was even suggested to have the potential to innovate current procedures by removing H_2O_2 gels entirely, and introducing a combination of plasma and saline solution [56].

1.1.5. CAP sources for dentistry

In order to maximize the efficacy of a plasma treatment, the control of all the plasma components is required and can be achieved through the tuning of operating conditions and the development of safe plasma devices exploitable in real oral environment. By means of the use of specific mode of plasma generation such as dielectric barrier discharge (DBD), resistive barrier discharge (RDB) and microwave or pulsed discharge, the current-to-transit arcing is prevented by limiting the current flow. Generations of treatment safety, running the experiments under low-plasma-power operating conditions to maintain the temperature of the treated samples below a safe threshold value and to avert the formation of destructive filamentary electrical discharges [56]. Another challenge comes in terms of safety issues, as plasma is typically generated a few tens of millimeters away from the application region using high-voltage (HV) (often in the range of 1–10 kV) electrodes, with a non-negligible risk of touching the tissues in the oral cavity. This aspect, which is interconnected with the source's geometry and architecture, is almost always neglected, leading to investigations of the effects of plasma sources that are difficult to translate to the clinical environment [56]. The plasma devices that can be handheld, can easily access to the oral cavity and conveniently operated by dental practitioners in clinics, is still under development.

Currently, only one high-tech company focusing on medical devices in dental, orthopaedic, and cardiovascular areas has developed a handheld plasma device that can be used by dentist for multiple dental clinical applications. The source generates a plasma with a brush-like shape, that glides across the surface of the tooth, killing bacteria and preparing the dentin and enamel [126,127]. By the way, the application of the device is limited to treat only the exposed oral surfaces due to its configurations and it is unable to reach remote inner areas or to localize the plasma brush inside root canals.

A multi-purposes device based on CAP technology, exploitable in real dental clinics, has not yet fully developed.

1.1.6. Perspectives for CAP treatment in dentistry

By producing and delivering reactive species, including ions, radicals, and UV photons, CAP have exhibited various biological and chemical effects [11] such as its excellent antibacterial property, activation of (bio-)surfaces, polymerization, stimulation of blood coagulation, wound healing and cell migration, and tooth bleaching, and the application of plasma to oral tissues is potentially a fascinating novel technique in dental care [6]. In addition, since gas plasma can penetrate into irregular cavities and fissures, differently from laser beams which propagate linearly, CAP can be applied in conventional endodontic treatment for the root canals care [6,33]. For oral diseases like dental caries or periodontitis, CAP could enhance or replace the conventional surgical removal or usage of antibiotics [8].

Research activities conducted to date lay the foundations for future use of CAP in several areas of clinical dentistry, but the road remains littered with many obstacles [56]. Oral pathogens, including cariogenic bacteria, can be inactivated by plasma within a clinically relevant time frame and without damaging the normal tissue, but further studies are warranted with respect to the removal of mature and multispecies biofilms [11]. Significant increase in surface hydrophilicity is furnished on dental surfaces, including enamel, dentin, and resin/composite, reflecting plasma's capability to etch and introduce functional groups to surfaces. Enhanced penetration of adhesives has been observed on CAP-treated dental surfaces resulting in thicker hybrid layer, longer resin tags and, finally, higher bonding strength. However, more vigorous and clinically relevant storage shall be performed to gauge CAP's long-term influence to bonding. The enhancement of adhesion performances should be proved with a broader spectrum of restorative materials. Critically, it is troublesome that little effort has been directed toward the establishment of a guideline by which CAP can be rationally integrated into bonding procedures. More systematic CAP studies on dental restoration under clinically relevant settings are needed in the future [11].

To introduce plasma treatment intra-orally and chairside, the improvement of equipment and simplification of the process is required [128]. The user-friendly interface, the portability and a

compact size of equipment would gain more popularity [129]. It is worth mentioning that CAP is a new technology for the medical field, and the safety of the equipment has to be taken care [130,131]. Cost of the equipment, marketing, maintenance and availability are also some of the issues at present [8,132].

For CAP to reach the dental chair, future research activities should involve increasing numbers of dentists and move towards more *in vivo* studies and eventually the clinical studies in order to widely accept plasma treatment in dental procedures [56].

The birth of an awareness towards safe, developing, efficient and echo-friendly plasma technology will be inevitable steps [8].

1.1.7. Overview of experimental activities

Plasma dentistry is a field of the research characterized by a multidisciplinary approach involving physicians, engineers, biologists and, of course, expert practitioners of dental clinics. The planning and the performing of the experimental activities I conducted during my PhD studies were carried out with the precious collaboration of a team of dentists of the University of Studies of Brescia. Considering the worldwide literature about the applications of CAP in the field of dentistry joined the knowledge and experience of the conventional dental procedures, it was chosen to focus the study on the evaluation of the potentialities of a CAP treatment, performed with a Plasma Gun (PG) source, in the endodontic clinics. Plasma Gun source is a DBD helium plasma jet firstly developed by J.-M. Pouvesle's research group [133–136]; in these years I properly designed and developed a new plasma source, based on Plasma Gun configuration, for endodontic applications. As reported above, an endodontic treatment comprises sequential steps aimed at disinfecting the root canal and at restoring the tooth. Both goals are limited by different factors: an effective decontamination of the canal is difficult to achieve without the using of high toxic irrigants and bacteria placed in dentinal tubules and in the apical region are hard to reach with liquid disinfectants; on the other hand, the problem of the debonding, resulting in an adhesion failure between the filler materials and dental substrates, recurs frequently in the ceramic-based composite restoration. A Plasma Gun treatment can play an important role in this situation, supporting the endodontic treatment in terms of higher safety and higher performances.

On the lights of these considerations, a preliminary investigation on the efficacy in root canal decontamination of a Plasma Gun, specifically designed for real endodontic practices, was conducted with the aim to assess the possible synergy of plasma treatment with the conventional endodontic therapies. *E. faecalis* was used as target microorganism, being the main responsible for endodontic failures due to its high resistance to conventional cleaning methods, its ability to compete with other microorganisms, invade dentinal tubules and resist nutritional deprivation. The Plasma Gun

antibacterial potential was at first evaluated on Tryptone Soy Agar (TSA) plates contaminated with *E. faecalis* with the aim of selecting, a set of optimal operating conditions qualitatively evaluating the extension and neatness of the produced inactivation areas; the antibacterial efficacy of those operating conditions was then quantified treating infected sterile water. Moreover, the *in vitro* decontamination by means of a Plasma Gun source was investigated on realistic tooth models, perfectly representing the morphology of the root canal and thus enabling to capture the complex geometrical constraints encountered during endodontic therapy. The experiments were performed with the root canal both in dry and wet (using sterile water) conditions, since both cases can be envisioned in the clinical practice and the effects of plasma treatment are known to be strongly affected by the presence of a liquid medium. A chemical analysis of the pH and of the concentrations of reactive species in sterile water treated by Plasma Gun was also performed to support of the interpretation of the experimental results and to gather further insights on the plasma inactivation mechanisms in wet condition. Different protocols, based on realistic endodontic procedures for the decontamination of root canals, were adopted to explore and to evaluate the versatility of the Plasma Gun treatment; in particular, the effectiveness of plasma “indirect treatments”, where the contaminated root canals were irrigated with Plasma Gun activated sterile water (PAW), and “direct treatments”, where they were directly exposed to the Plasma Gun effluent, were compared in wet and dry environments. Furthermore, in order to compare the antibacterial efficacy of Plasma Gun treatment with the conventional antiseptic irrigants in endodontic clinics, 0.2% chlorhexidine (0.2% CHX) and 0.6% sodium hypochlorite (0.6% NaClO) were selected as positive controls both in wet and dry conditions. The results will be discussed not only with the aim of comparing the efficacy of different Plasma Gun treatments for root canal decontamination, but also in the prospect of possibly exploiting the synergies between the various plasma treatments investigated, envisioning an innovative multi-phase endodontic plasma-based procedure.

Wishing to move closer to a real clinic situation, the efficacy of a Plasma Gun treatment in the inactivation of young (24h) biofilm was evaluated along the whole root canal system of ex-vivo teeth by means of a confocal laser microscopy analysis. The extracted teeth were vertically split in two symmetric parts and subsequently contaminated with *E. faecalis*. After plasma treatment, the specimens were prepared with a suspension of SYTO® 9 and propidium iodide, for monitoring the viability of bacteria as a function of the integrity of their cell membrane. Live/Dead spatial distribution of bacterial load was obtained by means of a Zeiss LSM 510 Meta Confocal Microscope: sequential scanning of 20 µm in z-axis, plane by plane with a step of 0,5 µm, was performed in different regions of the root canal (coronal, medial and apical portions).

Moreover, driven by the desire of developing a multi-purposes CAP device for dental applications, tests, performed with Plasma Gun source operating in the same conditions used for biological studies, were run, aimed at investigating the improvement of the bonding strength of the dentin/adhesive system interface in realistic dental composite restorations on extracted teeth. Previous pushout tests results highlighted that 180 s of plasma treatment can greatly improve (>+100%) the mechanical properties of dentin-adhesive interface along the whole length of the tooth root canal, indifferently by the type of chelant agent used (EDTA and phytic acid) to remove the smear layer. Contact angle measurements and SEM analyses confirm how the plasma treatment of dentin favours the permeation of adhesive into dentinal tubules, hence enhancing the interface properties. Supported by these results regarding the adhesive materials used mainly for the restoration of coronal and medial region of root canal, the improvement of adhesive performances was evaluated also in the apical region of the canal system through pushout tests. Guttapercha, that is characterized by low adhesive properties, was usually applied in the apical region as filling material in order to completely seal the canal system avoiding any contacts of the sub-root nerves and blood vessels with the restorative materials and residual bacteria in the root canal. The effects of plasma treatment were evaluated in the case of filling with only guttapercha and in the case of pre-application of an endodontic cement over the dentin surface, that is generally used to increase the adhesion of guttapercha to the dentin substrate in spite of its relevant cytotoxicity. By means of a confocal laser microscope analysis, the penetration of restorative materials into dentinal tubules and dentin substrate was qualitatively evaluated.

The collection of the promising results obtained in the mentioned activities, regarding the enhancement of performances in cleaning and restorative phase of an endodontic procedure, achieved thank to a Plasma Gun treatment, have prompt the development of new CAP system, based on Plasma Gun configuration, for dental applications, closer to the requirements of medical safety and dental practices.

1.2.PG treatment to assist the decontamination of root canal in endodontic procedure

1.2.1. Materials & Methods

1.2.1.1. Plasma Gun architecture and operating conditions

The Plasma Gun employed in the present work was developed in our laboratory and specifically designed for dental applications. The schematic of the source is shown in Fig. 1.6. As high-voltage (HV) electrode, a 50 mm long tungsten wire having a 1 mm diameter is used; the wire is positioned on the axis of a borosilicate glass capillary (4 and 6 mm of inner and outer diameter, respectively) having a relative dielectric constant $\epsilon_r = 7$. A polytetrafluoroethylene (PTFE) support is used to guarantee the coaxial geometry of the HV wire and the borosilicate glass capillary, while it is also machined to provide the inlet for the gas injection. As grounded electrode, a 40 mm width aluminum foil was wrapped outside the dielectric capillary. In order to make the Plasma Gun suitable for endodontic applications, the borosilicate glass capillary terminates with a 25 mm long section characterized by an inclination of 75° and a tapered orifice (inner diameter of 2 mm), resembling in shape typical endodontic instruments. As working gas, 99.999% pure He is introduced for sustaining and propagating the plasma; a plasma plume is produced downstream the source orifice, where the mixing of He plasma with the surrounding ambient air occurs.

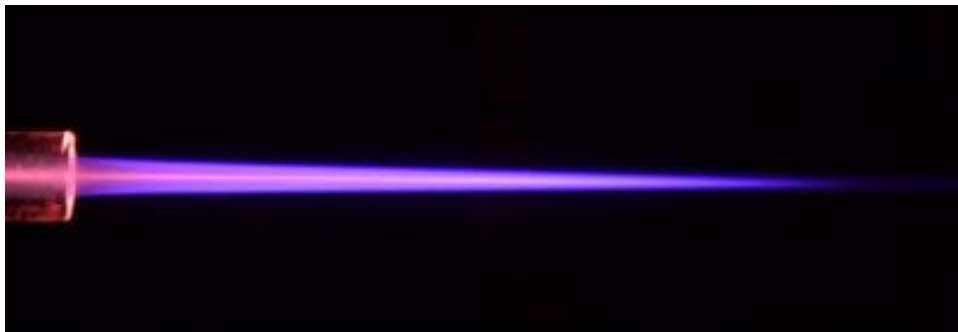
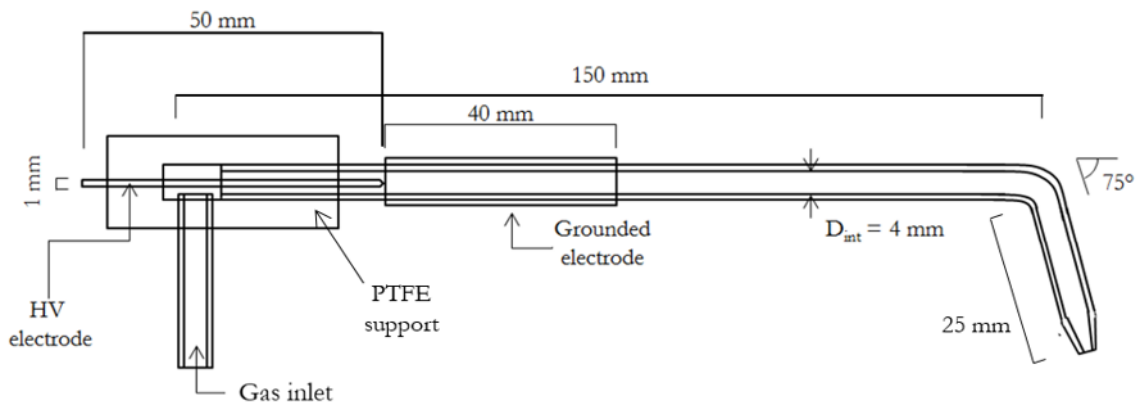


Fig. 1.6. 2D schematic of the Plasma Gun (top) and picture of the plasma plume produced by the Plasma Gun in air (bottom).

The plasma source is driven by a micropulsed generator producing high-voltage sinusoidal pulses having a peak voltage (*PV*) of 7–18 kV, frequency (*f*) of 20-50 kHz, variable pulse duration (around 700 μ s at the lowest duty cycle (*DC*) of 7%) and fixed pulsed repetition frequency (*PRF*) of 100 Hz. In this work, the Plasma Gun was operated at $f = 22$ kHz, with $DC = 7.5\%$ and for different *PVs*, as reported in the following paragraph. A variable He flow rate (*Q*), from 1 to 8 slpm, was used in the experiments; the electrical characteristics of the plasma source were observed to be unaffected by the variation of He flow rate. Voltage and current were monitored by means of high voltage (Tektronix P6015A) and current (Pearson 6585) probes connected to an oscilloscope (Tektronix DPO 40034).

1.2.1.2. Screening of PG operating conditions by means of qualitative analysis of bacterial growth inhibition areas on agar plates

A bacterial suspension was prepared in physiological saline solution (0,9% NaCl) starting from an overnight culture of *Enterococcus faecalis* (ATCC® 29212) on Brain Heart Infusion (BHI) agar plates incubated aerobically at 37°C; the suspension was adjusted to approximately 0.5 McFarland units (i.e. $\sim 1,5 \times 10^8$ CFU/ml), basing on turbidity standards. Ten-fold serial dilutions were prepared and spread on Tryptone Soy Agar (TSA) plates in order to accurately quantify the suspension by colony counting method. One milliliter of the standardized suspension was uniformly spread over the entire agar plate surface, which was dried at room temperature for 30 min and then plasma treated. Plasma treatments were performed for 3 minutes with $f=22$ kHz, $DC=7,5\%$, with a 5 mm gap between the source outlet and the agar surface) and for different values of *PV* and *Q*, as reported in Tab.1.1.

Test	Peak Voltage (PV)	He flow rate (Q)
*	0 kV	8 slpm
A	15 kV	2 slpm
B	15 kV	4 slpm
C	15 kV	6 slpm
D	15 kV	8 slpm
E	13 kV	8 slpm
F	11 kV	8 slpm
G	9 kV	8 slpm
H	7 kV	8 slpm

Tab. 1.1. Plasma Gun operating conditions investigated during the preliminary tests on contaminated TSA. During the experiments frequency, duty cycle, gap and treatment time were kept constant at 22 kHz, 7,5%, 5mm and 3 min, respectively.

After aerobic incubation at 37°C for 24h, the bacterial growth inhibition area on TSA plates was measured by means of the open-source software Icy and its neatness evaluating the absence or the number of bacterial colonies [133]. The best operating conditions resulting from the analysis of

dimension and neatness of the inhibition areas of these preliminary tests were then selected and adopted for all the experiments described in the following paragraphs.

1.2.1.3. Evaluation of the bacterial load reduction in liquid suspensions

A bacterial suspension was prepared in sterile water starting from an overnight culture of *Enterococcus faecalis* (ATCC® 29212) on Brain Heart Infusion (BHI) agar plates incubated aerobically at 37°C; the suspension was adjusted to approximately 0.5 McFarland units (i.e. $\sim 1,5 \times 10^8$ CFU/ml), basing on turbidity standards, and diluted achieving $10^6 - 10^7$ CFU/ml. 100 μ l of the suspension (correspondent to $\sim 10^5$ CFU, which is a value in the range $10^3 - 10^7$ CFU/root canal frequently reported in literature [50] for persistent or secondary infections associated to retreatment cases) were placed in the wells (7 mm deep) of a 96 wells-plate and plasma treated in the following operating conditions: $PV=15$ kV, $f=22$ kHz, $DC=7,5\%$, $Q=3$ slpm; in this case the gap, defined as the distance between the source outlet and the liquid surface was kept constant at 12 mm. The experiments were performed for three different treatment times (1 min, 3 min and 5 min). Moreover, the effect of gas (no plasma) treatment (He 3 slpm, 5 min treatment time) was also evaluated. Immediately after treatment, 50 μ l of the suspensions was used to prepare ten-fold serial dilutions: these were plated on BHI agar plates in order to quantify the amount of survived bacteria by colony counting method. In addition, untreated samples were used as reference.

The antibacterial effect of plasma was calculated following the Log reduction formula: $\text{LogR} = \text{Log}(N_0/N_t)$, where N_0 is the number of viable bacterial CFU recovered in untreated samples and N_t is the number of viable bacterial CFU recovered after plasma treatment. To ensure the reproducibility of experimental results, each experiment was performed in triplicate and results are presented both as mean of survivors CFU/100 μ l \pm standard error of the mean (SEM) and as mean $\text{LogR} \pm \text{SEM}$ of two different experiments.

1.2.1.4. Decontamination tests on realistic tooth models

Tooth models of mandibular premolar representing a realistic anatomy of the canal root were used for the quantitative decontamination tests; different plasma treatment procedures, resembling realistic endodontic procedures for the disinfection of the root canal, were evaluated: indirect treatment, with plasma treatment used to produce plasma activated sterile water (PAW), which is then injected in the contaminated tooth models, as well as direct treatment, performed on the contaminated tooth models both in *wet* and *dry* conditions. The preparation and contamination of the tooth models, as well as the plasma treatment protocols investigated are described in the following paragraphs; in particular, both direct and indirect treatments of the contaminated tooth models that will be described in the following

were performed at fixed (“standard”) operating conditions: $PV = 15$ kV, $f = 22$ kHz, $Q = 3$ slpm, $DC = 7,5\%$.

1.2.1.4.1. Standardization of realistic tooth models

Transparent tooth models of mandibular premolar (TrueTooth™ Mandibular Premolar Replica - DELendo), obtained with the support of the MicroCT scanner 3D analysis of dental and root canal morphology, were used to evaluate the antibacterial the plasma assisted decontamination in a realistic anatomy of root mono-canal system. The tooth model was standardized shaping the root canal by means of a conventional endodontic procedure (Protaper next X1, X2, X3, Dentsply Maileffer, 250 Rpm torque 3,5). After the shaping procedure, the volume of the root canal was about 50 μ l and its diameter was 3 mm in the coronal region and 0.30 mm in the apical region.

Before performing each plasma treatment, the tooth models were sterilized by immersion in ethanol (70%) for 10 min, washed with sterile water twice for 10 min in order to remove residues of alcohol and finally exposed to UV light for 1h.

1.2.1.4.2. PG Activated Water for the indirect treatment of contaminated tooth models

Under the indirect treatment procedure, plasma treatment was adopted to produce plasma activated sterile water (PAW), which was then irrigated in the root canal model for its disinfection. As shown in Fig. 1.7, PAW was prepared treating 100 μ l of sterile water for 1, 3 and 5 minutes in wells of a 96-wells plate, at the standard operating conditions, with a gap of 12 mm and injected in the contaminated tooth models with no delay time after treatment.

The root canal was contaminated following two different procedures, in either a *wet* or *dry environment*. In the first case (*wet environment*), 25 μ l of a bacterial suspension (about $2,5 \times 10^5$ CFU), prepared in sterile water as described in paragraph 2.3, were used to inoculate the root canals; 25 μ l of PAW were then added, filling the root canal model. At certain time lapses after the injection of PAW (contact times of 1, 3 and 5 min), the total liquid volume was recovered and added to 950 μ l of PBS with pH 7.4; ten-fold serial dilutions were prepared for colony counting of survivors on BHI agar plates (aerobic incubation at 37°C for 24 h). Experiments were performed in triplicate and the same procedure was also repeated using 25 μ l of untreated sterile water instead of PAW as the negative control (5 min of contact time). As positive controls, 25 μ l of NaClO solution (0,6%) and 25 μ l of CHX solution (0,2%) were used as disinfecting agent for the decontamination of the root canal system filled with 25 μ l of the bacterial suspension.



Fig. 1.7. Picture of the Plasma Gun treatment of 100 μ l of sterile water for PAW production.

3 min of contact time were selected, as reported in Jablonowski's study [63] and after the treatment, the aspirated suspension was neutralized for 20 min. CHX was neutralized by 50 μ l of Lipofundin MCT 20% (B.Braun, Melsungen, Germany), while NaClO by 50 μ l of sodium thiosulfate solution (5 g/l).

In the second case (*dry environment*), 50 μ l of a bacterial suspension (about 5×10^6 CFU), prepared in sterile NaCl 0,9% as described in the paragraph 2.2, were injected in the tooth model, which was then incubated at 37°C for 2 h in order to promote bacterial adhesion to the inner surfaces of the root canal and the evaporation of the solution; the remaining suspension was finally removed with a needle. 50 μ l of PAW were then added, filling the root canal model; at certain time lapses after the injection of PAW (contact times of 1, 3 and 5 min), the total liquid volume was recovered and added to 950 μ l of PBS with pH 7,4; ten-fold serial dilutions were prepared for colony counting of survivors on BHI agar plates (aerobic incubation at 37°C for 24 h), similarly to the case of *wet environment*. Experiments were performed in triplicate and the same procedure was also repeated using 50 μ l of untreated sterile water instead of PAW as the negative control (5 min of contact time). As positive controls, 50 μ l of NaClO solution (0,6%) and 50 μ l of CHX solution (0,2%) were used as disinfecting agent for the decontamination of the dry root canal with a contact time of 3 min. After the antiseptic was aspirated, neutralization for 20 min was accomplished: for the case of CHX by 50 μ l of Lipofundin MCT 20% (B.Braun, Melsungen, Germany), while for NaClO by 50 μ l of sodium thiosulfate solution (5 g/l).

1.2.1.4.3. Direct PG treatment of contaminated tooth models

In these experiments, plasma was used to directly treat the contaminated root canal models. Similarly to the case of the indirect treatment, experiments were performed for both wet and dry environments. In particular, the *wet environment* was created injecting in the root canal 50 µl of a standardized suspension of *E. faecalis* (about 5×10^5 CFU) prepared as described in paragraph 2.3. The Plasma Gun was then used for the treatment of the bacterial suspension inside the tooth model. For these experiments, the treatments were performed at standard operating conditions, with a gap of 5 mm and different exposure times (1, 3 and 5 min) were tested. Immediately after treatment, the liquid volume was recovered from the wells, added to 950 µl of PBS and ten-fold serial dilutions were prepared for colony counting of survivors on BHI agar plates (aerobic incubation at 37°C for 24 h). Experiments were performed in triplicate; as a negative control for the procedure, 50 µl of untreated suspension were used. The positive controls with NaClO and CHX irrigants for the *wet environment* were performed as described in the paragraph 2.4.2.

On the other side, following the protocol described in [63], the *dry environment* was prepared injecting 50 µl of a standardized suspension of *E. faecalis* (about 5×10^6 CFU), prepared as described in paragraph 2.2, in the root canals of the tooth models, which were then incubated at 37°C for 2 h in order to promote the bacterial adhesion to the inner surfaces and the evaporation of the solution; the remaining suspension was subsequently removed with a needle. Plasma Gun treatment of the dry root canal was performed with a gap of 2 mm (defined as the distance between the plasma source outlet and the root canal inlet section, in analogy to what reported in [63]) as operating conditions and different exposure times (1, 3 and 5 min); the plasma plume was able to propagate inside the entire tooth model. After plasma treatment, remaining bacteria were rinsed out of the tooth model using 50 µl of sterile PBS and a plastic needle; as negative control, 50 µl of sterile PBS were used to rinse a root canal not subjected to plasma treatment. The recovered liquid volumes were then added to 950 µl of PBS and ten-fold serial dilutions were prepared for colony counting of survivors on BHI agar plates (aerobic incubation at 37°C for 24 h). The positive controls with NaClO and CHX irrigants for the *dry environment* were performed as described in the paragraph 2.4.2.

1.2.1.5. Peroxides, nitrates, nitrites and pH measurements

A semi-quantitative chemical analysis of peroxide, nitrate and nitrite concentrations produced in plasma treated sterile water was performed to support the understanding of the experimental results obtained for the cases of indirect treatment and direct treatment in *wet environment* (as described above in paragraphs 2.4.2 and 2.4.3); for these measurements Quantofix® test strips were used.

Moreover, the pH of the sterile water was measured before and after plasma treatment by means of the pH meter InLab Micro Pro. The measurements were carried out in triplicate, by dipping the sensitive part of the pH meter in the liquid.

1.2.1.6. Decontamination tests on realistic monocal premandibular tooth

Premandibular monocal extracted teeth were chosen as models for ex-vivo experiments and contaminated with a 24h-grown biofilm of *E. faecalis*. The bactericidal efficacy was evaluated on extracted tooth models by means of a LIVE/DEAD analysis observed with a confocal microscopy. In particular, the effects of the direct plasma treatment in “dry” condition was compared with a positive control, in which teeth were treated with NaClO solution (0,6%) and with a negative control, performed with a physiological solution washing. The preparation and contamination of the tooth, as well as the plasma and control treatment protocols investigated are described in the following paragraphs; in particular, as in the experiments on root canal models, the Plasma Gun source operated at the same “standard” conditions: $PV = 15$ kV, $f = 22$ kHz, $Q = 3$ slpm, $DC = 7,5\%$.

An illustration of protocol procedure is presented below the paragraph 3.1.6.2. in Fig. 1.8.

1.2.1.6.1. Standardization of extracted tooth

The extracted teeth were immersed in thymol 0,1% gel until their use for the designed experiments. The standardization comprised sequential steps: the coronal region of the tooth was removed to obtain a root canal system 15 mm long, measured by means of *k-files* with a pin diameter of 15 μm ; the canal was regularly shaped through the milling machine Protaper Next X1 17.04, X2 25.06, X3 30.07 intercutting with washing of 2 ml of NaClO 5,25% ed EDTA 17% e physiological solution to remove the inorganic and smear layer over the dentin surface. In order to ensure a correct cutting along the longitudinal line of root canal, the shaped teeth were incorporated and fixed in a silicone mould; afterwards teeth were vertically cut to obtain two sections of the canal. Each part was sterilized through an autoclave cycle. Finally, each half-tooth was conserved in 1 ml Eppendorf by fixing with composite material (A2) polymerized for 20 s.

1.2.1.6.2. Contamination of extracted tooth

A bacterial suspension in NaCl 0,9% with a standard turbidity of 0,5-1 McFarland ($1,5-3 \times 10^8$ CFU/ml) was prepared starting from an over-night culture of *E. faecalis*. Then a working suspension in BHI broth was prepared diluting 1:100 the starting suspension to achieve a final OD405 of 0,05 (3×10^6 CFU/ml). The effective amount of CFU in the final suspension were calculated preparing ten serial dilutions and evaluating the growth of bacterial colonies after 24h of incubation at 37°C. In order to contaminate also the dentinal tubules, the procedure provided repeating sequential spin cycles

(5 min each one) with 500 μ l of fresh suspension each time. For each half tooth, the bacterial contamination procedure consists in: 2 spin cycle at 1400 rpm, 1 spin cycle at 2000 rpm, 1 spin cycle at 3600 rpm, 2 spin cycle at 5600 rpm. Then the samples were incubated in 1 ml of BHI at 37°C for 24 h to promote the growth of a young biofilm.

1.2.1.6.3. Treatments of contaminated tooth

Each half tooth was washed with sterile water and dried with absorbing paper. Then the whole tooth was recreated joining the two half parts in the silicone structure previously used (see paragraph 3.1.6.1). Then, the samples were treated depending on its associated group:

- Negative control (G1): washing with physiological solution for 3 min.
- Positive control (G2): washing with NaClO 0,6% solution for 3 min.
- Direct “dry” plasma treatment (G3): 5 min of plasma exposure; the tooth drying procedure and details of treatment are the same reported in paragraph 3.1.4.3.

After the treatment, each sample was irrigated with sterile water for 1 min.

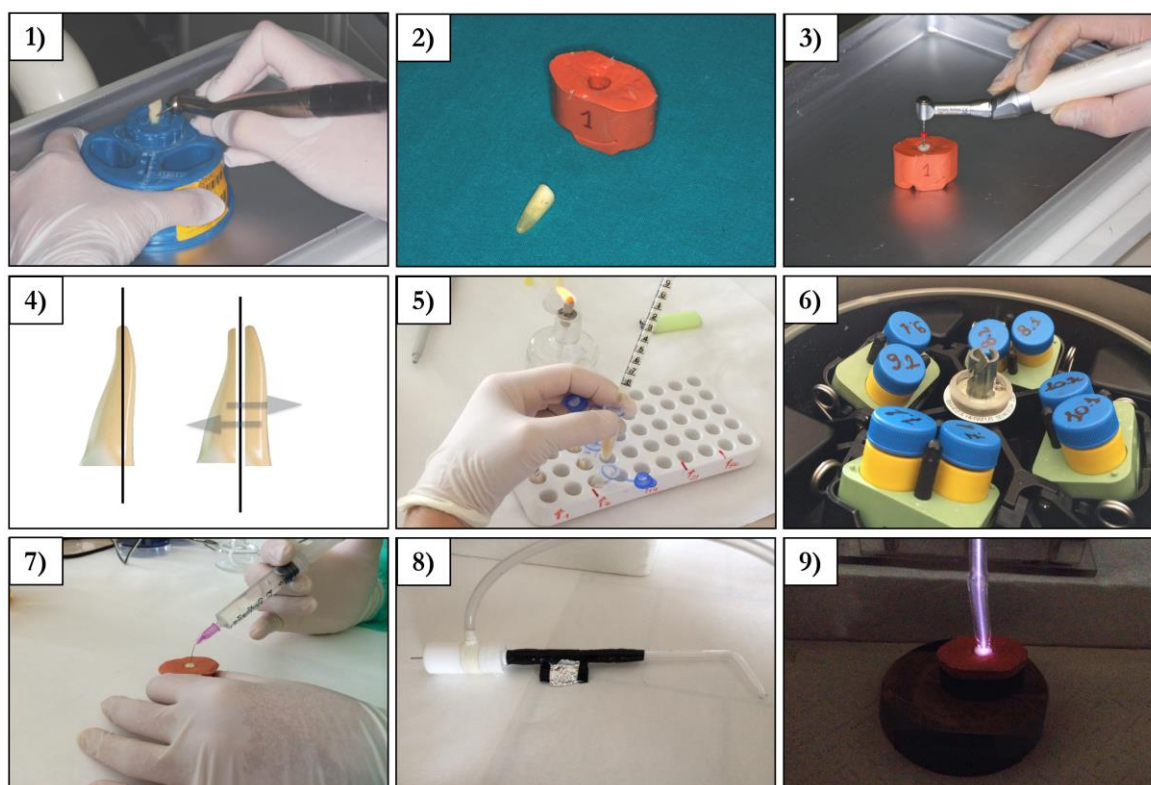


Fig.1.8. Biological protocol for treatment of contaminated ex-vivo teeth: 1) external cleaning of the tooth, 2) realization of the silicon holder, 3) shaping of root canal in apposite silicon holder, 4) longitudinal cutting, 5) contamination of root canal with bacterial suspension of *E. faecalis* in BHI broth, 6) spin cycles to contaminate the dentinal tubules, 7) rinsing with physiological solution as negative control, 8-9) direct plasma treatment.

1.2.1.6.4. Staining LIVE/DEAD analysis through Confocal Laser Scanning Microscopy (CLSM)

The *LIVE/DEAD BacLight viability stain* kit containing SYTO 9 and propidium iodide fluorescent molecules was used to evaluate the viability of bacterial cells. When used alone, the SYTO 9 stain generally labels all bacteria in a population those with intact membranes and those with damaged membranes. In contrast, propidium iodide penetrates only bacteria with damaged membranes, causing a reduction in the SYTO 9 stain fluorescence when both dyes are present. The excitation/emission maxima for these dyes are about 480/500 nm for SYTO 9 stain and 490/635 nm for propidium iodide. The background remains virtually non-fluorescent. Thus, bacteria with intact cell membranes stain fluorescent green, whereas bacteria with damaged membranes stain fluorescent red [134]. The application of fluorescent kit (1:1 = 3 μ l SYTO 9 + 3 μ l propidium iodide in 1 ml of sterile water; 100 μ l of mixture for each half-tooth) took 15 min in dark environment. To eliminate extra colourant, samples were then washed 3 times immersing the half-tooth in 2 ml of sterile water for 1 min. An additional group (G0) was prepared for CLSM analysis containing non-contaminated tooth, to assess the selectivity of the fluorescent kit to interact only with prokaryotic cells and not with the dentin substrate. Then the samples were served in 1 ml of physiological solution at 4°C until the CLSM analysis.

For CLSM analysis, Achroplan 10x/0,25 lens with an additional 2x or 3x zoom was used to acquire 3D images of apical, medial and coronal regions of the root canal system. Imaging scanning was performed with the following parameters: 40 focal plane acquisitions with a step size of 0,5 μ m (total investigated depth of 20 μ m), planar X-Y size of 0,70x0,70 mm². An example of confocal analysis is schematically reported in Fig.1.9.

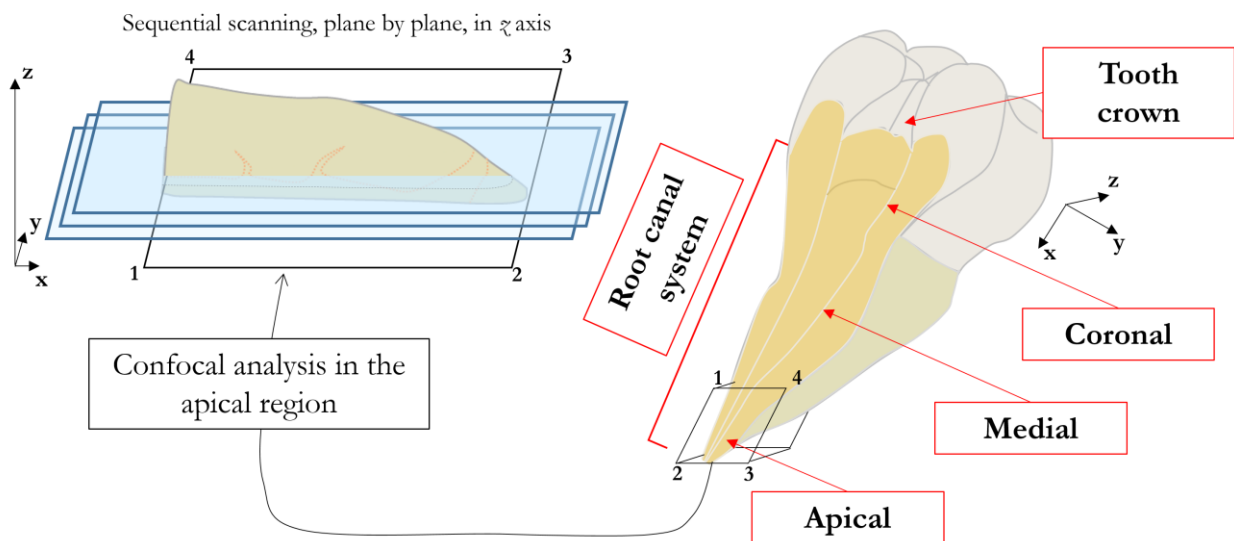


Fig.1.9. Description of confocal analysis in the apical region of root canal system.

1.2.2. Results

1.2.2.1. Analysis of the growth inhibition area on contaminated TSA plates

As reported in Fig. 1.10, results for tests on agar plates contaminated with *E. faecalis* were used to select Plasma Gun operating conditions to be used in all the other experiments in terms of *PV* and He flow rate: the dimensions of growth inhibition area after plasma treatment (in mm^2) can be observed: the increase of either *PV* or He flow rate results in a monotonic increase of the dimension of the growth inhibition area; similarly higher the applied voltage higher the current recorded. For the cases with higher *PV* (15 kV), the inhibition area is always greater than 50 mm^2 (tests: A, B, C, D), independently of the flow rate; on the other hand, for the cases with higher *Q* (8 slpm) a steep decrease in inhibition area is observed for *PV* lower than 11 kV (tests: H, G, F). As expected, the greatest inhibition area, around 140 mm^2 , was observed for the higher values of the operating parameters tested (test D: *PV* = 15 kV, *Q* = 8 slpm); however, in this case, similarly to case C, several bacterial colonies remained inside the inactivation area highlighting a low level of neatness.

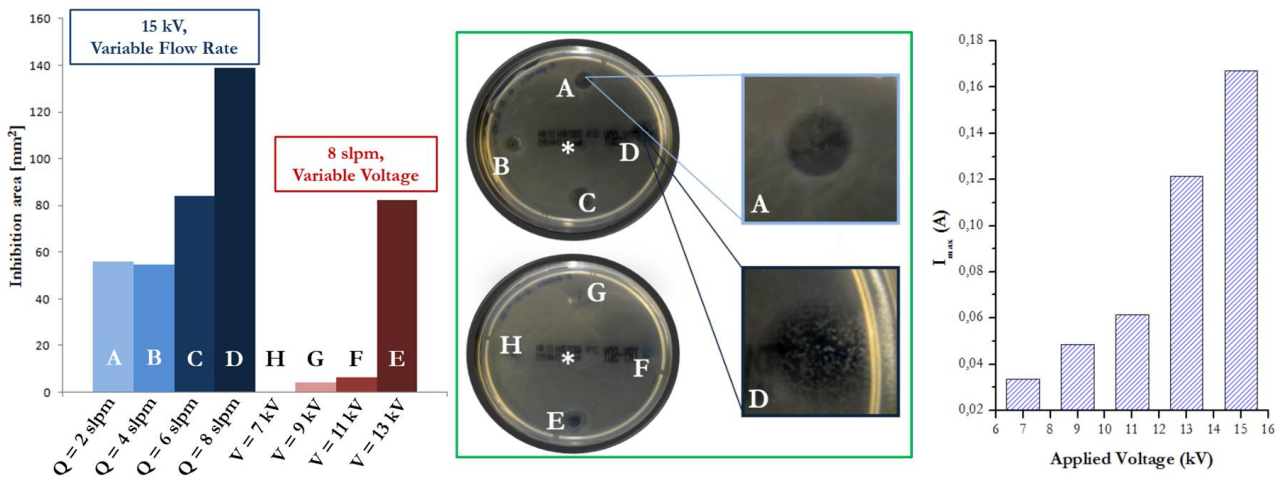


Fig. 1.10. A histogram (left) reporting the dimensions of inhibition areas (mm^2), for the different operating conditions (labeled with alphabetic letters) reported in Table 1. Agar plates with the growth inhibition area obtained for each operating condition, after 24 h of incubation, and zoom of the inactivation area for the conditions A and D in order to emphasize their neatness (center). A histogram of the maximum current value recorded for different applied voltage at fixed flow rate ($f=22\text{kHz}$, $\text{DC}=7,5\%$).

On the contrary, experimental conditions A and B, characterized by the same *PV* (15 kV) of test D, but lower He flow rates (2-4 slpm), resulted in completely neat growth inhibition areas, larger than 50 mm^2 (corresponding approximately to 8 mm diameter), without any bacterial colonies detectable inside the inactivation spots. Since almost no difference in the characteristics of the inhibition areas

were found for the operating conditions A and B, the operating conditions adopted for the following experiments were: $PV = 15$ kV and $Q = 3$ slpm ($f=22$ kHz, $PRF=100$ Hz, $DC=7,5\%$). It should also be noticed that the diameter of the tooth crown section of the standardized cavity access is lower than 3 mm, thus significantly lower than the growth inhibition area observed for the selected operating conditions.

1.2.2.2. Quantitative evaluation of bacterial load reduction in bacterial suspensions

In Fig. 1.11, the survivors (CFU/0,1 ml) after the tested plasma treatments are reported. After 1 minute of plasma exposure no reduction of bacterial load was observed, while for treatment times equal to or above 3 minutes total decontamination of the suspension was achieved ($\text{LogR} \geq 5$).

For the gas-only control, a slightly higher number of survivors CFU were recovered compared to the untreated control; this was probably due to partial evaporation of the contaminated suspension during the gas-only treatment, which caused an increase of the bacteria concentration.

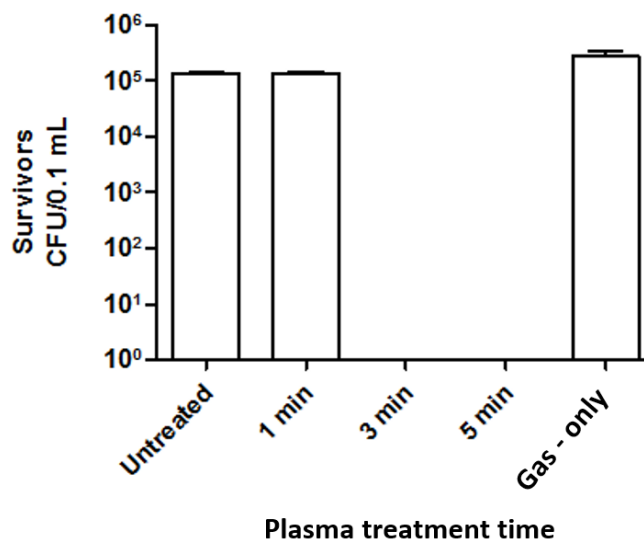


Fig. 1.11. Histogram of survivors CFU in 0,1 ml of bacterial suspension for different treatments: untreated (negative control), 1-3-5 min plasma treatments and 5 min gas-only.

1.2.2.3. Decontamination of root canal models

1.2.2.3.1. Indirect plasma treatment: wet and dry environment

Results for the survival CFU after indirect treatment in *wet environment*, are reported in Fig. 1.12. The higher the plasma treatment time of the sterile water, the greater the antibacterial effects of PAW. In fact, PAW obtained from 1 min treatment of sterile water (PAW 1 min) led to a LogR of $0,23 \pm 0,01$, while PAW produced after a 5 min treatment (PAW 5 min) to a LogR of $2,8 \pm 0,5$ (considering a

contact time of 5 min). Interestingly, it was also noticed that PAW 5 min exerted a $2,13 \pm 0,22$ LogR after just 1 minute of contact time.

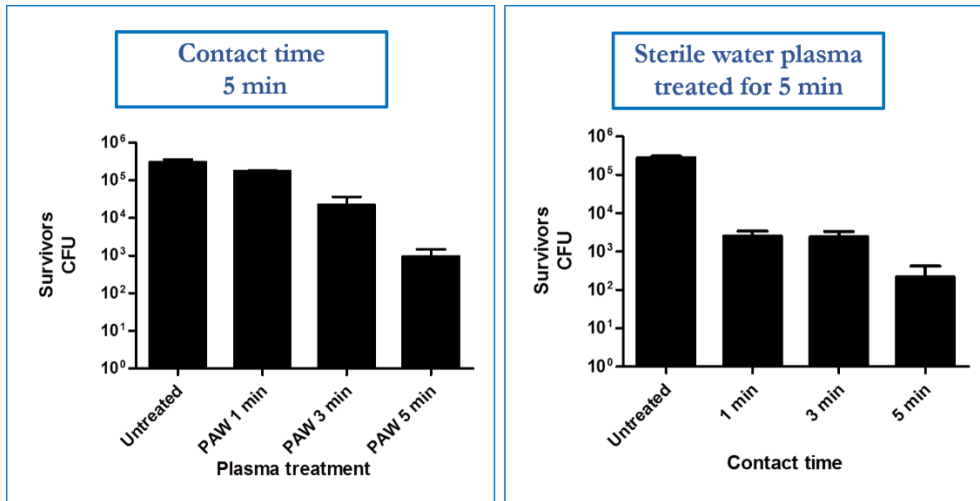


Fig. 1.12. Histograms of survivors CFU after the indirect treatment in *wet environment* performed for (left) fixed contact time of 5 min using PAW prepared with different plasma treatment times and (right) variable contact times using PAW prepared with a 5 min plasma treatment.

In Fig. 1.13, the survival CFU after the indirect plasma treatment in *dry environment* are reported. Similarly to the previous case, the higher the plasma treatment time for PAW production, the lower the residual CFU recovered; on the contrary, a LogR of only $1,6 \pm 0,4$ was achieved with a PAW 5 min kept in contact with the contaminated tooth models for 5 minutes. Notably, no difference in LogR was observed when using PAW 5 min for shorter contact times.

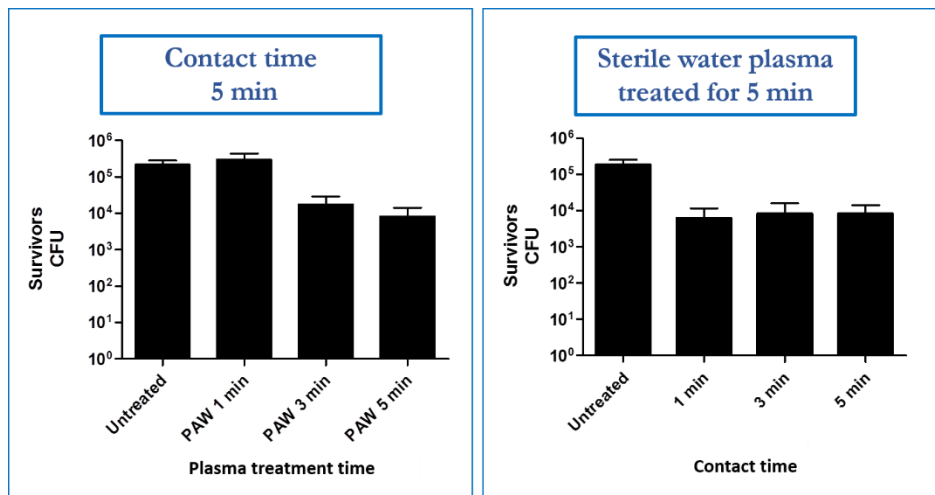


Fig. 1.13. Histograms of survivors CFU after the indirect treatment in *dry environment* for (left) fixed contact time of 5 min using PAW prepared with different plasma treatment times and (right) variable contact times using PAW prepared with a 5 min plasma treatment.

1.2.2.3.2. Direct plasma treatment: wet and dry environment

Results concerning the plasma treatment of tooth models contaminated with 50 μl of bacterial suspension (*wet environment*), reported in Fig. 1.14, denote that the achieved decontamination was always lower than Log1; no significant influence of treatment time on decontamination was then observed.

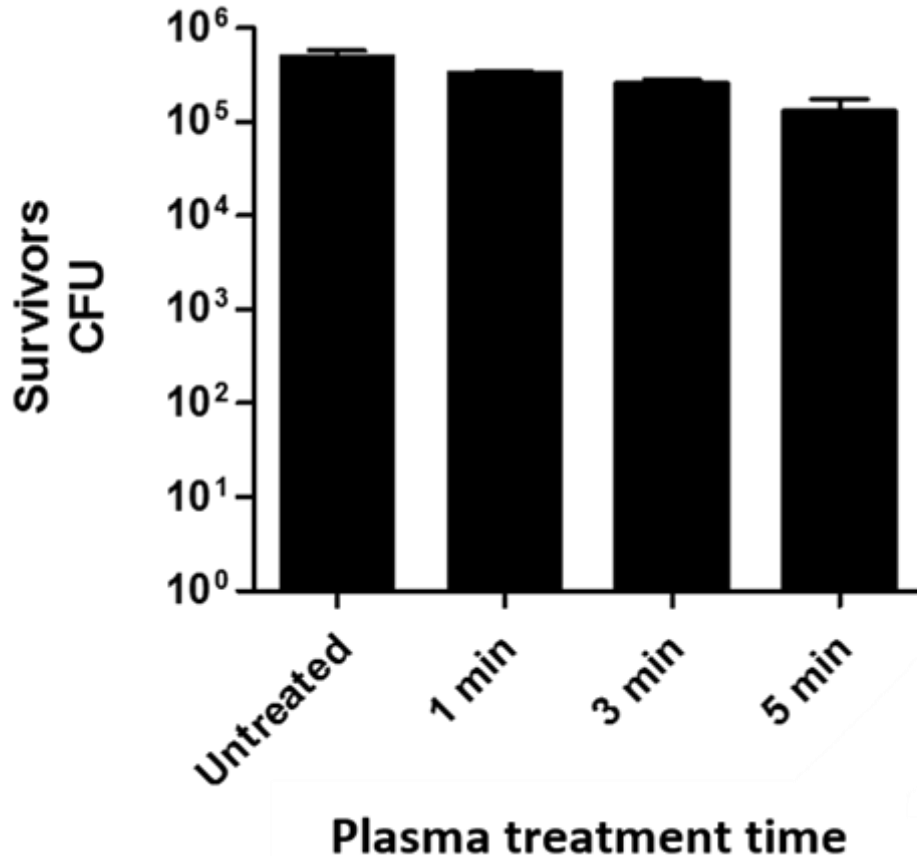


Fig. 1.14. Histogram of survivors CFU for the untreated model and after direct plasma treatments in *wet environment* performed for 1, 3 and 5 min.

The survivor CFU for the direct treatment in *dry environment* are presented in Fig. 1.15; where an exponential decrease of survivor bacteria is observed for increasing treatment times. Indeed, while a 1 min plasma treatment induced a limited decontamination ($\text{LogR} < 1$) with respect to the negative control, after 5 min of plasma treatment bacterial load logarithmic reduction of $4,1 \pm 0,3$ was observed.

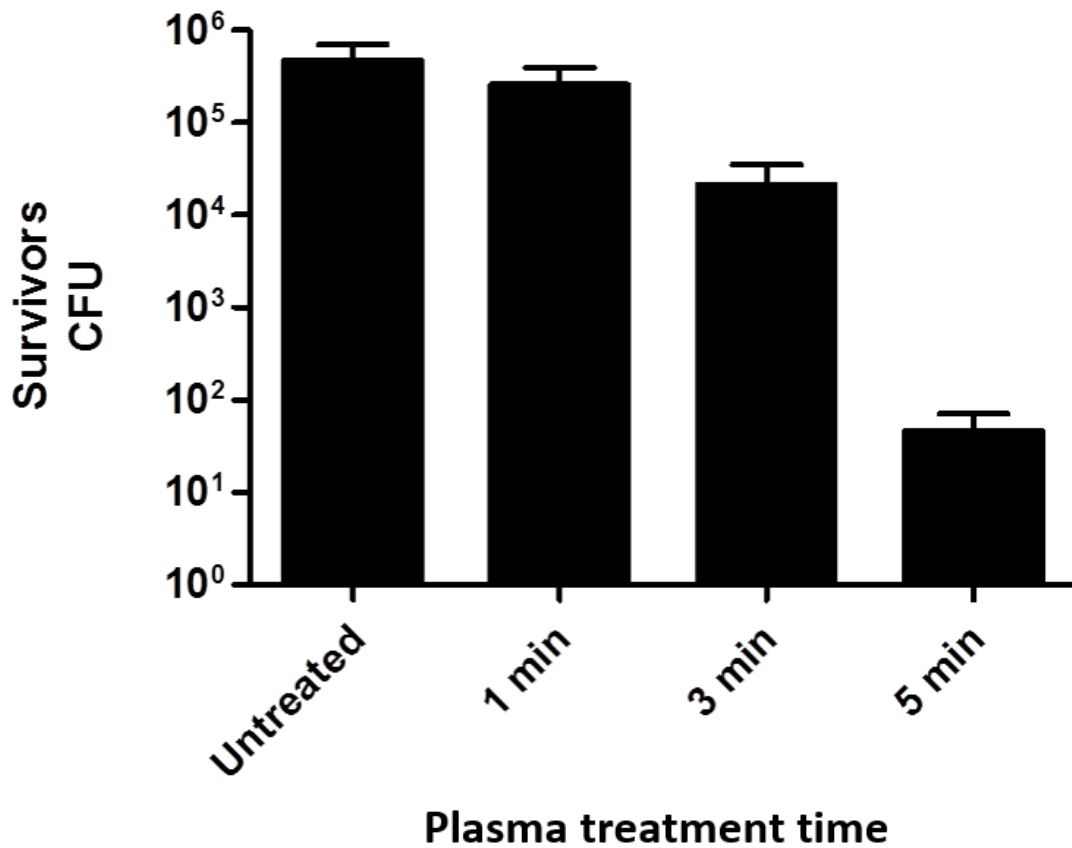


Fig. 1.15. Histogram of survivors CFU for the untreated model and after direct plasma treatments *dry environment* performed for 1, 3 and 5 min.

1.2.2.3.3. Positive controls with 0,2% CHX and 0,6% NaClO

In Fig.1.16, the bacterial load reduction (LogR), achieved by CHX and NaClO treatments, is shown. The highest values of LogR are obtained with the NaClO irrigant both in *wet* (LogR>5) and *dry* (LogR=2,77) *environment*, while with the CHX solution a LogR=2,82 for the wet condition and a LogR=2,35 for the dry conditions are reached.

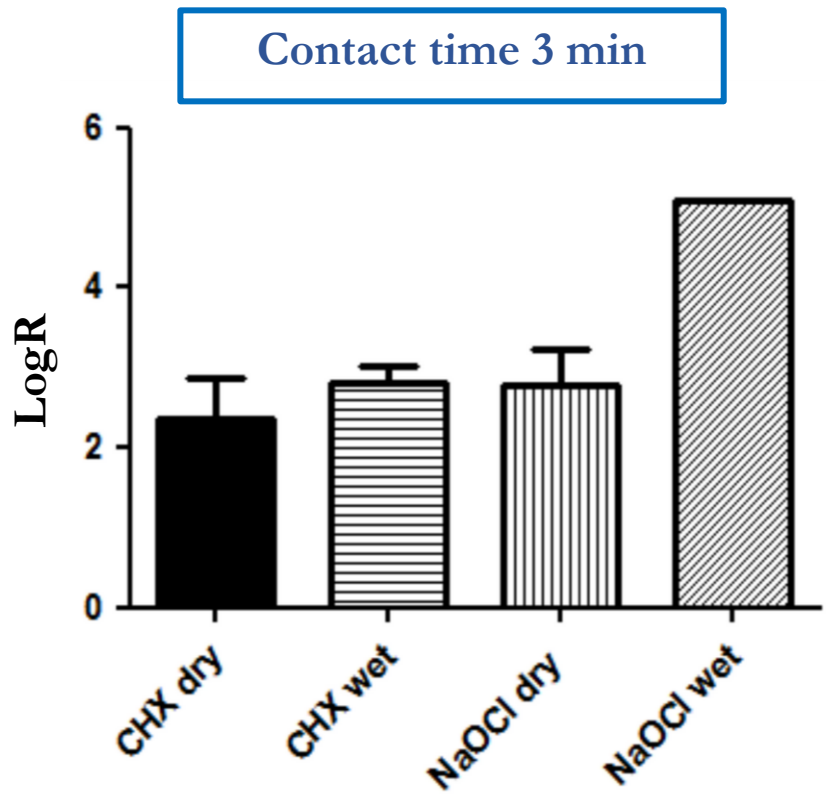


Fig. 1.16. Histogram of bacterial load log-reduction (LogR) after 3 min of 0,2% CHX and 0,6% NaClO treatments in wet and dry conditions.

Regarding the disinfection of the contaminated root canal models in *wet environment*, a complete decontamination is observed only with the NaClO irrigant.

1.2.2.3.4. Chemical analysis of pH and reactive species produced in sterile water treated by Plasma Gun

Results of chemical analysis of PAW produced either plasma treating 100 μ l of sterile water in wells of 96-wells plate or 50 μ l of sterile water in standardized tooth models are reported in Fig. 1.17. A decrease of pH was observed for PAW produced from sterile water in wells: after 1 min of plasma exposure, the pH was $3,43 \pm 0,06$ and decreased to the value of $2,20 \pm 0,44$ after 5 min of irradiation; moreover, increasing treatment times resulted in an increase of peroxides and nitrites concentrations, while nitrates concentrations appeared unaffected.

For the case of PAW prepared treating sterile water in tooth models, a lower pH decrease ($3,43$ after 3 min and 5 min treatments) and lower concentrations of reactive species were registered with respect to the pH measured for PAW prepared treating sterile water in wells.

Finally, no pH variation and no production of reactive species were observed for treatments performed in gas-only conditions.

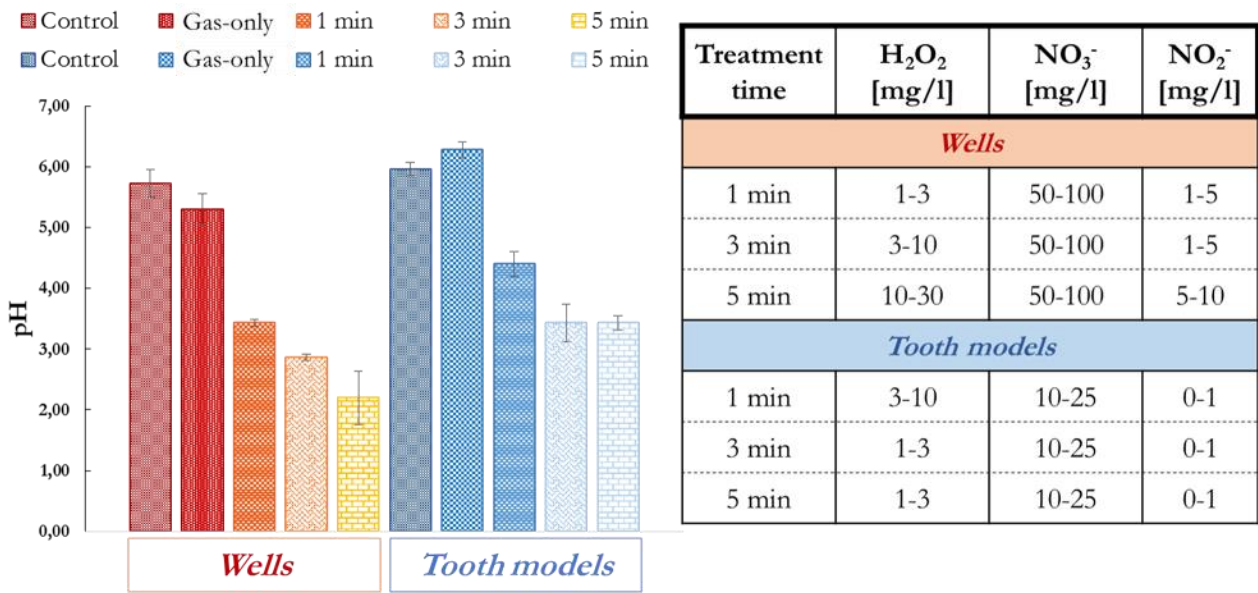


Fig.1.17. pH values (Left) and concentrations [mg/l] of peroxides, nitrites and nitrates (right) measured in untreated sterile water, sterile water treated in gas-only condition ($Q = 5$ slpm) and in PAW produced treating for 1, 3 and 5 min sterile water contained either in wells or in tooth models.

1.2.2.4. Decontamination of ex-vivo extracted teeth through CLSM analysis

The collection of CLSM images is reported below in Fig.1.18. A good contamination of dentin surface and dentinal tubules was confirmed by the negative control images. The same images also proved the effectiveness of fluorescent method used for the analysis as a really low red signal was detected in the negative control. A bactericidal efficacy of plasma treatment was observed along the whole length of canal although a greater inactivate bacterial load was detected in the coronal region in respect of the apical region of the root canal. The ability of plasma to penetrate tubules was proved; however, as shown in the 3D visualization images, in the dentin surface the dead bacteria population was greater than the alive one while in the dentinal tubules more alive bacteria were detected. The positive control highlighted how a treatment with 0,6% NaClO solution could achieved higher level of young biofilm inactivation than plasma treatment for the whole length of canal and in the lateral tubules.

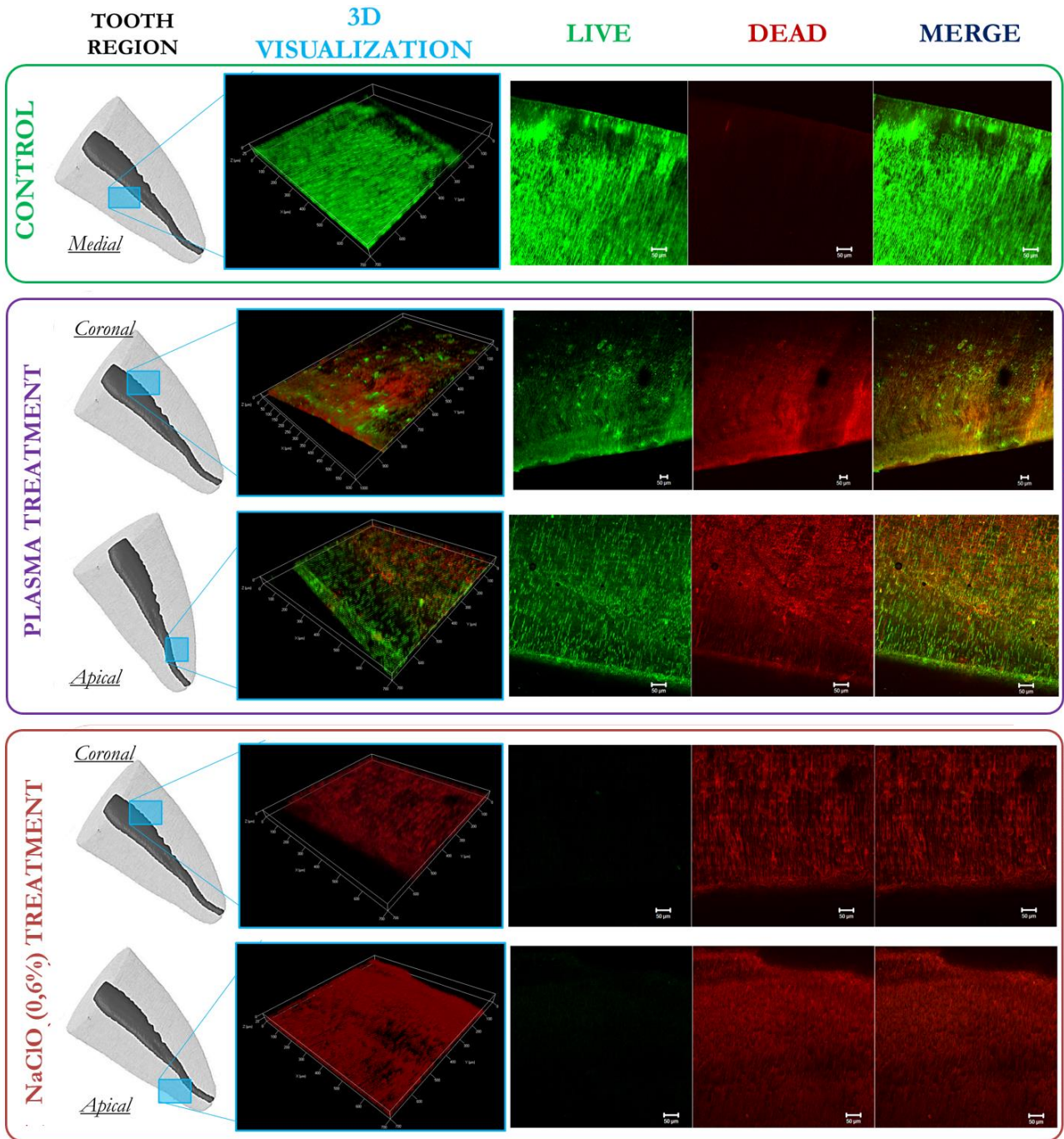


Fig.1.18. Collection of CLSM images for negative control, plasma treatment and positive control (0,6% NaClO solution). TOOTH REGION: region of root canal system analyzed by CLSM (coronal, medial or apical. 3D VISUALIZATION: tridimensional overlap of 8 focal planes with a single z-step of 7µm. LIVE: 2D map of SYTO 9 fluorescence, representing the LIVE bacterial population (single focal plane). DEAD: 2D map of propidium iodide fluorescence, representing the DEAD bacterial population (single focal plane). MERGE: Merge of LIVE and DEAD 2D maps representing the whole bacterial viability (single focal plane).

1.2.3. Discussion of results

The results reported for the preliminary tests on contaminated TSA plates highlight the role of PV and He flow rate in the decontamination process. In particular, higher He flow rates led to larger growth inhibition areas, as shown in Fig. 3, possibly also as a consequence of the fluid dynamic behavior of the plasma plume when impinging on the substrate. Indeed, it was previously demonstrated [135], albeit using a different plasma source, that at the contact point of the plasma plume with the substrate, turbulent wave fronts are formed and spread radially along the surface, extending the area affected by the reactive species produced in the plasma region.

Even though at higher He flow rates a wider radial expansion over the surface, leading to a larger growth inhibition area, of the turbulent wave fronts is expected, the neatness of the growth inhibition areas was observed to decrease as the flow rate was increased. On the other hand, an increase of PV was observed to induce an increase in the dimension of the growth inhibition area as well as in its level of neatness. This can be explained as a PV increase causes a higher local electric field produced in the plasma plume which, in turn, produces a higher electron concentration that enhances the production of excited species, as observed in [136]. Furthermore, it was previously reported that increasing voltage induces also a faster and more intense ionization wave, penetrating further into the plasma plume and resulting as well in a higher production of reactive species [137]. Therefore, the antibacterial efficacy of a plasma source is generally enhanced when PV is increased. The analysis of the results at fixed flow rate, highlights a non-linear relation between the applied voltage and the dimension of the bacterial inactivation area: a strong amplification of bactericidal effects was observed changing the applied voltage from $V=11\text{kV}$ to $V=13\text{kV}$. This behavior is also supported by the maximum value of current recorded during the experiments as shown in Fig. 1.10, that follows a similar profile.

The results of bacterial load reduction in contaminated suspensions in 96 wells-plate showed that complete decontamination could be achieved after 3 minutes of Plasma Gun treatment, while no reduction was observed in the gas-only control. Furthermore, a non-linear behavior between the antibacterial efficacy of the plasma treatment and the exposure time was detected, in agreement with Morfill's study [138]: in fact, a LogR of 5 was reached after 3 minutes of plasma treatment while the decontamination after 1 minute was negligible. Through a chemical analysis of the plasma treated sterile water, a reduction of pH of the solution, down to 2,2, and relevant concentrations of nitrites, nitrates and peroxides were measured, confirming the formation of a solution with bactericidal properties. In fact, when the liquid environment is characterized by a $\text{pH} < 4$, reactive species such as nitrates, nitrites and peroxides, generated in liquid during the treatment, participate in the degradation of bacteria membranes [139,140].

Results for the Plasma Gun indirect treatment of contaminated tooth models have highlighted that with PAW 5 min with 5 minutes of contact time in *wet environment* a $\text{LogR} = 2,8 \pm 0,5$ could be obtained; this result being in the same range of effectiveness as the one obtained for the 0,2% CHX positive control. pH variation and concentrations of reactive species formed in water strongly depended on the plasma treatment time. As expected, since the antimicrobial activity of PAW is related to resulting concentration in treated water of pH, NO_2^- and H_2O_2 , that are the precursors of the peroxyntirite which participates directly in the degradation of bacterial membranes [139], the higher antibacterial efficacy was achieved in the case of PAW with the lower induced value of pH and higher concentration of reactive species. Generally, contact time longer than 1 min did not increase the LogR both in the case of *wet* and *dry environment*. In particular, the indirect treatment in *wet environment* presented the highest bacterial load reduction, since the suspended bacteria resulted to be more affected by PAW than bacteria adherent to the inner surface of the root canal model, in agreement with what previously reported for bacteria adhering on solid substrates [141].

Concerning the Plasma Gun direct treatment of contaminated tooth models, the decontamination efficacy was dramatically affected by the root canal environment; the best results were obtained in the case of *dry environment*, where the plasma plume could propagate in the entire root canal (as shown in Fig. 12) and an exponential increase in decontamination efficacy with treatment time was observed (LogR as high as $4,1 \pm 0,3$ after after 5 minutes of Plasma Gun exposure). On the other hand, no relevant inactivation was obtained for the direct treatment of the root canal in *wet environment*; this result is in marked contrast with results obtained treating bacterial suspensions in 96-well plates, even though the volume of solution in wells was significantly bigger, in accordance with the higher pH and lower concentration of reactive species measured in the sterile water treated in tooth model than that treated in wells for identical treatment times. Two possible explanations are advanced to explain this behaviour; first, the liquid surface directly exposed to the plasma discharge irradiation was considerably smaller in the tooth model than in the well of the 96-well plate, and so, the area interested in the diffusion and interaction between the reactive species produced in air and the liquid surface was considerably reduced. Second, in the decontamination tests on suspensions in wells, the plasma plume remained in contact with the liquid surface for the whole duration of the experiment, while during the tests on the tooth models the plasma discharge was in contact with the suspensions only for the first thirty seconds of the treatment then, due to the evaporation of the solution, the plume was observed to attach on the upper surface of the tooth model, as shown in Fig.1.19; therefore, after the first 30 sec the bacterial suspension was exposed to the afterglow of the plasma plume, resulting in a reduced bactericidal efficacy as only long living species can reach the contaminated liquid [142].

Although in the dry conditions the chemistry induced in liquid by plasma irradiation was not present, the direct plasma treatment in *dry environment* achieved the highest values of bacterial load reduction among all the tested plasma based procedures and even higher than NaClO and CHX controls in the same protocol conditions (LogR=2,77 and LogR=2,35, respectively).

Since the drying procedures of root canal by means of paper points or pressured air syringes are common in endodontic practices [143], a direct Plasma Gun treatment in dry conditions seems really exploitable in actual dental applications as independent method or in support of the conventional cleaning methods for the decontamination of root canal.

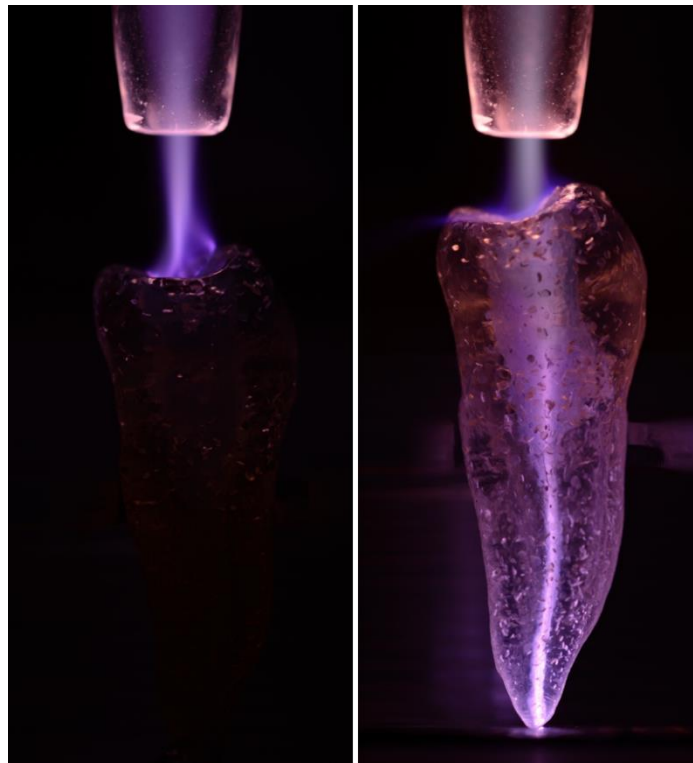


Fig. 1.19. Plasma plume in the different experimental setup for *wet* and *dry* conditions: plasma plume after 1 minute of treatment on a tooth model filled with liquid with a gap of 5 mm (left) and the plasma plume propagation inside a dry tooth model positioned 2 mm away from the Plasma Gun outlet (right).

Regarding the confocal analysis, a more realistic clinic situation was investigated. Pathogenic bacteria are usually in the state of biofilm in oral environment, and the morphology of a root canal system is more complex of a simple root canal model due to the presence of isthmuses, ramifications and lateral dentinal tubules, that could be contaminated. The CLSM images highlighted the capability of plasma of reaching the apical region ensuring a partial inactivation of the biofilm; moreover, dead bacteria were found also in the lateral tubules of dentin both in the coronal and apical sections. The effectiveness of plasma treatment was not fully uniform along the canal and higher inactivation was

observed in the coronal region. A negative gradient of the bactericidal efficacy moving from the dentin surface, where the red signal (indicating dead bacteria) exceeds the green one, towards the inner dentinal substrate was also observed. On the other hand, the positive control performed with sodium hypochlorite solution showed a quasi-fully destruction of biofilm in the whole root canal system, underlining a higher efficacy in comparison with the alone plasma treatment. Although these qualitative images seemed in contrast with the results obtained in the decontamination of root canal models, it is worth mentioning that bacteria in biofilm state have stronger and different mechanisms of defence against antiseptic agents. The complex structure of a biofilm, characterized by a multilayered morphology, protects the inner bacteria avoiding the direct contact with plasma and the easy diffusion of reactive and charge species inside the bacterial matrix [39,41]. Sladek et al. supported the idea that the deactivation of biofilm cells is associated to short-lived reactive species, such as atomic oxygen and OH radicals [40]. In particular, in the studies of Perni et al. [144] and Goree et al. [29] the major contribution of bacterial deactivation was attributed to the monoatomic oxygen. Furthermore, electrostatic process are involved in the opening or destruction of cellular membranes, due to the charging of cell membrane for the delivery of charge species in the plasma effluent [145]. These considerations are fully in agreement with CLSM acquisitions. The lower inactivation in the dentinal tubules, in respect to the levels achieved over the dentin surface, can be related to the diffusion of the only long-lived RONS. Oxygen atoms and OH radicals don't have enough time to reach the bacteria deeply in tubules; the delivery of charged species is confined in the plasma plume mainly in contact with the dentin substrate. Thus, CAP results more affected by the state of bacteria (planktonic or biofilm) than a conventional disinfecting irrigant as NaClO solution, that interacts with prokaryotic cells with the same chemical agents everywhere. Sladek and co-workers observed similar results, where a *S. mutans* biofilm was completely inhibited with CHX while plasma treatment did exhibit only growth inhibitory effects against the biofilm [40].

By the way, a safe and less aggressive alternative treatment to conventional irrigants (NaClO, CHX,..) would be highly desirable [40] and this should pave the way for further researches aimed at evaluating the potentialities of CAP treatment in synergy with conventional clinics. Future studies in *ex vivo* and *in vivo* samples, contaminated with multi-species biofilms, should be carried out to support the feasibility of Plasma Gun treatment in realistic dental therapies.

1.3. PG treatment to assist the restoration of root canal in endodontic procedure

1.3.1. Preliminary results on coronal-medial canal restoration and overview on guttapercha obturation of apical region

Different endodontic materials are usually adopted for the restoration of coronal-medial and apical region of the root canal system. Previously experimental activities were performed in our laboratories to evaluate the enhancement of bonding strength at adhesive/dentine interface after a plasma treatment of dentine [146]. In particular, the study was focused on the restorative materials used for the obturation of upper (coronal and medial) region of canal which are generally chosen for their adhesion and structural performances since the scope of this endodontic phase is the obturation of the canal system and the anchorage of the restored tooth crown.

For these experiments, the plasma-induced enhancement of bonding strength in a restoration procedure performed with a 2-step (or “self-etch”) adhesive system, which has steadily growing popularity in today’s dental practices. Extracted monocanal teeth were standardized. Teeth were then embedded in epoxy resin cylinders using a custom molding procedure designed to ensure the accurate alignment of the specimens during the pushout tests. Then the dentine surface was pre-treated (or not) with different chelating agents (EDTA and IP6) and exposed (or not) to plasma for 3 min. The self-etch adhesive system was finally applied and polymerized. After that, luting cement was used to seal the root canal. After 24h of storage in water at 37°C, the teeth were sectioned in slices (2 mm thick) obtained from the coronal and medial portions. The adhesion between the dentine and the adhesive system was evaluated by means of pushout tests: specimens were axially loaded on the cement section (\varnothing 1,6 mm) with a cylindrical metallic plunger (\varnothing 1,4 mm) controlled by a universal testing machine (Instron 8033) at a cross-head speed of 0,5 mm/min.

Pushout results clearly showed a significant enhancement of the bonding strength as a consequence of plasma dentine pre-treatment. The results reported an improvement of bonding strength of more than +100% along the whole axial length of root canal when plasma was applied on its dentine after the application of a chelating agent.

Moreover, the contact angle measurements, performed on dentine surface with both water and the etcher-primer component of the adhesive system, supported the hypothesis that the improvement of bonding strength is mainly driven by the plasma-induced increase in wettability of the dentine surface. By means of SEM analysis, was observed an increase, with respect to control, of the amount of dentinal tubules filled with luting material when the dentine was pre-treated with a chelating agent followed by plasma exposure.

Regarding the apical sealing, different materials are usually used in order to avoid an endodontic failure due to a new bacterial colonization resulting in hazardous abscess. The main features of a good sealing material in the apical region are recognized to be [93]:

- Easy to manipulate.
- Amenable to different obturating methods.
- Stable in the oral environment.
- Radiopaque.
- Biocompatible.
- Antimicrobial.
- Non shrinking or expanding more than 0.5% during polymerization.
- Self-adhesive.
- Forms a stable bond to dentine that does not degrade with time and function.
- Forms a bond that is not affected by oxidizing agents like sodium hypochlorite.
- Strengthens the tooth.
- Easily removed for post placement or retreatment.

Nowadays, guttapercha is the adopted sealing material for apical restoration. Cold and thermal plasticity, high stability after polymerization, inert and biocompatible, low thermal conductivity are the main advantages of guttapercha with respect to other conventional sealers [147–151]. The conventional application of guttapercha, procedure known as “down-packing”, comprises the sequential heating of different pluggers with different diameters aimed at sealing the root canal by a thermal expansion of guttapercha in a plastic state. To enhance the adhesion performances of guttapercha to dentinal surfaces, an endodontic sealer (liquid cement) is usually spread in the canal system before sealing.

1.3.2. Materials & Methods

1.3.2.1. Tooth sample preparation

The procedure adopted for the preparation of teeth sample follows the protocol described in [146]. Forty-four maxillary and mandibular monoradicular human teeth, extracted for periodontal, prosthetic or orthodontic diseases, with straight roots and regular single canals were selected for this study. Teeth were stored in 0,1% thymol solution at 4°C to serve their structural properties and ensure good hydration. The crown was sectioned off at the cemento-enamel junction using a water-cooled diamond blade on a cutting machine (Isomet, Buhler, Lake Bluff, NY, USA) to expose the root canal.

Although guttapercha is used for sealing apical foramen with diameter lower than 1 mm, to standardize the study, the first 8 mm of the canal were shaped to a regular diameter of 1,6 mm by means of a cylindrical diamond bur (Komet 837/016, Brasseler, Lemgo, D). Teeth were then embedded in epoxy resin cylinders (Enamel Temp Plus, Micerium) using a custom molding procedure (described in Fig. 1.20 and Fig. 1.21) designed to ensure the accurate alignment of the specimens for pushout tests. The mold presents a pin on its base designed to hold the tooth in position during the resin curing and ensure the alignment of the root canal along the cylinder axis.

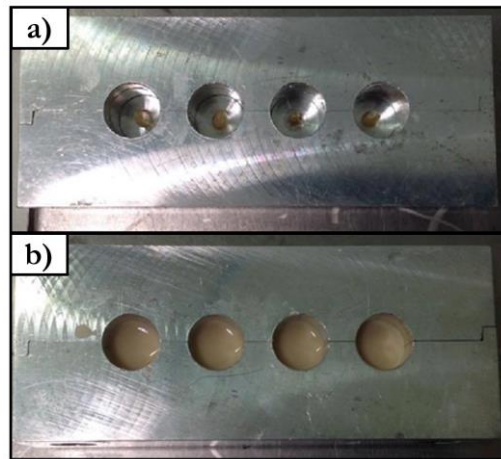


Fig. 1.20. Molding procedure before (a) and after (b) resin casting.

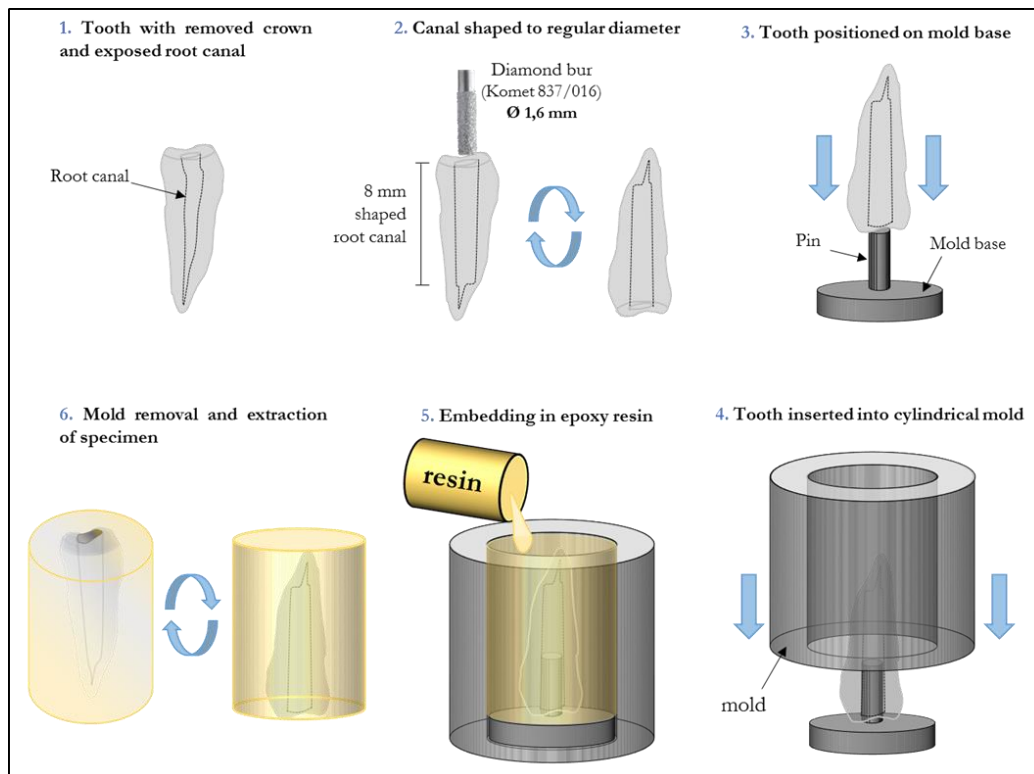


Fig. 1.21. Molding procedure to ensure the alignment of the root canal along the resin cylinder axis

[146].

As later described, this procedure ensures an accurate alignment of the specimens during pushout tests. After curing of the epoxy resin the tooth results as perfectly embedded in the mold. A solution of EDTA 17% (most popular chelant agent adopted in endodontic clinics) was rinsed for 1 min for the cleansing of each root canal and for the removal of smear layer. Then, teeth were dried with paper points to eliminate any residuals of chalent agent. The samples were randomly distributed into 4 groups and conditioned with different type of dentine pre-treatment: two control groups subjected to standard procedures (G1, G3) and two experimental groups including the conditioning of dentine through a plasma treatment (G2, G4). Plasma treatment was carried out by means of a Plasma Gun source operating in the same conditions used in the bacterial inactivation experiments (see paragraph 1.2.1.4) and in [146] for 3 minutes.

As reported in Tab.1.2, G1 included the teeth subjected to no dentine surface conditioning and directly filled with guttapercha (Calamus Dual System – Calamus Flow, Dentsply, Maillefer). Back-packing procedure was used for the application of guttapercha for a better 3D polymerization [152] by means of manual plugger. G2 comprised a plasma treatment of the root canal before guttapercha sealing. The group G3 was characterized by the application of an endodontic sealer (Top Seal, Dentsply, Maillefer), conventionally used as adhesive material to bond guttapercha with apical dentine. G4 provided a plasma pre-treatment od dentine surface before sealer application.

Group	Filling procedure
1	Guttapercha
2	CAP + Guttapercha
3	Sealer + Guttapercha
4	CAP + Sealer + Guttapercha

Tab. 1.2. Sealing protocol applied to each group after root canal shaping.

Photos of each single step of the procedure were collected in Fig. 1.22.

Specimens were stored for 1 week at 37°C in saturated environment. According to the procedure reported in [153], after water storage, the samples were sectioned transversally to the long axis of the tooth by means of a diamond saw (Isomet) irrigated with water. Tooth sections 1,6 mm-thick were obtained from coronal and apical portions of the root canal as schematically described in Figure 1.23. The coronal and apical sections were respectively cut 4 and 1 mm above the apical terminal. Thanks to the molding system procedure, the accurate positioning of the specimens in the pushout testing machine was guaranteed in spite of the tooth irregular external shape. Images of sample slices preparation and collection are reported in Fig. 1.24 and Fig. 1.25.

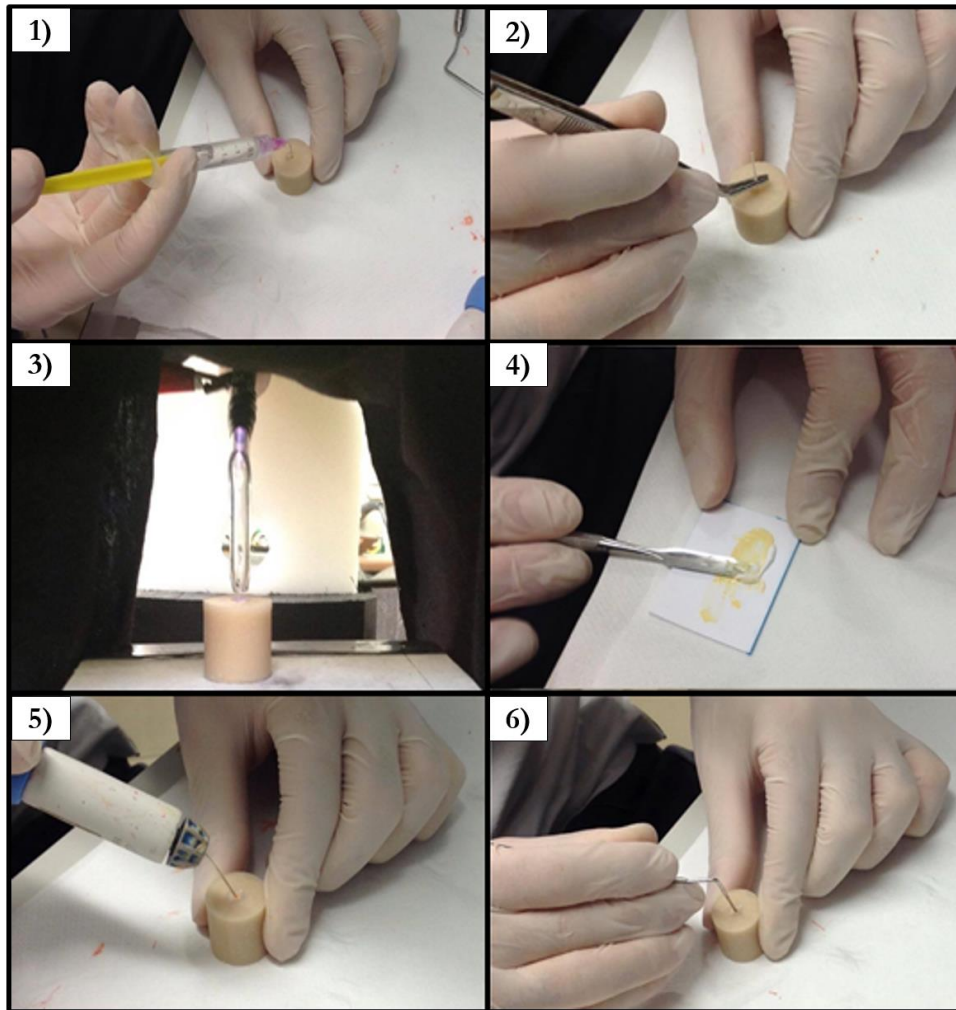


Fig. 1.22. Different steps of experimental procedures: 1) EDTA rinsing; 2) drying with paper points; 3) CAP treatment; 4) sealer preparation; 5) guttapercha obturation with Calamus Flow; 6) manual compaction/compression of guttapercha.

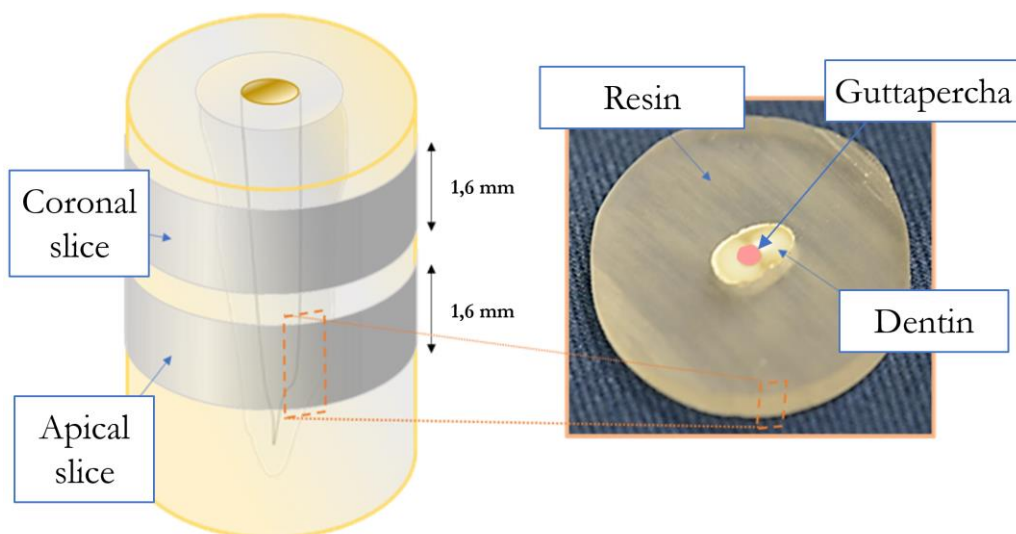


Fig. 1.23. Tooth coronal and apical section specimens for pushout test.



Fig. 1.24. Isomet diamond saw for the samples section cutting.

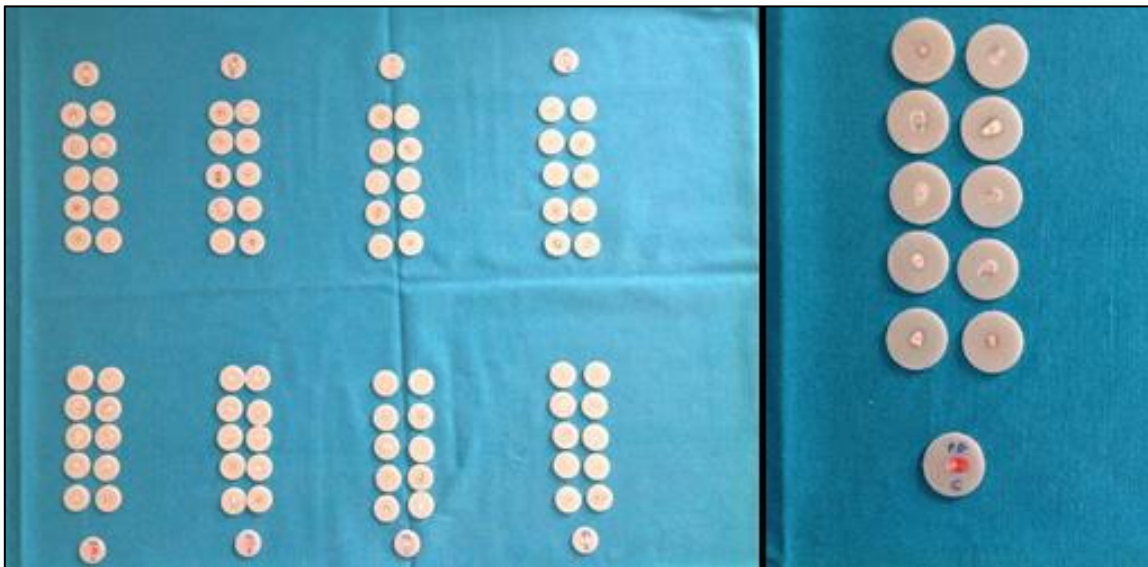


Fig. 1.25. Specimens prepared for pushout test.

1.3.2.2. Pushout test

In accord with [146] and in order to support and widen the results described in paragraph 4.1, the pushout tests were performed following the same procedure. In particular, the pushout test [153–155] was used to evaluate the bonding strength of dentine-adhesive system interface in prepared specimens. A representative photo of pushout tests is reported in Fig. 1.26. Tests were performed using a universal testing machine (Instron model 5848, load cell HBM U2A 200 kg, Micro Tester MTS electronic Test Star IIs). Specimens were axially loaded on the luting material section (\varnothing 1,6

mm) with a cylindrical metallic plunger (\varnothing 1,4 mm) at a cross-head speed of 1 mm/min. When dislodgement occurred, the maximum failure load was recorded in volts (V) and then converted into newton (N). For the final conversion into MPa the surface of the adhesive-dentine interface was estimated from the height of each specimen measured with a digital calliper. Statistical analysis was performed applying one-variable analysis of variance (ANOVA) as post-hoc comparison at a significance level set at $p < 0,05$.



Fig. 1.26. Picture of the pushout tests setup.

1.3.2.3. CLSM analysis

In order to observe the penetration of sealing materials in dentinal tubules and support the discussion of the results, a red-fluorescent molecule (Eosin Yellowish 1B 425, Chroma-Gesellschaft, red emission around 532 nm) was used for confocal analysis. A colourant with eosin 0,1% was prepared. Teeth specimens were prepared as described in paragraph 4.2.1. As sealer was used in liquid state, a mixture of colourant-sealer was prepared and then used for G3 and G4 groups following the procedure discussed above. On the other hand, being guttapercha plugger in plastic-solid phase, for the case G1 and G2, the colourant was spread in the root canal before guttapercha filling. Thus, the red fluorescence represents the sealer penetration in the cases G3 and G4, while in the G1 and G2 groups the red signal shows the colourant itself pushed into dentinal tubules by the guttapercha penetration. The confocal analysis was performed by means of confocal microscope (510 META, Zeiss, Fig. 1.27)

with a 40x lens and an additional zoom of 3x as magnification factor. Pinhole was keep open at 100 μm for all acquisitions (512x512 px).

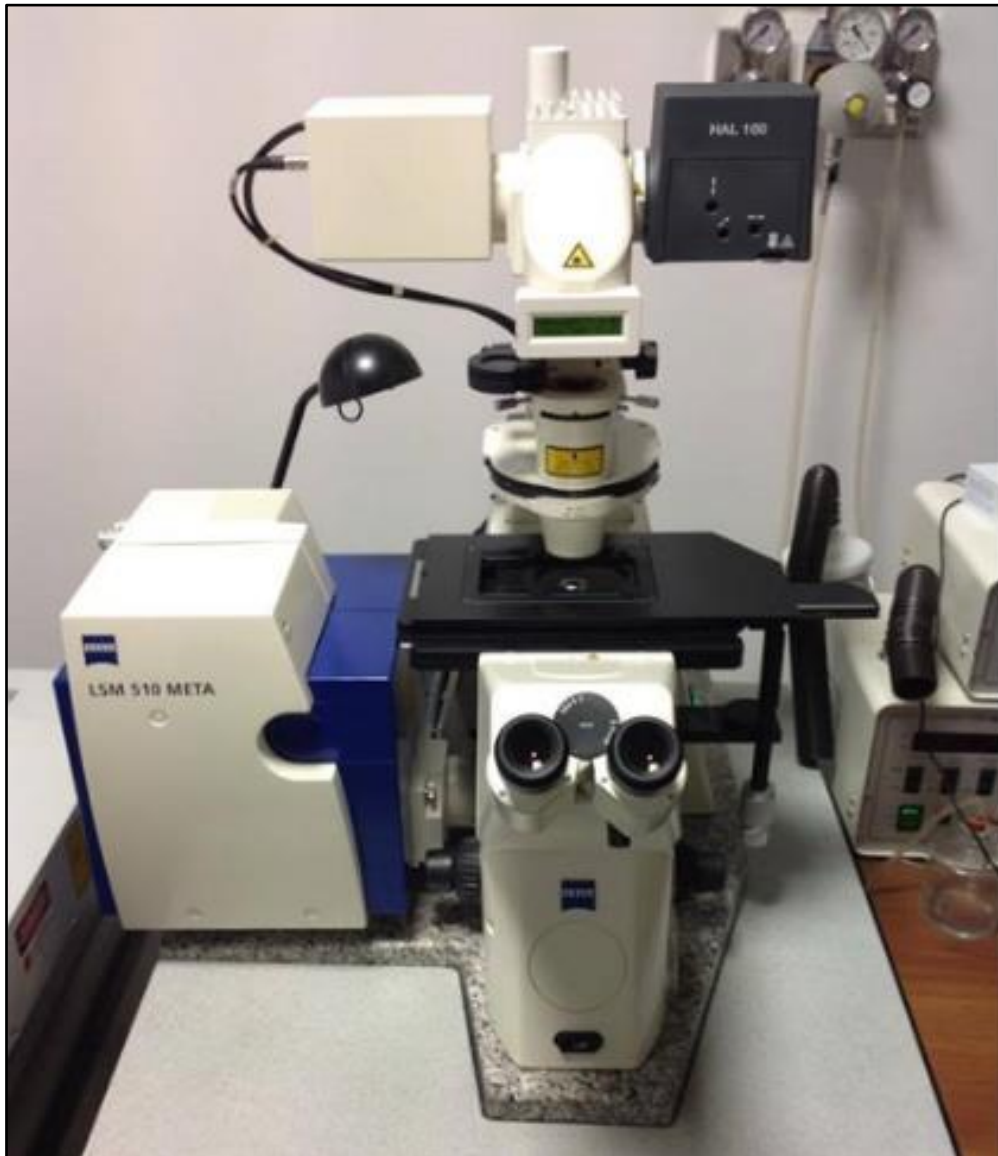


Fig. 1.27. Laser Scanning Microscope used for confocal analysis.

1.3.3. Results

1.3.3.1. Pushout tests

Table 1.3 shows the mean bonding strength evaluated through pushout tests. Data for coronal and apical sections are reported both separately and averaged. Results clearly show a statistically significant enhancement, around three times ($\sim +200\%$ with a $p < 0,05$) compared to control, of the bonding strength along the whole axial length of the root canal when plasma is applied on dentine before the direct application of guttapercha. Relevant increase of adhesion performances, around $+50\%$ ($p < 0,05$) is observed also in G4 both in coronal and apical sections, where sealer was used as in conventional treatment. The comparison of G2 and G3 groups, presenting similar values of average

bonding strength, highlights how a plasma treatment of the dentine could replace the application of endodontic sealer because the values of achieved bonding strength are similar to each other.

	Average bonding strength [MPa]	Increase [+%]
G1 – Coronal	1,05 ± 0,36	+ 238,1%
G2 (plasma) – Coronal	3,56 ± 1,04	
G1 – Apical	1,25 ± 0,40	+ 194,1%
G2 (plasma) – Apical	3,69 ± 1,21	
G3 – Coronal	3,10 ± 0,61	+ 58,6%
G4 (plasma) – Coronal	4,92 ± 0,85	
G3 – Apical	3,49 ± 0,78	+ 47,6%
G4 (plasma) – Apical	5,15 ± 0,71	

Tab. 1.3. Mean bonding strength ± standard deviation of sealing system (guttapercha or sealer+guttapercha) to dentine evaluated through pushout test. Last column reports the average % improvement in bonding strength due to plasma application with respect to untreated control.

1.3.3.2. CLSM analysis

In Fig. 1.28 the confocal acquisitions are reported for the case G1, G2, G3 and G4. Comparing the control groups G1 and G3, a higher penetration is observed in the case in which guttapercha was directly posed in contact with the dentine substrate without any differences between coronal and apical regions. For both cases (G2 and G4), characterized by a CAP pre-treatment of dentine, the penetration of guttapercha (G2) and of endodontic sealer (G4) is extremely amplified for the whole length of the root canal.

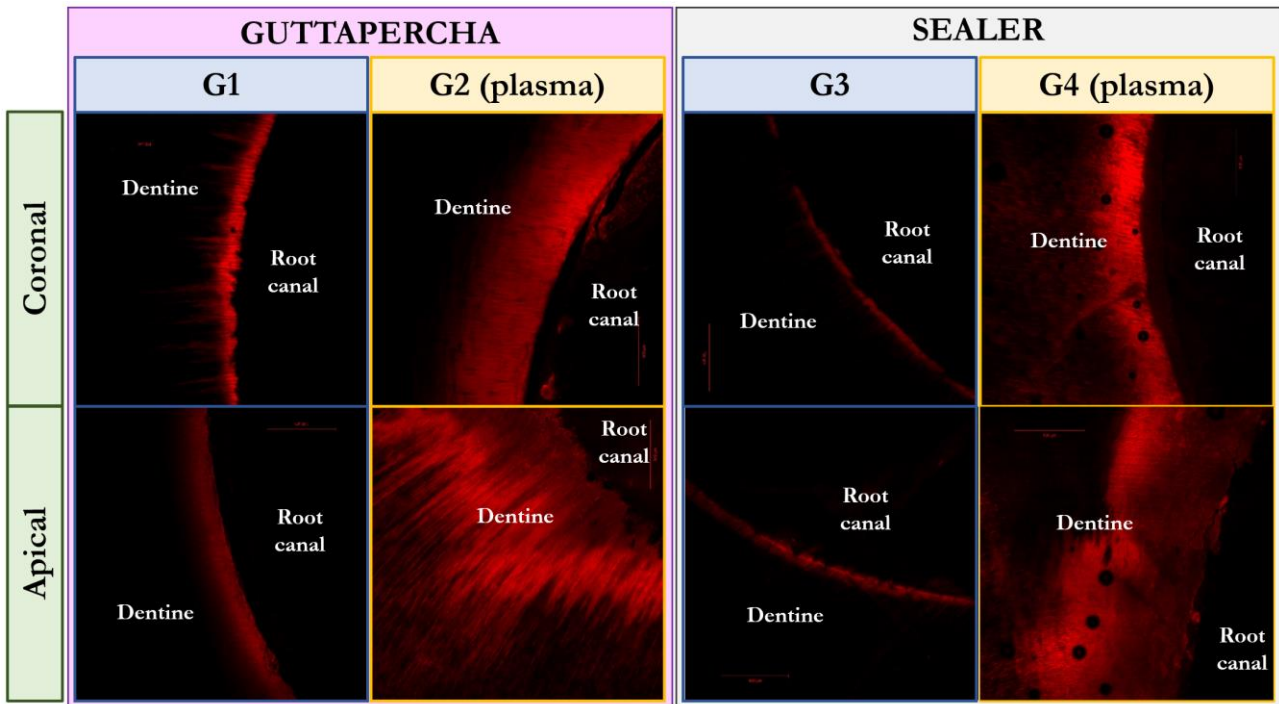


Fig. 1.28. Collection of CLSM images divided for each investigated group and for different sections of root canal.

1.3.4. Discussion of results

3D-obturation of the apical system has been recognized as the most critical phase of endodontic treatment with the final aim of sealing and avoiding any residual holes into the filled canal space [94,95]. The ideal 3D-filling of the apical region would form a monoblock, in which the root canal becomes a perfectly sealed, stable, solid mass with no gaps [93]. Adhesion between filling materials, such as guttapercha, and root dentine is desirable to stabilize the apical seal without any dislodgement of the sealing block. Since guttapercha does not adhere spontaneously onto the dentinal walls due to its chemical properties and solid-viscous state, filling material system often consists of guttapercha associated with a root canal sealer. The sealer serves as a lubricant when inserting the guttapercha point, as a filling material to fill the irregularities of the preparation, and as adhesive system between dentine and guttapercha [96,156,157].

Adhesion depends on the surface energy of the adhesive materials (dentine or guttapercha), the surface tension of the adhesive (sealer), the adhesive's quality to be spread over the surfaces [158]. Moreover, an effective bonding, based both on chemical and micromechanical mechanisms [158], requires a dentinal surface that is free of debris and pulp residues from an imperfect mechanical and chemical treatment of the canal [93].

The control groups (G1 and G3) report pushout values in accordance with literature, highlighting the low bonding strength of guttapercha with the dentine substrate [156,157], while the application of an

endodontic sealer before guttapercha filling leads to values of mean adhesion strength around 3 MPa, as also found by Lee et al. [96]. The adhesion of endodontic sealers is lower (< 6 MPa) [93,96,97] than the adhesion strength offered by the adhesive resins used in coronal dentine bonding (ca. 20–25 MPa) (as in the previously results reported paragraph 4.1 [146] and in [96]).

Pushout results clearly show a relevant enhancement of the mean bonding strength between the plasma treated dentine and the filling materials used in these experiments, guttapercha or endodontic sealer as well. G4, that represents the conventional apical sealing procedure supported by a plasma pre-treatment of dentine surface, shows an improvement around +50% underlining an enhanced interaction of endodontic sealer with the dentinal substrate. The sealer used in these experiments was the Topseal (Dentsply Maillefer), an epoxy resin sealer also marketed as AH Plus, and it interacts with the (bio-)substrates through an epoxide amine chemistry. Epoxy-resin based sealers have also been used for many years with clinical success [96]. Topseal consists of a paste–paste system: an epoxide paste containing radiopaque fillers and aerosol, and an amine paste composed by three different types of amines [159]. Advantageous features of Topseal are recognized to be its good mechanical properties, high radiopacity, low solubility, little shrinkage and good tissue compatibility, low discolouration and low release of formaldehyde [159], eugenol-free which inhibits the polymerization of resins [93]. These advantages are mainly supported by its resin nature, flow and long setting time [160,161], which promote a greater intertwining of the sealer with dentine structure [161].

A substrate exposed to a CAP produced in air (or generally O₂/N₂ mixture gases) is functionalized and grafted by the insertion of carbonyl and amine functional groups, resulting in an increased amount of O and N content in the surface [55,99,128,162], generally leading to an increase of surface wettability. The epoxy resin-based sealer should be able to react with any exposed amino groups in collagen to form covalent bonds with dentine collagen when the epoxide ring opens [96]. Moreover, as Topseal operates in fluid state characterized by a polar component (amine paste), it could be spread better in a plasma-activated surface with higher hydrophilicity resulting in deeper resin infiltration into the demineralized dentine and, thus, in a thicker hybrid layer [93].

Although CLSM acquisitions are focused on the infiltration of filling material essentially in dentinal tubules, they support anyway the hypothesis of an enhanced penetration of sealer into dentine substrate along the whole length of root canal. It is worth mentioning that the formation of resin tags in lateral tubules contributes only for a percentage <15% to the total adhesion strength [93,163,164], while hybridization is considered the primary process involved in ceramic-base restoration [93].

Surprisingly, the adhesion performances of group G2 show an unexpected increase (+238%, $p < 0,05$), revealing how guttapercha was able to “self-bond” directly with the dentine substrate without any sealer application.

As synthetically reported in paragraph 1.3.1, pure guttapercha is a material rigid at ordinary temperatures, becomes pliable at 25° to 30°C, softens at 60°C, and melts at 100°C with partial decomposition. The common guttapercha points used in endodontic clinics are composed by an organic component (guttapercha; wax and/or resin) and an inorganic component (zinc oxide, metal sulfates), in proportion 1:1 regardless of the brand [165]. The filling procedure is designed to plastically deform the guttapercha and fill the irregularities and crevices of the root canal [165]. Thus, this material does not present any chemical characteristic that can promote an adhesive restoration. In light of these considerations, the pushout results appear even more interesting. The idea is that the enhanced wettability of dentine surface can support the spreading of guttapercha in viscous state during the filling procedure. Compared to the resin tags formed by sealers or adhesive systems, which are characterized by high rigidity, guttapercha tags could probably play a major role of anchor of the sealed block to the dentine thanks to their higher flexibility. As a matter of fact, CLSM images show the higher penetration of guttapercha in lateral tubules both in coronal and apical region, and pushout results of G2 group highlight that the achieved adhesion performances are comparable to ones obtained with the application of endodontic sealer before guttapercha filling. 180 sec of CAP treatment increase the adhesion by an enhanced mechanical anchorage of guttapercha into dentine substrate, as well as endodontic sealer can favour the formation of hybrid layer promoting, chemically and micromechanically, the adhesion of a monoblock to dentine. However, the highest value of adhesion of sealed monoblock and dentine is achieved performing the conventional procedure (sealer + guttapercha) with a CAP pre-treatment of the disinfected root canal (G4).

It is worth mentioning that the primary function of the guttapercha is to seal the apical region avoiding gaps, which can provide pathways for bacteria and toxins to the periapex and apical connective tissues, and not to promote a stable adhesion with apical surfaces [166]. Although endodontic sealers enhance the sealing ability of guttapercha and allows the adhesion of the monoblock to root canal [167], ensuring a perfect sealing of apical region is still a challenging task, as shown in Fig. 1.29 and Fig. 1.30 [95].

Even if CLSM acquisitions cannot confirm the absence of gaps in the whole coronal-apical perimeter, confocal images of group G2 and G4 clearly show a higher infiltration and spreading of both materials (sealer and guttapercha) into dentine substrate because of plasma treatment, that may result in an enhancement of apical sealing.

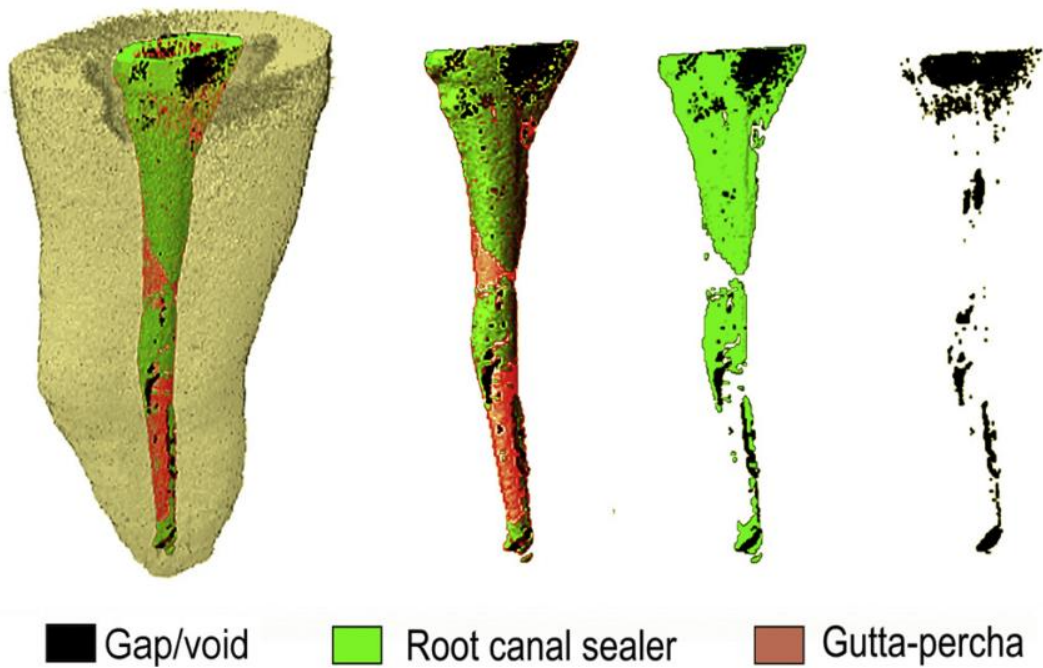


Fig. 1.29. 3-D visualisations of root canals that were obturated using the sealer and guttapercha.

Based on grey scale thresholds, virtual-coloured images were generated showing the different components of the root filling and interfacial gaps and voids within the root (far left), without the root dentine (left), without the root dentine and gutta-percha (right), and depiction of the interfacial gaps and voids alone (far right) [95].

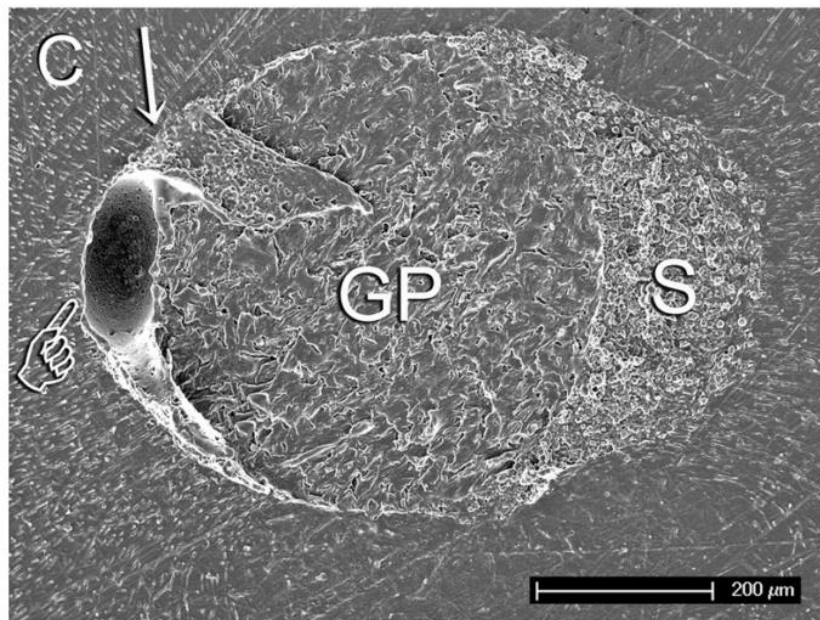


Fig. 1.30. SEM image of an axial surface taken from the 8-mm level of a obturated canal obturated with guttapercha (GP) and sealer (S), showing an interfacial gap (arrow) that is continuous with an interfacial void (pointer) [95].

Moreover, the results of G2 group gain interest and importance in the context of biological safety. Though resin-based sealers are increasingly gaining popularity, their toxicity and mutagenicity are well documented [168–171] and may become hazardous for patient in the case of possible extrusion of sealers into the periapical region during treatment [168,172]. Although Topseal is recognized to be one of the most biocompatible sealers on the market, it was demonstrated that its cytotoxicity can be related to the contained small amount of formaldehyde and to the release of the amine and epoxy resin components from this material [171]. Generally, the biological risk of using an endodontic sealer is critically dependent on both the cytotoxicity of the material and the practitioner's ability to seal the root canal [168]. CAP can reduce the cytotoxic risk favouring an apical 3D obturation performed with the use of only guttapercha characterized by adhesion and sealing performances comparable to the ones achieved in conventional procedures.

In order to assess the potentialities of a CAP treatment in the restoration of root canals, future studies, focused on the ageing effect, are required to investigate the long-term stability of adherent monoblock to dentine surface and to evaluate the sealing performances by means of dye filtration tests or total-canal scanning imaging.

1.4. Conclusions

Great effort has been given by the scientific research community aiming at providing evidences of efficacy and advantages of CAP technology in the field of dentistry, even though plasma technologies are yet far from a real exploitation in actual dental procedures. With the aim of defining procedures useful for future clinical practices in the use of cold atmospheric plasma for the treatment of tooth root canal, a thorough investigation of different plasma based procedures assisted by a handheld Plasma Gun source, whose geometry and characteristics would allow its insertion in the mouth of a patient, was carried out.

Firstly, the efficacy of Plasma Gun treatment was evaluated in the disinfection of contaminated root canals. *Enterococcus faecalis* was selected as bacterial strain for the experimental decontamination treatments due to its relevance in endodontic infections. The antibacterial potentialities of the plasma source were investigated on contaminated TSA plates and quantitatively evaluated on bacterial suspensions, in order to take into account the role of a liquid medium during the Plasma Gun treatment. Then, two different plasma assisted decontamination strategies (direct and indirect CAP treatment) were assessed on realistic tooth models; furthermore, since the root canal during the endodontic procedure can be dry, wet or partially wet depending on the phase of the clinical practice as well as on the conventional procedures of the dentist, Plasma Gun treatments were performed both in wet and dry environments, prepared following two different contamination and treatment protocols. Finally, in order to evaluate the plasma gun treatment in real clinical condition, the obtained results were compared with NaClO and CHX treatments as positive controls. The direct treatment of root canals in dry environment was shown to cause the highest level of bacterial inactivation, but a relevant bacterial load reduction ($\text{LogR} > 2$) was obtained also when the root canal system was irrigated with PAW. Moving towards a more realistic condition, the Plasma Gun was used to treat extracted teeth contaminated with a 24h *E. faecalis* biofilm and the antibacterial efficacy of the plasma treatment in dry environment was evaluated by means of CLSM analysis. CAP preserved its bactericidal properties for the whole length of root canal, even though the positive control, performed with NaClO solution, achieved better results against biofilm. However, these results suggest the possibility of combining direct and indirect CAP treatments in an innovative multi-phase endodontic procedure in synergy with CAP treatments with increased overall antibacterial efficacy. The presented experimental activity resulted in the publication of a paper “*Preliminary investigation of the antibacterial efficacy of a handheld Plasma Gun source for endodontic procedures*” in Clinical Plasma Medicine international journal [177].

Regarding the restoration phase of an endodontic treatment, the feasibility of adopting CAP technology to increase adhesive performances of filling materials, resulting in a reduction of dental

restorations failures, has been demonstrated. Acquired data, on *ex-vivo* teeth, show how the simple addition of a 180s plasma treatment to the conventional procedures can lead to a statistically relevant enhancement of the mean bonding strength along the entire root canal length. Moreover, considering the results obtained in a previous study [146], the effects of Plasma Gun treatment were observed for both kinds of materials (self-etch adhesive systems and sealer+guttapercha) used respectively in the coronal and apical regions of the root canal. In particular, the study highlighted the possibility to avoid the use of cytotoxic endodontic sealers in the apical sealing in terms of adhesion performances between the guttapercha and the plasma treated dentine. Confocal images confirmed the higher spreading and penetration of both guttapercha and sealer into dentinal tubules. Thus, the pushout test results support the applicability of a Plasma Gun treatment for the activation of dentine surfaces before filling procedures, gaining positive effects in the entire restoration of root canal system.

The experimental results, obtained during these years, demonstrated the efficacy of plasma treatment, with a Plasma Gun source operating in the same conditions for both disinfection and restoration of the root canal. Concluding, even if future clinical *in vivo* studies are still required the potential for a future success of a CAP-assisted endodontic procedure appears day by day more certain.

1.5. Bibliography

- [1] World Health Organisation. Oral health. vol. N°318. 2012.
- [2] Reena P. The State of Oral Health in Europe. 2012.
- [3] Erik Petersen P. Priorities for research for oral health in the 21 st Century – the approach of the WHO Global Oral Health Programme. *Community Dent Health* 2005;22:71–4.
- [4] Wilson N. Priorities for oral and dental research. *Indian J Dent Res* 2016;27:227.
- [5] Palincsar AS. Guest Editorial. *Sci Child* 2013;2:10–5.
- [6] Kim GC, Lee HW, Byun JH, Chung J, Jeon YC, Lee JK. Dental applications of low-temperature nonthermal plasmas. *Plasma Process Polym* 2013;10:199–206.
- [7] Khalili J. Periodontal disease: an overview for medical practitioners. *Likars'ka Sprav* 2008:10–21.
- [8] Arora V. Cold Atmospheric Plasma (CAP) In Dentistry. *Dentistry* 2014;4:189.
- [9] Tenuta LMA, Zamataro CB, Del Bel Cury AA, Tabchoury CPM, Cury JA. Mechanism of fluoride dentifrice effect on enamel demineralization. *Caries Res* 2009;43:278–85.
- [10] Watson T, Fox CH, Rekow ED. Priorities for future innovation, research, and advocacy in dental restorative materials. *Adv Dent Res* 2013;25:46–8.
- [11] Liu Y, Liu Q, Yu QS, Wang Y. Nonthermal Atmospheric Plasmas in Dental Restoration. *J Dent Res* 2016.
- [12] Sladek REJ, Stoffels E, Walraven R, Tielbeek PJ a., Koolhoven R a. Plasma treatment of dental cavities: a feasibility study. *IEEE Trans Plasma Sci* 2004;32:2002–5.
- [13] Fridman G, Peddinghaus M, Ayan H, Fridman A, Balasubramanian M, Gutsol A, et al. Blood coagulation and living tissue sterilization by floating-electrode dielectric barrier discharge in air. *Plasma Chem Plasma Process* 2006;26:425–42.
- [14] Liu D, Xiong Z, Du T, Zhou X, Cao Y, Lu X. Bacterial-killing effect of atmospheric pressure non-equilibrium plasma jet and oral mucosa response. *J Huazhong Univ Sci Technol [Medical Sci]* 2011;31:852–6.
- [15] Molnar I, Papp J, Simon A, Anghel SD. Deactivation of *Streptococcus mutans* Biofilms on a Tooth Surface Using He Dielectric Barrier Discharge at Atmospheric Pressure. *Plasma Sci Technol* 2013;15:535–41.
- [16] Lunov O, Churpita O, Zablotskii V, Deyneka IG, Meshkovskii IK, Jäger A, et al. Non-thermal plasma kills bacteria: Scanning electron microscopy observations. *Appl Phys Lett* 2015;106:1–6.
- [17] Marsh PD, Head DA, Devine DA. Dental plaque as a biofilm and a microbial community - Implications for treatment. *J Oral Biosci* 2015;57:185–91.
- [18] Whiley RA, Fraser H, Hardie JM, Beighton D. Phenotypic differentiation of *Streptococcus intermedius*, *Streptococcus constellatus*, and *Streptococcus anginosus* strains within the “*Streptococcus milleri* group.” *J Clin Microbiol* 1990;28:1497–501.
- [19] Osman SA, McCabe JF, Walls AWG. Bonding of adhesive resin luting agents to metal and amalgam. *Eur J Prosthodont Restor Dent* 2008;16:171–6.

- [20] Sculley D V., Langley-Evans SC. Salivary antioxidants and periodontal disease status. *Proc Nutr Soc* 2002;61:137–43.
- [21] Riep B, Edesi-Neuß L, Claessen F, Skarabis H, Ehmke B, Flemmig TF, et al. Are putative periodontal pathogens reliable diagnostic markers? *J Clin Microbiol* 2009;47:1705–11.
- [22] Zijngje V, Van Leeuwen MBM, Degener JE, Abbas F, Thurnheer T, Gmür R, et al. Oral biofilm architecture on natural teeth. *PLoS One* 2010;5:1–9.
- [23] Spencer HR, Ike V, Brennan P a. Review: the use of sodium hypochlorite in endodontics--potential complications and their management. *Br Dent J* 2007;202:555–9.
- [24] Rupf S, Lehmann A, Hannig M, Schafer B, Schubert A, Feldmann U, et al. Killing of adherent oral microbes by a non-thermal atmospheric plasma jet. *J Med Microbiol* 2010;59:206–12.
- [25] Stuart CH, Schwartz S a., Beeson TJ, Owatz CB. *Enterococcus faecalis*: Its role in root canal treatment failure and current concepts in retreatment. *J Endod* 2006;32:93–8.
- [26] Huang C, Yu QS, Hsieh FH, Duan YX. Bacterial deactivation using a low temperature argon atmospheric plasma brush with oxygen addition. *Plasma Process Polym* 2007;4:77–87.
- [27] Zhou X, Xiong Z, Cao Y, Lu X, Liu D. The antimicrobial activity of an atmospheric-pressure room-temperature plasma in a simulated root-canal model infected with *enterococcus faecalis*. *IEEE Trans Plasma Sci* 2010;38:3370–4.
- [28] Alkawareek MY, Gorman SP, Graham WG, Gilmore BF. Potential cellular targets and antibacterial efficacy of atmospheric pressure non-thermal plasma. *Int J Antimicrob Agents* 2014;43:154–60.
- [29] Goree J, Liu B, Drake D, Stoffels E. Killing of *S. mutans* bacteria using a plasma needle at atmospheric pressure. *IEEE Trans Plasma Sci* 2006;34:1317–24.
- [30] Kieft IE, Broers JL V, Caubet-Hilloutou V, Slaaf DW, Ramaekers FCS, Stoffels E. Electric discharge plasmas influence attachment of cultured CHO K1 cells. *Bioelectromagnetics* 2004;25:362–8.
- [31] Naitali M, Kamgang-Youbi G, Herry J-M, Bellon-Fontaine M-N, Brisset J-L. Combined Effects of Long-Living Chemical Species during Microbial Inactivation Using Atmospheric Plasma-Treated Water. *Appl Environ Microbiol* 2010;76:7662–4.
- [32] Yamazaki H, Ohshima T, Tsubota Y, Yamaguchi H, Jayawardena JA, Nishimura Y. Microbicidal activities of low frequency atmospheric pressure plasma jets on oral pathogens. *Dent Mater J* 2011;30:384–91.
- [33] Cha S, Park YS. Plasma in dentistry. *Clin Plasma Med* 2014;2:4–10.
- [34] Fricke K, Koban I, Tresp H, Jablonowski L, Schröder K, Kramer A, et al. Atmospheric pressure plasma: A high-performance tool for the efficient removal of biofilms. *PLoS One* 2012;7:1–8.
- [35] Hannig C, Hannig M. The oral cavity - A key system to understand substratum-dependent bioadhesion on solid surfaces in man. *Clin Oral Investig* 2009;13:123–39.
- [36] Paster BJ, Boches SK, Galvin JL, Ericson E, Lau CN, Levanos VA, et al. Bacterial Diversity in Human Subgingival Plaque. *J Bacteriol* 2001;183:3770–3783.
- [37] Größner-Schreiber B, Teichmann J, Hannig M, Dörfer C, Wenderoth DF, Ott SJ. Modified

- implant surfaces show different biofilm compositions under in vivo conditions. *Clin Oral Implants Res* 2009;20:817–26.
- [38] Zitzmann NU, Berglundh T. Definition and prevalence of peri-implant diseases. *J Clin Periodontol* 2008;35:286–91.
- [39] Yang B, Chen J, Yu Q, Li H, Lin M, Mustapha A, et al. Oral bacterial deactivation using a low-temperature atmospheric argon plasma brush. *J Dent* 2011;39:48–56.
- [40] Sladek REJ, Filoche SK, Sissons CH, Stoffels E. Treatment of *Streptococcus mutans* biofilms with a nonthermal atmospheric plasma. *Lett Appl Microbiol* 2007;45:318–23.
- [41] Blumhagen A, Singh P, Mustapha A, Chen M, Wang Y, Yu Q. Plasma deactivation of oral bacteria seeded on hydroxyapatite disks as tooth enamel analogue. *Am J Dent* 2014;27:84–90.
- [42] Koban I, Holtfreter B, Hübner NO, Matthes R, Sietmann R, Kindel E, et al. Antimicrobial efficacy of non-thermal plasma in comparison to chlorhexidine against dental biofilms on titanium discs in vitro - Proof of principle experiment. *J Clin Periodontol* 2011;38:956–65.
- [43] Sundqvist G, Figdor D, Persson S, Sjögren U. Microbiologic analysis of teeth with failed endodontic treatment and the outcome of conservative re-treatment. *Oral Surgery, Oral Med Oral Pathol Oral Radiol Endod* 2017;85:86–93.
- [44] Roach RP, Hatton JF, Gillespie MJ. Prevention of the Ingress of a Known Virulent Bacterium into the Root Canal System by Intracanal Medications. *J Endod* 2017;27:657–60.
- [45] Cho B-H, Han G-J, Oh K-H, Chung S-N, Chun B-H. The effect of plasma polymer coating using atmospheric-pressure glow discharge on the shear bond strength of composite resin to ceramic. *J Mater Sci* 2011;46:2755–63.
- [46] Wang R, Zhou H, Sun P, Wu H, Pan J. The Effect of an Atmospheric Pressure , DC Nonthermal Plasma Microjet on Tooth Root Canal , Dentinal Tubules Infection and Reinfection Prevention. *Plasma Med* 2011;1:143–55.
- [47] Haapasalo M, Ørstavik D. In vitro Infection and of Dentinal Tubules. *J Dent Res* 1987;66:1375–9.
- [48] Wu MK, Dummer PMH, Wesselink PR. Consequences of and strategies to deal with residual post-treatment root canal infection. *Int Endod J* 2006;39:343–56.
- [49] Gendron R, Grenier D, Maheu-Robert LF. The oral cavity as a reservoir of bacterial pathogens for focal infections. *Microbes Infect* 2000;2:897–906.
- [50] Siqueira JF, Rôças IN. Clinical Implications and Microbiology of Bacterial Persistence after Treatment Procedures. *J Endod* 2008;34.
- [51] Colak M, Evcil S, Bayindir YZ, Yigit N. The effectiveness of three instrumentation techniques on the elimination of enterococcus faecalis from a root canal: An in vitro study. *J Contemp Dent Pract* 2005;6:094–106.
- [52] Menezes MM, Valera MC, Jorge AOC, Koga-Ito CY, Camargo CHR, Mancini MNG. In vitro evaluation of the effectiveness of irrigants and intracanal medicaments on microorganisms within root canals. *Int Endod J* 2004;37:311–9.
- [53] Heling, Chandler. Antimicrobial effect of irrigant combinations within dentinal tubules. *Int Endod J* 1998;31:8–14.

- [54] Bergmans L, Moisiadis P, Teughels W, Van Meerbeek B, Quirynen M, Lambrechts P. Bactericidal effect of Nd:YAG laser irradiation on some endodontic pathogens ex vivo. *Int Endod J* 2006;39:547–57.
- [55] Lehmann A, Rueppell A, Schindler A, Zylla IM, Seifert HJ, Nothdurft F, et al. Modification of enamel and dentin surfaces by non-thermal atmospheric plasma. *Plasma Process Polym* 2013;10:262–70.
- [56] Gherardi M, Tonini R, Colombo V. Plasma in Dentistry: Brief History and Current Status. *Trends Biotechnol* 2017;xx:1–3.
- [57] Nakamura VC, Cai S, Candeiro GTM, Ferrari PH, Caldeira CL, Gavini G. Ex vivo evaluation of the effects of several root canal preparation techniques and irrigation regimens on a mixed microbial infection. *Int Endod J* 2013;46:217–24.
- [58] Zehnder M. Root Canal Irrigants. *J Endod* 2006;32:389–98.
- [59] El Karim I, Kennedy J, Hussey D. The antimicrobial effects of root canal irrigation and medication. *Oral Surg Oral Med Oral Pathol Oral Radiol Endod* 2007;103:560–9.
- [60] Bergmans L, Moisiadis P, Van Meerbeek B, Quirynen M, Lambrechts P. Microscopic observation of bacteria: Review highlighting the use of environmental SEM. *Int Endod J* 2005;38:775–88.
- [61] Pan J, Sun K, Liang Y, Sun P, Yang X, Wang J, et al. Cold plasma therapy of a tooth root canal infected with enterococcus faecalis biofilms in vitro. *J Endod* 2013;39:105–10.
- [62] Lu X, Cao Y, Yang P, Xiong Q, Xiong Z, Xian Y, et al. An RC plasma device for sterilization of root canal of teeth. *IEEE Trans Plasma Sci* 2009;37:668–73.
- [63] Jablonowski L, Koban I, Berg MH, Kindel E, Duske K, Schröder K, et al. Elimination of E. faecalis by a new non-thermal atmospheric pressure plasma handheld device for endodontic treatment. a preliminary investigation. *Plasma Process Polym* 2013;10:499–505.
- [64] Chen W, Huang J, Du N, Liu X-D, Wang X-Q, Lv G-H, et al. Treatment of enterococcus faecalis bacteria by a helium atmospheric cold plasma brush with oxygen addition. *J Appl Phys* 2012;112:13304.
- [65] Zhou X, Xiong Z, Cao Y, Lu X, Liu D. The antimicrobial activity of an atmospheric-pressure room-temperature plasma in a simulated root-canal model infected with enterococcus faecalis. *IEEE Trans Plasma Sci* 2010;38:3370–4.
- [66] Cao Y, Yang P, Lu X, Xiong Z, Ye T, Xiong Q, et al. Efficacy of Atmospheric Pressure Plasma as an Antibacterial Agent Against Enterococcus Faecalis in Vitro. *Plasma Sci Technol* 2011;13:93–8.
- [67] Xiong Z, Cao Y, Lu X, Du T. Plasmas in Tooth Root Canal. *Science (80-)* 2011;39:1–2.
- [68] Bussiahn R, Brandenburg R, Gerling T, Kindel E, Lange H, Lembke N, et al. The hairline plasma: An intermittent negative dc-corona discharge at atmospheric pressure for plasma medical applications. *Appl Phys Lett* 2010;96:10–3.
- [69] Petersen PE. Oral health. *J Public Health Dent* 2008;4:677–85.
- [70] Ferracane J, Fisher J, Eiselé JL, Fox CH. Ensuring the Global Availability of High-quality Dental Restorative Materials. *Adv Dent Res* 2013;25:41–5.
- [71] Buonocore M. A Simple Method of Increasing the Adhesion of Acrylic Filling Materials to

Enamel Surfaces. *J D Res* 1955;34:849–53.

- [72] Soderholm K-JM. Dental adhesives how it all started and later evolved. *J Adhes Dent* 2007;9 Suppl 2:227–30.
- [73] Pashley DH, Tay FR, Breschi L, Tjaderhane L, Carvalho RM, Carrilho M, et al. State of the art etch-and-rinse adhesives. *Dent Mater* 2011;27:1–16.
- [74] Van Meerbeek B, Yoshihara K, Yoshida Y, Mine A, De Munck J, Van Landuyt KL. State of the art of self-etch adhesives. *Dent Mater* 2011;27:17–28.
- [75] Drummond JL. Degradation, fatigue, and failure of resin dental composite materials. *J Dent Res* 2008;87:710–9.
- [76] Opdam NJM, Loomans BAC, Roeters FJM, Bronkhorst EM. Five-year clinical performance of posterior resin composite restorations placed by dental students. *J Dent* 2004;32:379–83.
- [77] Endo K, Sano H, Oguchi H. In vivo Degradation of Resin-Dentin Bonds in Humans Over 1 to 3 Years 2000.
- [78] Nicholson JW. Adhesive dental materials and their durability. *Int J Adhes Adhes* 2000;20:11–6.
- [79] Van Landuyt KL, Snauwaert J, De Munck J, Peumans M, Yoshida Y, Poitevin A, et al. Systematic review of the chemical composition of contemporary dental adhesives. *Biomaterials* 2007;28:3757–85.
- [80] Schwartz RS, Fransman R. Adhesive dentistry and endodontics: materials, clinical strategies, and procedures for restoration of access cavities: a review. *J Endod* 2005;31:151–65.
- [81] Goldberg M, Kulkarni AB, Young M, Boskey A. Dentin: structure, composition and mineralization. *Front Biosci (Elite Ed)* 2012;3:711–35.
- [82] Bowes JH, Murray MM. The chemical composition of teeth: The composition of human enamel and dentine. *Biochem J* 1935;29:2721–7.
- [83] Marshall GWJ, Marshall SJ, Kinney JH, Balooch M. The dentin substrate: structure and properties related to bonding. *J Dent* 1997;25:441–58.
- [84] Garberoglio R, Brännström M. Scanning electron microscopic investigation of human dentinal tubules. *Arch Oral Biol* 1976;21:355–62.
- [85] Van Meerbeek B, Inokoshi S, Braem M, Lambrechts P, Vanherle G. Morphological aspects of the resin-dentin interdiffusion zone with different dentin adhesive systems. *J Dent Res* 1992;71:1530–40.
- [86] Oliveira SSA, Pugach MK, Hilton JF, Watanabe LG, Marshall SJ, Marshall GW. The influence of the dentin smear layer on adhesion: A self-etching primer vs. a total-etch system. *Dent Mater* 2003;19:758–67.
- [87] Stansbury JW. Curing dental resins and composites by photopolymerization. *J Esthet Dent* 2000;12:300–8.
- [88] Nakabayashi N, Nakamura M, Yasuda N. Hybrid layer as a dentin-bonding mechanism. *J Esthet Dent* 1963;3:133–8.
- [89] Spencer P, Ye Q, Park J, Topp EM, Misra A, Marangos O, et al. Adhesive/dentin interface: The weak link in the composite restoration. *Ann Biomed Eng* 2010;38:1989–2003.

- [90] Kanca III J. Improving Bond Strength Through Acid Etching of Dentin and Bonding to Wet Dentin Surfaces. *J Am Dent Assoc* 2017;123:35–43.
- [91] Wang Y, Spencer P, Yao X. Micro-Raman imaging analysis of monomer/mineral distribution in intertubular region of adhesive/dentin interfaces. *J Biomed Opt* 2006;11:24005.
- [92] Nakabayashi N, Kojima K, Masuhara E. The promotion of adhesion by the infiltration of monomers into tooth substrates. *J Biomed Mater Res* 1982;16:265–73.
- [93] Schwartz RS. Adhesive Dentistry and Endodontics. Part 2: Bonding in the Root Canal System-The Promise and the Problems: A Review. *J Endod* 2006;32:1125–34.
- [94] Sjögren U, Hägglund B, Sundqvist G, Wing K. Factors affecting the long-term results of endodontic treatment. *J Endod* 1990;16:498–504.
- [95] Li GH, Niu LN, Selem LC, Eid AA, Bergeron BE, Chen JH, et al. Quality of obturation achieved by an endodontic core-carrier system with crosslinked gutta-percha carrier in single-rooted canals. *J Dent* 2014;42:1124–34.
- [96] Lee K-W, Williams M, Camps JJ, Pashley DH. Adhesion of Endodontic Sealers to Dentin and Gutta-Percha. *J Endod* 2002;28:684–8.
- [97] McComb D, Smith DC. Comparison of physical properties of polycarboxylate-based and conventional root canal sealers. *J Endod* 1976;2:228–35.
- [98] Thompson VP, Watson TF, Marshall GW, Blackman BRK, Stansbury JW, Schadler LS, et al. Outside-the-(Cavity-prep)-Box Thinking. *Adv Dent Res* 2013;25:24–32.
- [99] Ritts AC, Li H, Yu Q, Xu C, Yao X, Hong L, et al. Dentin surface treatment using a non-thermal argon plasma brush for interfacial bonding improvement in composite restoration. *Eur J Oral Sci* 2010;118:510–6.
- [100] Zhang Y, Yu Q, Wang Y. Non-thermal atmospheric plasmas in dental restoration: Improved resin adhesive penetration. *J Dent* 2014;42:1033–42.
- [101] Han GJ, Kim JH, Chung SN, Chun BH, Kim CK, Seo DG, et al. Effects of non-thermal atmospheric pressure pulsed plasma on the adhesion and durability of resin composite to dentin. *Eur J Oral Sci* 2014;122:417–23.
- [102] Koban I, Duske K, Jablonowski L, Schröder K, Nebe B, Sietmann R, et al. Atmospheric plasma enhances wettability and osteoblast spreading on dentin in vitro: Proof-of-principle. *Plasma Process Polym* 2011;8:975–82.
- [103] Silva NRFA, Coelho PG, Valverde GB, Becker K, Ihrke R, Quade A, et al. Surface characterization of Ti and Y-TZP following non-thermal plasma exposure. *J Biomed Mater Res - Part B Appl Biomater* 2011;99 B:199–206.
- [104] Valverde GB, Coelho PG, Janal MN, Lorenzoni FC, Carvalho RM, Thompson VP, et al. Surface characterisation and bonding of Y-TZP following non-thermal plasma treatment. *J Dent* 2013;41:51–9.
- [105] Hirata R, Teixeira H, Paula A, Ayres A, Machado LS, Paulo /, et al. Long-term Adhesion Study of Self-Etching Systems to Plasma-Treated Dentin 2015;17.
- [106] Epailard F, Brosse JC, Legeay G. Plasma-induced polymerization. *J Appl Polym Sci* 1989;38:887–98.

- [107] Gong X, Dai L, Mau AWH, Griesser HJ. Plasma-Polymerized Polyaniline Films : Synthesis and Characterization. *J Polym Sci Part A Polym Chem* 1998;36:633–43.
- [108] Çökeliler D, Erkut S, Zemek J, Biederman H, Mutlu M. Modification of glass fibers to improve reinforcement: A plasma polymerization technique. *Dent Mater* 2007;23:335–42.
- [109] Simionescu BC, Leanca M, Ananiescu C, Simionescu CI. Plasma-induced polymerization - 3. Bulk and solution homopolymerization of some vinylic monomers. *Polym Bull* 1980;3:437–40.
- [110] Chen M, Zhang Y, Yao X, Li H, Yu Q, Wang Y. Effect of a non-thermal, atmospheric-pressure, plasma brush on conversion of model self-etch adhesive formulations compared to conventional photo-polymerization. *Dent Mater* 2012;28:1232–9.
- [111] Özkurt Z, Kazazoğlu E. Zirconia Dental Implants: A Literature Review. *J Oral Implantol* 2011;37:367–76.
- [112] Rupp F, Scheideler L, Eichler M, Geis-Gerstorfer J. Wetting behavior of dental implants. *Int J Oral Maxillofac Implant* 2011;26:1256–66.
- [113] Kawai H, Shibata Y, Miyazaki T. Glow discharge plasma pretreatment enhances osteoclast differentiation and survival on titanium plates. *Biomaterials* 2004;25:1805–11.
- [114] Shibata Y, Hosaka M, Kawai H, Miyazaki T. Glow Discharge Plasma Treatment of Titanium Plates Enhances Adhesion of Osteoblast-like Cells to the Plates Through the Integrin-Mediated Mechanism. *Int J Oral Maxillofac Implant* 2002;17:771–7.
- [115] Giro G, Tovar N, Witek L, Marin C, Silva NRF, Bonfante EA, et al. Osseointegration assessment of chairside argon-based nonthermal plasma-treated Ca-P coated dental implants. *J Biomed Mater Res - Part A* 2013;101 A:98–103.
- [116] Duske K, Koban I, Kindel E, Schröder K, Nebe B, Holtfreter B, et al. Atmospheric plasma enhances wettability and cell spreading on dental implant metals. *J Clin Periodontol* 2012;39:400–7.
- [117] Lee J-H, Choi E-H, Kim K-M, Kim K-N. Effect of non-thermal air atmospheric pressure plasma jet treatment on gingival wound healing. *J Phys D Appl Phys* 2016;49:75402.
- [118] Kalghatgi SU, Fridman G, Cooper M, Nagaraj G, Peddinghaus M, Balasubramanian M, et al. Mechanism of blood coagulation by nonthermal atmospheric pressure dielectric barrier discharge plasma. *IEEE Trans Plasma Sci* 2007;35:1559–66.
- [119] Lim MY, Lum SOY, Poh RSC, Lee GP, Lim KC. An in vitro comparison of the bleaching efficacy of 35% carbamide peroxide with established intracoronary bleaching agents. *Int Endod J* 2004;37:483–8.
- [120] Tavares M, Stultz J, Newman M, Smith V, Kent R, Carpino E, et al. Light augments tooth whitening with peroxide. *J Am Dent Assoc* 2003;134:167–75.
- [121] Jones a H, Diaz-Arnold a M, Vargas M a, Cobb DS. Colorimetric assessment of laser and home bleaching techniques. *J Esthet Dent* 1999;11:87–94.
- [122] Lee HW, Kim GJ, Kim JM, Park JK, Lee JK, Kim GC. Tooth Bleaching with Nonthermal Atmospheric Pressure Plasma. *J Endod* 2009;35:587–91.
- [123] Park JK, Nam SH, Kwon HC, Mohamed AAH, Lee JK, Kim GC. Feasibility of nonthermal atmospheric pressure plasma for intracoronary bleaching. *Int Endod J* 2011;44:170–5.

- [124] Lee HW, Nam SH, Mohamed AAH, Kim GC, Lee JK. Atmospheric pressure plasma jet composed of three electrodes: Application to tooth bleaching. *Plasma Process Polym* 2010;7:274–80.
- [125] Claiborne D, McCombs G, Lemaster M, Akman MA, Laroussi M. Low-temperature atmospheric pressure plasma enhanced tooth whitening: The next-generation technology. *Int J Dent Hyg* 2014;12:108–14.
- [126] Smitha T, Chaitanya Babu N. Plasma in dentistry: an update. *Indian J Dent Adv* 2010;2:1–7.
- [127] Santosh Kumar CH, Sarada P, Sampath Reddy CH, Surendra Reddy M, Nagasailaja DSV. Plasmatorch toothbrush a new insight in fear free dentistry. *J Clin Diagnostic Res* 2014;8:7–10.
- [128] Kim J-H, Lee M-A, Han G-J, Cho B-H. Plasma in dentistry: a review of basic concepts and applications in dentistry. *Acta Odontol Scand* 2014;72:1–12.
- [129] Cha S, Park Y-S. Plasma in dentistry. *Clin Plasma Med* 2014;2:1–7.
- [130] Moreau M, Orange N, Feuilloley MGJ. Non-thermal plasma technologies: New tools for bio-decontamination. *Biotechnol Adv* 2008;26:610–7.
- [131] Weltmann K-D, von Woedtke T. Basic requirements for plasma sources in medicine. *Eur Phys J Appl Phys* 2011;55:13807.
- [132] Martin M. From distant stars to dental chairs-Plasmas May Promise Pain-free and durable Restorations. *AGD Impact* 2009;37:46.
- [133] Fridman G, Brooks AD, Balasubramanian M, Fridman A, Gutsol A, Vasilets VN, et al. Comparison of direct and indirect effects of non-thermal atmospheric-pressure plasma on bacteria. *Plasma Process Polym* 2007;4:370–5.
- [134] Molecular Probes I. LIVE/DEAD® BacLight™ Bacterial Viability Kits. LIVE/DEAD® BacLight™ Bact Viability Kits 2004:1–8.
- [135] Boselli M, Colombo V, Ghedini E, Gherardi M, Laurita R, Liguori a., et al. Schlieren high-speed imaging of a nanosecond pulsed atmospheric pressure non-equilibrium plasma jet. *Plasma Chem Plasma Process* 2014;34:853–69.
- [136] Boselli M, Colombo V, Gherardi M, Laurita R, Liguori A, Sanibondi P, et al. Characterization of a Cold Atmospheric Pressure Plasma Jet Device Driven by Nanosecond Voltage Pulses 2014:1–13.
- [137] Norberg S a, Johnsen E, Kushner MJ. Formation of reactive oxygen and nitrogen species by repetitive negatively pulsed helium atmospheric pressure plasma jets propagating into humid air. *Plasma Sources Sci Technol* 2015;24:35026.
- [138] Boxhammer V, Morfill GE, Jokipii JR, Shimizu T, Klämpfl T, Li Y-F, et al. Bactericidal action of cold atmospheric plasma in solution. *New J Phys* 2012;14:113042.
- [139] Lukes P, Dolezalova E, Sisrova I, Clupek M. Aqueous-phase chemistry and bactericidal effects from an air discharge plasma in contact with water: evidence for the formation of peroxyxynitrite through a pseudo-second-order post-discharge reaction of H₂O₂ and HNO₂. *Plasma Sources Sci Technol* 2014;23:15019.
- [140] Lukeš P. Water treatment by pulsed streamer corona discharge. *Environmental Technology*, 2001.

- [141] Kamgang-Youbi G, Herry JM, Meylheuc T, Brisset JL, Bellon-Fontaine MN, Doubla a., et al. Microbial inactivation using plasma-activated water obtained by gliding electric discharges. *Lett Appl Microbiol* 2009;48:13–8.
- [142] Norberg S a, Tian W, Johnsen E, Kushner MJ. Atmospheric pressure plasma jets interacting with liquid covered tissue: touching and not-touching the liquid. *J Phys D Appl Phys* 2014;47:475203.
- [143] Wakabayashi H, Masumoto K, Tachibana H, Tuzuki N. A new instrument for drying root canals. *Int Endod J* 1987;20:298–9.
- [144] Perni S, Shama G. Probing bactericidal mechanisms induced by cold atmospheric plasmas with *Escherichia coli* mutants.pdf. *Appl Phys Lett* 2007;90:1–12.
- [145] Dobrynin D, Fridman G, Friedman G, Fridman A. Physical and biological mechanisms of direct plasma interaction with living tissue. *New J Phys* 2009;11.
- [146] Stancampiano A. Design and diagnostic of non-equilibrium atmospheric plasma sources for cell treatment and bacterial decontamination. *Alma Mater Studiorum - University of Bologna*, 2016.
- [147] Schilder H, Goodman A, Aldrich W. The thermomechanical properties of gutta-percha. Part V. Volume changes in bulk gutta-percha as a function of temperature and its relationship to molecular phase transformation. *Oral Surg Oral Med Oral Pathol* 1985;59:285–96.
- [148] Goodman A, Schilder H, Aldrich W. The thermomechanical properties of gutta-percha. Part IV. A thermal profile of the warm gutta-percha packing procedure. *Oral Surg Oral Med Oral Pathol* 1981;51:544–51.
- [149] Schilder H, Goodman A, Aldrich W. The thermomechanical properties of gutta-percha. 3. Determination of phase transition temperatures for gutta-percha. *Oral Surg Oral Med Oral Pathol* 1974;38:109–14.
- [150] Goodman A, Schilder H, Aldrich W. The thermomechanical properties of gutta-percha. II. The history and molecular chemistry of gutta-percha. *Oral Surg Oral Med Oral Pathol* 1974;37:954–61.
- [151] Schilder H, Goodman A, Aldrich W. The thermomechanical properties of gutta-percha. I. The compressibility of gutta-percha. *Oral Surg Oral Med Oral Pathol* 1974;37:946–53.
- [152] Ruddle CJ. Filling root canal systems the calamus 3D obturation technique. *Adv Endod* 2010:1–7.
- [153] Boschian Pest L, Cavalli G, Bertani P, Gagliani M. Adhesive post-endodontic restorations with fiber posts: Push-out tests and SEM observations. *Dent Mater* 2002;18:596–602.
- [154] Haller B, Thull R, Klaiber B TM. An extrusion test for determination of bond strength to dentin. *J Dent Res* 1991.
- [155] Cheylan J, Eid N, Degrange M. Adherence of different luting agents using a push-out method. *Proc. 35th Annu. IADR/CED Meet.*, 1999.
- [156] Pommel L, About I, Pashley D, Camps J. Apical Leakage of Four Endodontic Sealers. *J Endod* 2003;29:208–10.
- [157] Hata G ichiro, Kawazoe S, Toda T, Weine FS. Sealing ability of Thermafil with and without sealer. *J Endod* 1992;18:322–6.

- [158] Saleh IM, Ruyter IE, Haapasalo M, Ørstavik D. The effects of dentine pretreatment on the adhesion of root-canal sealers. *Int Endod J* 2002;35:859–66.
- [159] Gopikrishna Dr. V, Parameswaren A. Coronal sealing ability of three sectional obturation techniques - Simplifill, thermafil and warm vertical compaction - Compared with cold lateral condensation and post space preparation. *Aust Endod J* 2006;32:95–100.
- [160] Almeida JFA, Gomes BPF, Ferraz CCR, Souza-Filho FJ, Zaia AA. Filling of artificial lateral canals and microleakage and flow of five endodontic sealers. *Int Endod J* 2007;40:692–9.
- [161] Teixeira CS, Alfredo E, Thomé LHDC, Gariba-Silva R, Silva-Sousa YTC, Sousa-Neto MD. Adhesion of an endodontic sealer to dentin and gutta-percha: shear and push-out bond strength measurements and SEM analysis. *J Appl Oral Sci* 2009;17:129–35.
- [162] Grace JM, Gerenser LJ. Plasma Treatment of Polymers. *J Dispers Sci Technol* 2003;24:305–41.
- [163] Tagami J, Tao L, Pashley DH. Correlation among dentin depth, permeability, and bond strength of adhesive resins. *Dent Mater* 2017;6:45–50.
- [164] Pereira PN, Okuda M, Sano H, Yoshikawa T, Burrow MF, Tagami J. Effect of intrinsic wetness and regional difference on dentin bond strength. *Dent Mater* 1999;15:46–53.
- [165] Friedman CE, Sandrik JL, Heuer MA, Rapp GW. Composition and physical properties of gutta-percha endodontic filling materials. *J Endod* 1997;3:304–8.
- [166] Geurtsen W, Leyhausen G. Biological aspects of root canal filling materials--histocompatibility, cytotoxicity, and mutagenicity. *Clin Oral Investig* 1997;1:5–11.
- [167] Skinner RL, Himel VT. The sealing ability of injection-molded thermoplasticized gutta-percha with and without the use of sealers. *J Endod* 1987;13:315–7.
- [168] Bouillaguet S, Wataha JC, Lockwood PE, Galgano C, Golay A, Krejci I. Cytotoxicity and sealing properties of four classes of endodontic sealers evaluated by succinic dehydrogenase activity and confocal laser scanning microscopy. *Eur J Oral Sci* 2004;112:182–7.
- [169] Bratel J, Jontell M, Dahlgren U, Bergenholtz G. Effects of root canal sealers on immunocompetent cells in vitro and in vivo. *Int Endod J* 1998;31:178–88.
- [170] Eldeniz AU, Mustafa K, Ørstavik D, Dahl JE. Cytotoxicity of new resin-, calcium hydroxide- and silicone-based root canal sealers on fibroblasts derived from human gingiva and L929 cell lines. *Int Endod J* 2007;40:329–37.
- [171] da Silva PT, Pappen FG, Souza EM, Dias JE, Bonetti Filho I, Carlos IZ, et al. Cytotoxicity evaluation of four endodontic sealers. *Braz Dent J* 2008;19:228–31.
- [172] Bernáth M, Szabó J. Tissue reaction initiated by different sealers. *Int Endod J* 2003;36:256–61.

2. Plasma Gun for cancer applications

2.1. Overview of literature and of experimental activities

2.1.1. Cancer therapy: induction of apoptosis

In the last decade the use of CAP on tumour cells has been gaining great interest in the research field of plasma medicine. More and more promising results, achieved worldwide by many different research groups, have been promoting CAPs as new therapy opportunity in the treatment of cancer. It was demonstrated, mainly *in vitro* but also in few preliminary *in vivo* studies, that CAP treatments are able to arrest the tumour cells growth inducing apoptosis, with higher effectiveness in respect to some standard treatments including radiation and chemotherapy [1]. Apoptosis causes minimal inflammation and damage to the healthy tissue, and thus apoptotic induction-based therapy has been the centre of attraction for the research of innovative anticancer drugs. Moreover, first results showed high CAP selectivity for cancer cells comparing to the non-malignant cells [1–3]. Since this chapter is focused on the Plasma Gun ability to selectively kill tumor cells inducing apoptotic pathways, a brief explanation on the fundamental biochemical mechanisms involved in cellular apoptosis is here reported.

Apoptosis is an important cellular process that allows cells to die in a programmed fashion; in particular this cell death mechanism plays an important role in removing faulty cells [4].

Apoptosis is extended over 3 steps: initiation, execution and phagocytosis. In apoptosis, the cell is broken down from within by proteins called caspases [5–7]. For apoptosis to occur, these caspases first need to be activated. Caspase activation can happen via two distinct pathways, called extrinsic and intrinsic pathways [8,9].

The extrinsic pathway is initiated by signals coming from outside the cells. This pathway is often triggered by other cells, commonly by means of surface ligand molecules, which are secreted by many cells, like T lymphocytes. These lymphocytes are characterized by a FAS ligand (or Fas-L) in the cellular membrane. The extrinsic pathway is initiated when Fas-L binds to Fas-receptor on the surface of the targeted cell. This sets off a chain of intracellular events that will ultimately result in apoptosis. The sequence is mediated by a FAS Associated Death Domain or FADD [8–11]. Similarly, TNF α (another ligand molecule of lymphocytes) can bind to the TNF α -receptor in the outer membrane of the cell. Sequentially the TNF-receptor associated protein with death domain (TRADD) at the cytoplasmic side of the receptor is activated. Activated FADD or TRADD can recruit pro caspase-8 [8–11]. This protease is able to auto-catalyse the hydrolysis of its inhibiting segments, leading to active caspase-8, which disassociates from the receptor. Caspases activate each other in a self-amplifying process called caspase cascade [5–7]. Apoptosis is then initiated as the active caspases begin the breakdown of cellular materials.

On the other hand, the intrinsic pathway is initiated by signals from within the cell. This intrinsic pathway is regulated by maintaining a balance between two sets of proteins in the mitochondrial membrane, belonging to the Bcl-2 family: anti-apoptotic proteins, such as BCL-2 and BCL-X, and pro-apoptotic proteins, such as BAX and BAK [10,11]. In a healthy cell, the anti-apoptotic proteins bind the pro-apoptotic ones, thereby blocking their action. The most frequent signals that activate intrinsic initiation are irreparable and irreversible DNA lesions. These lesions lead to the activation of ATM, a protein that is able to activate the tumor suppressor protein p53. In addition to many other proteins, p53 is able to activate the protein BAX and BAK [12]. Moreover, if a cell is damaged, or if it stops receiving survival signals, BCL-2 and BCL-X can be blocked in turn. Switching the mitochondrial protein balance toward pro-apoptotic conditions, BAX and BAK form pores in the outer membrane of mitochondria: Ca^{2+} ions, protons and other molecules, which are located in the inner membrane region, may leak into the cytosol. One of these molecules is the protein cytochrome C. Cytochrome C binds to APAF (Apoptotic Protease Activating Factor) and may then associate with an inactive form of pro caspase-9 [13,14]. As a consequence, the inhibiting domain of the pro caspase is hydrolysed and dissociated from the protease. By this mechanism, caspase-9 becomes active. Active caspase-9 is able to cleave additional caspases and to destroy many other proteins. In this way, caspase-9 initiates the caspase cascade. This cascade denotes a stepwise cascade of proteases that cleave and thus activate each other. The concentration of active proteases in the cell increases rapidly leading to the destruction of many different proteins.

Important steps of the execution phase are the cleavage of DNA and the cleavage of cytoskeleton. In the normal cell, DNAase is linked to an inhibitor and it is inactive. After initiation and activation of caspase cascade, the active caspase-3 is able to cleave this inhibitor. Activated DNAase cleaves DNA. Moreover, caspase-3 was demonstrated to cleave many other proteins such as proteins of the cytoskeleton [14]. Hereby the cell loses its structure. Next, other proteins cause the cell to collapse into vesicles, the so-called apoptotic blebs. The rapid breakup of the cell and of the formed vesicles is thus avoided preventing an inflammatory reaction in the surrounding tissue.

The various processes of execution phase lead to significant modification of the structure and composition of the outer membranes of cells and apoptotic blebs [15]. Based on the modified membrane structure, phagocytes like macrophages can recognize the blebs. In the cytosol of the phagocytosing cell, the blebs fuse with lysosomes. These organelles contain enzymes that finally metabolized the blebs and their components.

An illustration of the main pathway steps involved in cellular apoptosis are reported in Fig. 2.1.

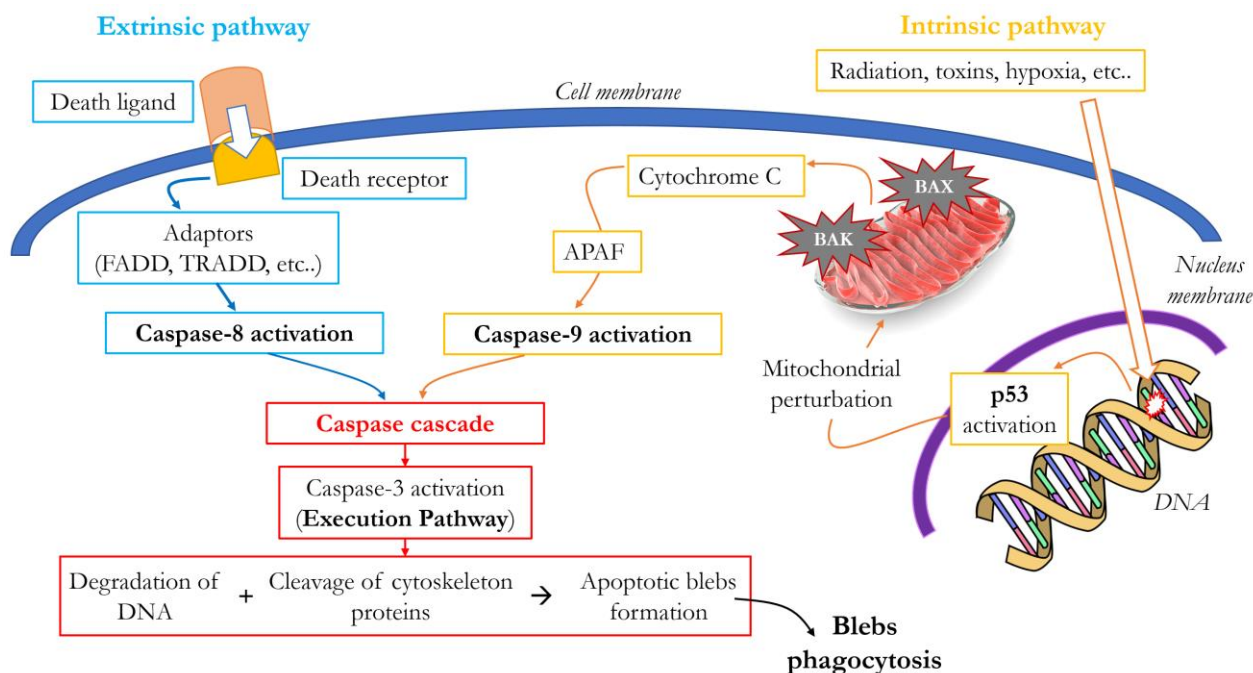


Fig. 2.1. Schematic illustration of cellular apoptosis induced by extrinsic (blue) and intrinsic (orange) pathways.

2.1.2. Plasma & Oncology

The first study aimed at evaluating the CAP potentialities as innovative therapy for the treatment of cancer was conducted by the research group of Eva Stoffles [16]. It was the first time in which a temporary loss of cell adhesion (detachment) and apoptosis were identified as a consequence of CAP treatment. Although at the beginning the experiments were driven by plasma research groups and thus an essential scientific contribution from clinician and biologists lacked, in the last years research groups involved in the field of medicine and biology posed their interest and effort in these studies. This multidisciplinary approach led to prove the efficacy of CAP to induce apoptosis in several cancer cell lines. For example, Schlegel et al. [1] reviewed in 2013 a list of most important experiments *in vitro* and *in vivo* concerning CAP treatment of breast, brain, colon, lung, skin, and pancreas cancers. CAP are able to affect cell growth inhibition [17,18], inhibition of migration and invasion [19], induction of cell cycle arrest [20,21] and induction of apoptosis in a dose-dependent manner [2,22–26]. Recently, the anti-tumoral properties of Plasma Activated Medium (PAM) were investigated and proved [27]. Finally, studies underlined the possibility to combine CAP treatment to the conventional chemotherapies achieving synergistic effects in a combined therapy with gemcitabine chemotherapy *in vivo* for pancreas carcinoma [28] as well as both *in vitro* and *in vivo* murine neuroblastoma [29]. Different mechanisms were investigated to explain CAP and PAM-mediated selective antitumor action. Keidar and Yan supported the idea that aquaporins play the main role leading H₂O₂ to enter into cancer cells and, thus, inducing apoptosis [30,31]. Bauer suggested that the selectivity of CAP

treatment was related to the CAP-derived singlet oxygen, able to inactivate the oxidant defenses in outer membrane of tumor cells [32]. On the other hand, Miller and co-workers suggested a central role of immunological processes for selective CAP-mediated antitumor effects [33–35].

2.1.3. RONS in Plasma Activated Medium (PAM): selectivity and self-perturbation of apoptosis induction

Cancer cells manifest an enhanced intracellular oxidative status in respect to non-malignant cells. It is well documented that ROS and oxidant stress may induce cancer and that transformed cells generate more ROS for their growth and their survival; moreover, an increase ROS signaling leads to a stimulation of tumor cell cycle progression by growth factors. Thus, different cancer chemotherapies may be selectively toxic to tumor cells because they are able to induce an increase of oxidant stress, overcoming the oxidative limit for the cellular survival [36,37].

CAP treatment mainly sustains the HOCl and the NO/peroxynitrite signaling pathways that are well known to induce mitochondrial pathway of apoptosis [38–41]. The final products of HOCl and the NO/peroxynitrite signaling pathways are free hydroxyl radicals nearby the tumor cell membrane and thus a lipid peroxidation is caused with a subsequent apoptosis induction [3,42,43]. Intracellularly, an increase of abundant hydrogen peroxide is then provoked overcoming the threshold of intra-oxidative stress and caspase cascade is initialized [44].

Interestingly, cancer cells develop a specific membrane phenotype during their growth from transformed to tumor cell, with the aim to preserve and protect the cell by external oxidant agents [37,45,46]. Thus, in order to be selective for cancer cells, an oncological therapy should be able to recognize the malignant cells, overcome the membrane defenses and induce intracellularly an oxidant stress high enough to promote apoptosis inducing moderate damages to non-malignant cells.

As reported above, scientific literature, young but day by day more and more wide, has been demonstrating the high selectivity of CAP action with the respect of membrane phenotype of cancer cells, and the CAP ability to increase of intracellular RONS resulting into apoptosis in malignant cells [3]. Moreover, self-perpetuating process (by stander effect-like process) of apoptosis induction, also in tumor areas not directly treated by CAP constituents was observed [47–49].

The distinctive elements on the surface of tumor cells for the protection by exogenous nitro/oxidant agents are active NADPH oxidase-1 (NOX1), membrane-associated catalase, mitochondrial enzyme superoxide dismutase (SOD), the FAS receptor (death receptor expressed by FAS gene), proton pumps and aquaporins [50–54,38]. Bauer well resumed the protection system of tumor cells against exogenous RONS, Fig. 2.2.

RONS, among which superoxide anions ($O_2^{\bullet-}$), hydrogen peroxide (H_2O_2), hydroxyl radicals ($\bullet OH$), nitric oxide ($\bullet NO$), nitrogen dioxide ($\bullet NO_2$), peroxy nitrite “PON” ($ONOO^-$), nitrite (NO_2^-), nitrate (NO_3^-), and singlet oxygen (1O_2), are considered the major active components in CAP treatment [55]. Recently, Wende and co-worker showed how O-based reactions can lead to the formation of OCl⁻ and dichloride anion radicals ($Cl_2^{\bullet-}$), that are involved in apoptosis pathway signaling [56]. Both tumor cells and non-malignant cells express DUOX (dual oxidase) that consists of a peroxidase (POD) domain and a NOX-related domain that collaborate in the destruction of exogenous H_2O_2 for the formation of HOCl through the reaction with free chloride anion Cl^- [57].

Although a high membrane catalase activity can ensure an efficient decomposition of H_2O_2 , PON, and NO, the SOD concentration on the outer membrane is too low to dismutate efficiently the cell-derived superoxide anions, resulting in a local concentration nearby cellular membrane of $O_2^{\bullet-}$ [58]. Since H_2O_2 was completely consumed by catalysis, the presence of superoxide anions closed to tumor cells doesn't lead to the production of apoptosis-inducing species [3] and thus the CAP-derived $O_2^{\bullet-}$ are not likely candidates to account for selective apoptosis induction in tumor cells by CAP. Regarding the hydrogen peroxides produced by CAP treatment, they can be efficiently decomposed by tumor cell membrane-associated catalase and, therefore, it is not correct to consider H_2O_2 as a reactive specie able to interact selectively with targeted cells [3], although aquaporins could facilitate the diffusion of H_2O_2 into cells. Moreover, beyond a threshold concentration of H_2O_2 , non-malignant cells, characterized by the absence of membrane-associated catalase, can be expected to undergo apoptosis or necrosis [59].

As far as hydroxyl radical is concerned, OH radical is characterized by a very short diffusion pathway in liquid phase due to its high reactivity. This consideration supports the hypothesis the its extra- and intracellular presence is not directly related to direct OH production during the plasma treatment but as the result of secondary reaction pathways. Furthermore, OH radicals can induce apoptosis or necrosis to tumor cells as well as the non malignant ones, highlighting none selective properties [3]. Although NO radicals are involved in the synthesis of PON and together can react inducing NO/PON-dependent apoptosis, SOD and catalases defenses can efficient block these pathways when CAP-derived NO is present at moderate concentration. No $O_2^{\bullet-}$ is present outside non-malignant cells and extra cellular PON can't be formed, and thus NO can freely enter into cytosol. Within the cell, nitrogen oxide radicals can be counteracted by intracellular glutathione [60]. Except the case of really high concentration of CAP-derive NO that can lead to in the inactivation of catalase, nitrogen oxide can't induce apoptosis in a selective ways [3].

Free exogenous PON strongly induces apoptotic effect on healthy cells after formation of peroxy-nitrous acid and hydroxyl radicals and thus it is not possible to consider this molecule as a CAP selective component [59].

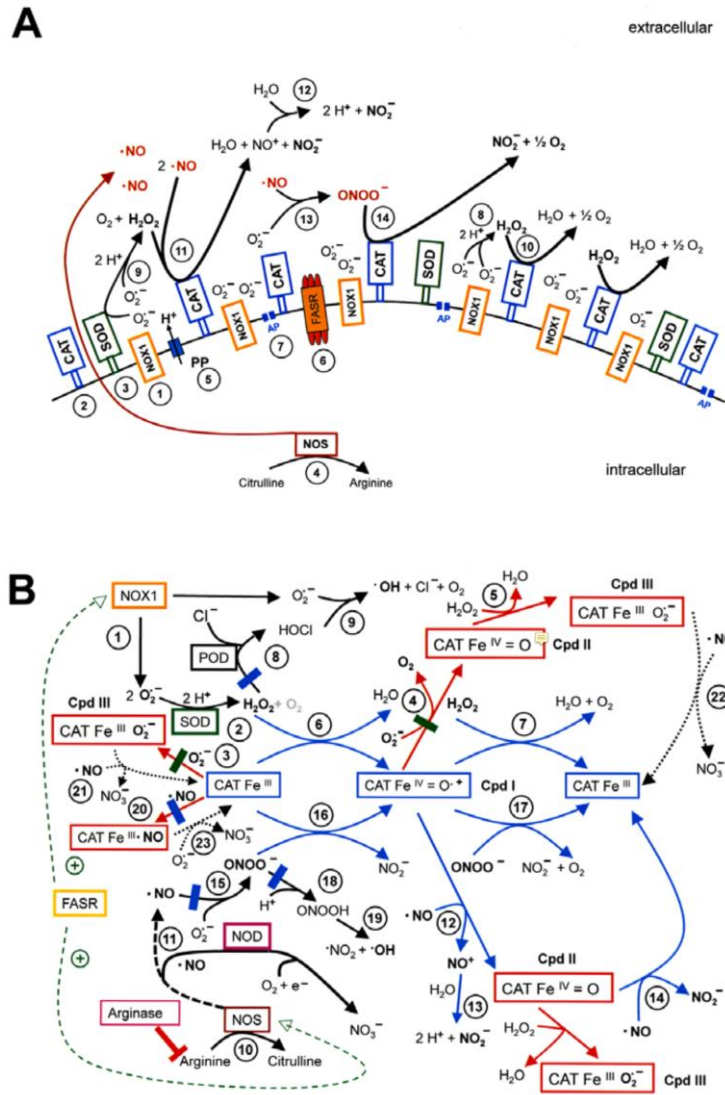


Fig.2.2. Protection of bona fide tumor cells towards intercellular ROS/RNS-mediated apoptosis-inducing signalling [61].

A. Overview. Tumor cells express NOX1 (at a higher level than transformed cells) (#1) and show a locally high concentration of membrane-associated catalase (CAT) (#2), as well as comodulatory SOD (#3). NO is generated by NOS (#4). Proton pumps (PP), the FAS receptor (FASR) and aquaporins (AP) (#5-#7) are additional important constituents in the membrane of tumor cells. H₂O₂ derived from spontaneous (#8) or SOD-catalyzed (#9) dismutation is decomposed by catalase (#10) and thus HOCl synthesis is prevented. The interaction of catalase with H₂O₂ leads to the formation of compound I that oxidizes NO in a two-step reaction (#11), resulting in the generation of NO⁺ and NO₂ (#12). Residual NO generates peroxynitrite (#13) that is decomposed by catalase (#14). **B.** Enzymatic details. Part of the superoxide anions generated by NOX1 (#1) are dismutated to H₂O₂ by SOD (#2) and thus superoxide anion-mediated inhibition of catalase (#3-#5) is prevented. H₂O₂ is decomposed by catalase in a two step reaction (#6, 7), involving the activity of compound I (CpdI). This prevents the HOCl signaling pathway (#8, 9). NO synthesis is mediated and controlled by steps # 10-11, involving arginine, arginase, NO synthase (NOS) and NO dioxygenase (NOD). NO is oxidated by compound I of catalase (#12-#14) in a two step reaction, involving compound II (CpdII). Eventually formed peroxynitrite through the interaction of residual NO with superoxide anions (#15) is decomposed by catalase (#16, 17) and thus apoptosis-inducing NO/peroxynitrite signaling (#18, 19) is prevented. NO has the potential to reversibly inhibit catalase (#20) but also to revert superoxide anion-mediated inhibition of catalase (#21, 22). Vice versa, superoxide anions revert NO-mediated inhibition of catalase (#23). Activated FAS receptor has the potential to enhance NOX1 activity and NOS expression.

Regarding the NO_2 radical, it is one of the products with OH radicals of peroxy-nitrous acid decomposition and thus it is not directly involved in the apoptosis induction [2]. By the way, NO_2 can be consumed with superoxide anions to form peroxy-nitrate (O_2NOO^-), a precursor of singlet oxygen that can trigger singlet oxygen-dependent auto-amplification with the final result of selective apoptosis induction in tumor cells [62,63]. Nitrite and nitrates have not been found to provoke alone apoptosis in malignant cells [64,65].

Bauer *et al* firstly supported the idea that extracellular singlet oxygen is the RONS mainly responsible of CAP selectivity thanks to its strong potential to trigger selective apoptosis induction in tumor cells [3,66]. $^1\text{O}_2$ has the potential to inactivate catalase, placed onto the malignant cell membrane, relying on the interaction between H_2O_2 and PON which, in the absence of active catalase, are no longer decomposed and begin to promote apoptotic signaling. Moreover, since the inactivation of catalases leads to a secondary production of free single oxygen and more and more weak oxidant defenses by tumor cells, the self-perpetuation of apoptosis induction in areas not directly reached by CAP can be warranted by $^1\text{O}_2$ -induced pathways.

CAP-derived OCl^- can be considered as a selective pro-apoptotic agent since it can be protonated into HOCl by means of proton pumps associated to tumor cellular membrane. HOCl can react with superoxide anions derived from NOX1 (other specific components of malignant phenotype), resulting in the generation of apoptosis-inducing hydroxyl radicals [58,67]. However, as catalase is not affected by OCl^- , CAP-induced apoptotic self-perpetuation of apoptosis induction, would not be supported [3]. On the other hand, the synergic presence of OCl^- and H_2O_2 can lead to the formation of secondary singlet oxygen [68] and thus this process can inactivate catalase and cooperate with self-propagation of apoptosis induction.

Similarly to OCl^- based pathways, CAP-derived dichloride anion radicals $\text{Cl}_2^{\bullet-}$ evolve into HOCl in aqueous environment and induce apoptotic signaling selectively in tumor cells [3,69]. As $\text{Cl}_2^{\bullet-}$ acts in isolated way (without any catalases inhibitor such as $^1\text{O}_2$), it is unable to trigger the self-perturbation of apoptosis induction [3].

On light of the exposed considerations, CAP-produced singlet oxygen can promote apoptosis through local catalase inactivation and can support the self-perturbation of selective apoptosis induction to neighboring tumor cells through secondary extracellular singlet oxygen production [3]. Bauer described this time-dependent RONS-associated apoptosis induction in Fig.2.3. The experimental studies, carried out by Bohm *et al.* and Heinzelmann *et al.*, showed how the adding of $^1\text{O}_2$ scavenger histidine leads to arrest the self-perturbation apoptosis induction $^1\text{O}_2$ -mediated [51,53].

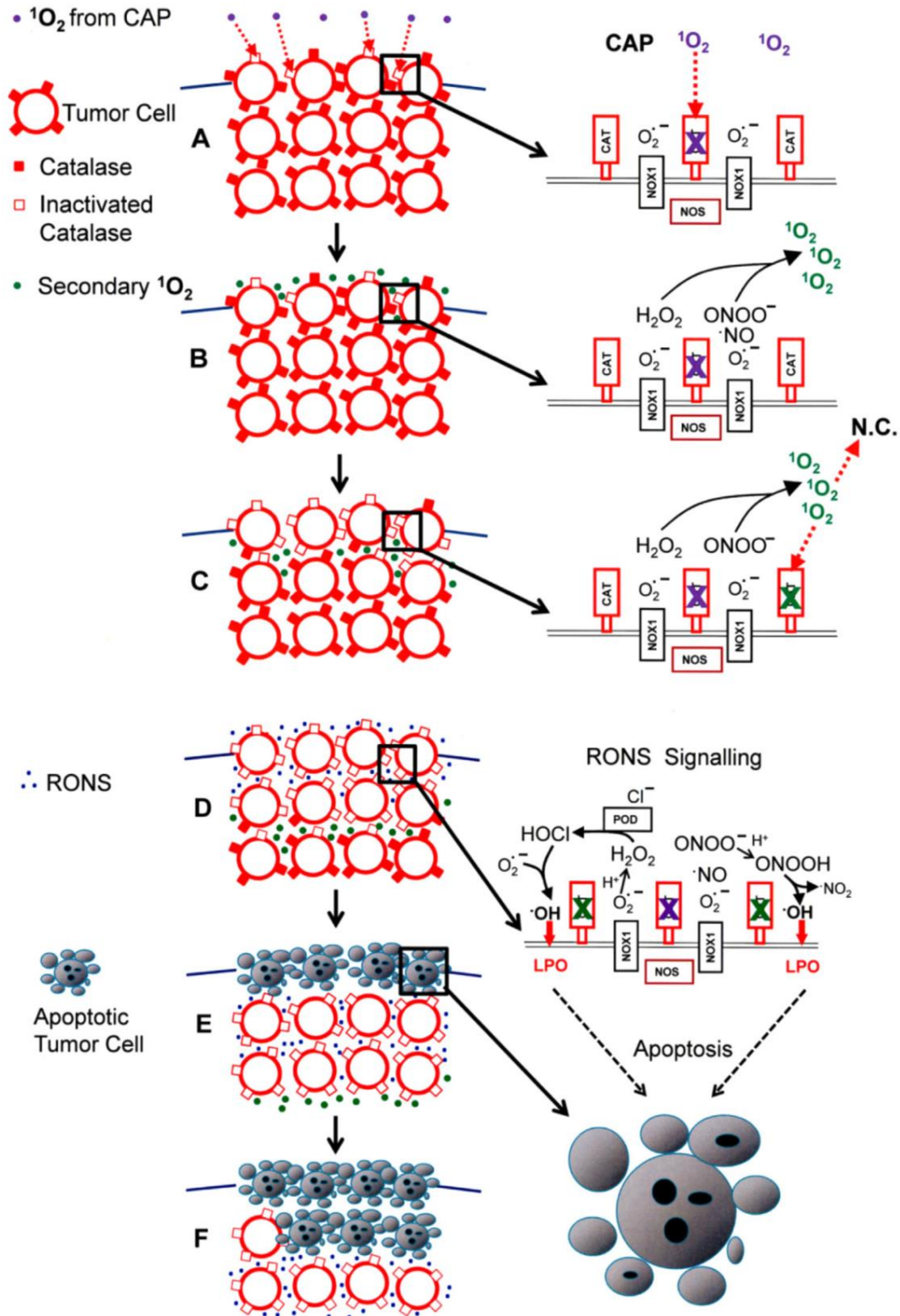


Fig.2.3. Hypothetical model to explain self-perpetuation of singlet oxygen triggered processes [3].
A: Singlet oxygen from CAP only reaches the surface of a tumor, and inactivates some membrane-associated catalase (CAT). **B and C:** At the site of local catalase inactivation, secondary singlet oxygen is generated by the tumor cells. This causes inactivation of more catalase molecules on the same cells and on neighboring cells. **D:** At the sites of optimal catalase inactivation intercellular RONS signaling is reactivated, while the generation of secondary singlet oxygen and catalase inactivation are spreading into deeper layers of the tumor. **E and F:** Apoptotic cells appear in the upper layers of the tumor, while the generation of secondary singlet oxygen, catalase inactivation, and RONS signaling are spreading further into deeper layers.

2.1.4. Overview of experimental activities

As well as the activities conducted in the field of dentistry, the research regarding the potentialities applications of a Plasma Gun treatment in oncology was driven in collaboration with the research group of Pharmacology and Toxicology, Alma Mater Studiorum – University of Bologna. The activities were involved in a project supported by a National SIR grant (RBSI14DBMB) named “*Non-thermal plasma as an innovative anticancer strategy: in vitro and ex vivo studies in leukemia models*”. This project brings together different research teams in the areas of physics/engineering, pharmacology and oncohematology, whose expertise and research competences are complementary. Through an integrated experimental approach, the project aims to contribute to a substantial progress in the understanding of the mechanisms of cell’s response to plasma. Since previous results showed that an indirect CAP treatment could induce apoptosis in tumor cells [70,71], the investigation on the antitumoral properties of cell culture medium activated by a Plasma Gun treatment was performed. The versatility of plasma technology raises the need for biological system standardized and consistent to uniformly define the fundamental mechanisms of the interaction process. Leukemia cell lines were chosen as target in this project because they are widely used in oncology for their easy cultivability and because are considered as a reference cell line for the preliminary fundamental studies of innovative therapies. Although the entire project was designed to investigate the effects of plasma treatment on leukemia cells with the aim at evaluating the selective apoptosis induction, efforts were addressed to the studies of the induction of apoptosis on acute T-lymphoblastic leukemia (Jurkat, CEM). In particular, cell culture medium, activated by Plasma Gun in different treatment conditions, was kept in contact with Jurkat cells and then the cyto-toxicological analysis was performed combining the results with quantitative chemical measurements of the RONS concentrations produced in the medium. A first analysis on the chemical composition of PAM focused on H₂O₂ and NO₂⁻ [64,65,72,73]. Thus, quantitative measurement of the mentioned species was performed by means of specific colorimetric kit assays. From a cyto-toxicological point of view, a discrimination of cell death mechanisms was carried out through a fluorescent technique. Survival, apoptotic and necrotic cell populations were evaluated at 24h and 48h after plasma treatment. Different phases (G0/G1, S and G2/M) occur during the mitosis cell cycle characterized by specific biochemical end-points related to DNA duplication. Thus, the distribution of cells in their cell reproduction cycle was investigated, determining at which end-points of reproduction phases PAM treatment induced the arrest of cell growth. To investigate the involvement of intrinsic pathway in the induction of apoptosis, an analysis of the perturbation of mitochondrial membrane potential was run. The involvement of mitochondria, characterized by perturbed membranes, could support the idea that CAP treatment induced a shift in the mitochondrial proteins balance towards the pro-apoptotic ones

leading to the activation of caspase-9. Finally, a valuation of the DNA damage caused by PAM was performed through the measurement of histones phosphorylation H2A.X, which is well recognized to be a marker of DNA breaks due to the involvement of histones in the cellular mechanisms for the DNA repair.

Further experimental activities will be carried out on *ex vivo* leukemia cell lines, both malignant (T lymphoblastoid) and non-malignant (T lymphocytes) in order to evaluate the performances of PAM treatment with more realistic target cells and, in particular, to analyze the selectivity of PAM treatment towards the malignant cells.

In light of the multidisciplinary approach that characterizes the project, it is worth underlining that my personal contribution was mainly focused on the use of Plasma Gun for the production of PAM, on the experimental setup development, on the planning of experimental activities, and on the discussion about the achieved results. Thus, I would like to acknowledge Ph.D. Romolo Laurita for his contribution in the chemical analysis of PAM, and Ph.D. Eleonora Turrini and co-workers for their effort dedicated to the cyto-toxicological analyses and cells management.

2.2. Materials & Methods

2.2.1. Cell culture

For the experiments, Jurkat T-lymphoblasts (standard LGC) cells were grown in suspension and propagated a medium composed by ~90% of Roswell Park Memorial Institute 1640 (RPMI, Sigma Aldrich), ~10% of inactivated fetal bovine serum (FBS), ~1% of penicillin/streptomycin solution and ~1% L-Glutamine 200mM (Sigma Aldrich). To maintain the exponential growth, the culture was divided every third day by dilution to a final concentration of $\sim 10^5$ viable cells/mL. Cells were cultured at 37°C / 5% CO₂.

2.3. Plasma treatment

The plasma device used for the experiments was the Plasma Gun source, previously described in paragraph. 1.2.1.1. The source was fed with 3 slpm of helium flow rate and operated at fixed frequency of 22 kHz and with a constant duty cycle of 7,5%. The distance between the source outlet and liquid to be treated was fixed at 11 mm. The activation of 1 ml of cell culture medium was performed in three different conditions, reported in Tab.2.1, in order to investigate the role of the applied voltage and treatment time.

Test	Applied Voltage [kV]	Treatment time [sec]
A	10	120
B	10	180
C	15	120

Tab. 2.1. Treatment conditions investigated for the activation of 1 ml of cell culture medium.

During the experiments frequency, duty cycle and gap were kept constant at 22 kHz, 7,5% and 11 mm respectively.

To standardize the procedure and to avoid any variables related to the kinetics of RONS in liquid phase, a delay time of 30 seconds was fixed before treatment with PAM. Then, 1×10^6 cells/100 μ l were added to the activated medium and incubated at 37°C for 1h, defined as contact time between PAM and cells. Finally, after a spin cycle of the cell suspension to place cells on the bottom of the plate, the recovery of medium was carried out and fresh medium enriched with 10% of FBS was added. The suspension was incubated at 37°C until the cytotoxicity analysis after 24h and 48h.

2.3.1. Cytotoxicity analysis

2.3.1.1. Discrimination of cell death mechanisms

Discrimination of cell death mechanisms between apoptotic and necrotic events was performed using the kit Guava Nexin®. The assay exploits the capacity of annexin V, conjugated to the Phycoerythrin (PE, fluorescent in yellow), to bind the phosphatidylserine (PS). Phosphatidylserine is a phospholipid that in healthy living cells is located on the inner side of the cell membrane; on the other hand, during apoptotic process it is everted on the external side of the cell membrane assuming a key role in the cell recognition by the cells of immune system, involved in the phagocytosis process of apoptotic cells. By the way, the fluorescent complex is able to penetrate inside the necrotic cell, because of the compromised membrane, resulting in the bonding between annexin V-PE and PS. To discriminate cells with integral membrane (living and apoptotic) from cells with compromised membrane (necrotic), 7-amino actinomycin (7-AAD, red fluorescence), a chemical compound unable to cross the integral cell membranes, was used for the cell viability stain. The procedure comprises the addition of 100 µl of Guava Nexin® to 100 M L of cell suspension (cell density between 2×10^5 and 1×10^6 cells/ml) and a subsequent incubation for 20 minutes in dark environment. Then, the viability analysis, based on the intensity of the yellow and red fluorescence, was carried out by means of a cytofluorimeter discriminating three cell populations: live (low yellow and red fluorescence), necrotic (high yellow and red fluorescence) and apoptotic (high yellow fluorescence and low red fluorescence). An example of cytofluorimeter signal distribution is reported in Fig.2.4.

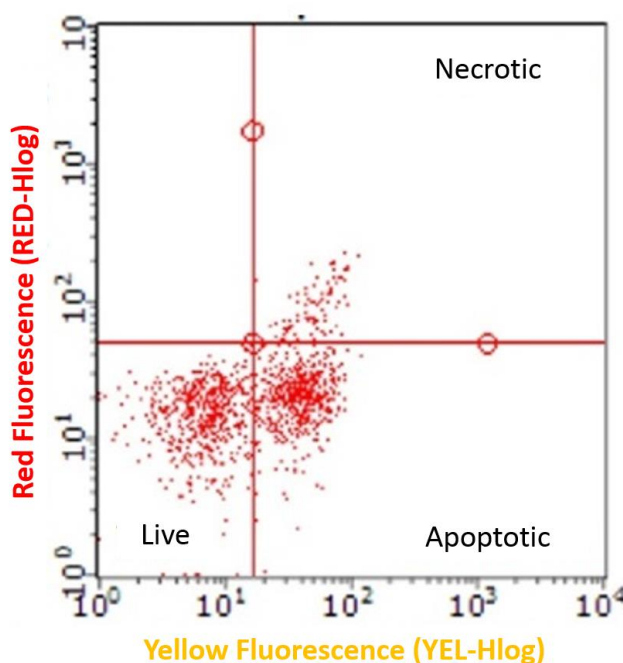


Fig.2.4. Example of distribution of yellow(x)-red(y) fluorescence signals in log-scale.

2.3.1.2. Analysis of the perturbation of mitochondrial membrane potential

The involvement of the intrinsic pathway in induced apoptosis, that is closely correlated to the permeability of the mitochondrial membranes, was evaluated through the study of the perturbation of mitochondrial membrane potential. The MitoProbe™ DiIC1 assay, containing the DiIC1 dye solution, was used for the assay. DiIC1 can penetrate the cytosol of eukaryotic cells and accumulates in healthy mitochondria. Thus, the greater the number of uncompromised mitochondria present in a cell, the higher the fluorescence intensity recorded. The cytotoxic substance carbonyl cyanide M-chlorophenyl hydrazone (CCCF) is used as a positive control as it alters the mitochondrial membrane potential.

24h post PAM treatment, after a centrifugation cycle, the cellular samples were resuspended in 1 ml of cell culture medium; for the positive control, cells were resuspended in 999 µl of medium + 1 µl of CCCF. Then, % min of incubation at 37°C occurred. Thereafter, all samples were added 5 µl DiIC1 and incubated at 37 °C for 20 min. Finally, the samples, resuspended in 500 µl of PBS, were analysed by means of a cytofluorimeter.

2.3.1.3. Cell cycle analysis

In order to evaluate the modulation of the cell replication cycle in a specific phase as a result of PAM treatment, the analysis was carried out with the Guava Cell Cycle® reagent, containing propidium iodide (PI, red fluorescence), which has the ability to bond DNA. The cells in the G0/G1 phase perform the normal metabolic functions and, during the phase of DNA duplication (phase S), a higher concentration of PI can be interspersed in the DNA, with proportional increase of the fluorescence intensity in the red. In the next G2/M phase, the DNA was fully duplicated and also the fluorescence associated with the PI is double in respect to the intensity measured during the phase G0/G1.

Firstly, cells were fixed for 1 h in ethanol at 70% at -18 °C. After a PBS washing, the cellular sample was resuspended in 200 µl of Guava Cell Cycle and incubated in dark environment at room temperature for 30 minutes before the cytofluorimetric analysis. As shown in Fig.2.5, the analysis of cell replication cycle was performed through the red fluorescence distribution.

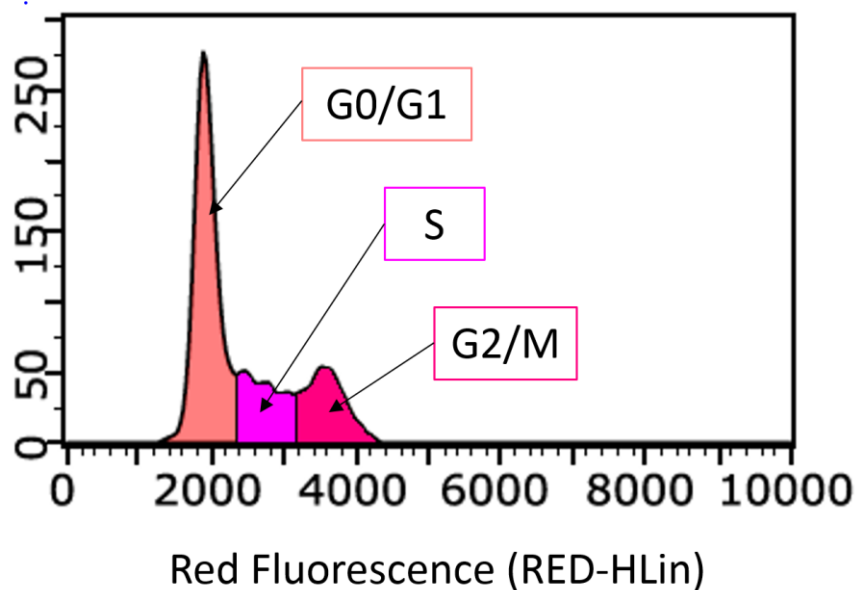


Fig.2.5. Example of cells distribution during the replication cycle achieved by fluorescent technique.

2.3.1.4. Analysis of histones phosphorylation H2A.X

Histone H2A.X is one of the main histone proteins 2A involved in the structure of chromatin in eukaryotic cells and in DNA repair. Phosphorylation of the histone H2A.X on serine-139 is an important signal of the presence of DNA breaks, in particular at the double filament level. The level of phosphorylation of the histone, after the phase of fixation and cell permeability, was measured through a specific antibody for H2A.X, whose fluorescence is directly proportional to the extent of the damage to the double filament. The phosphorylation analysis of histone H2A.X was carried out using the Millipore's FlowCollect™ Histone H2A.X Phosphorylation Assay Kit.

The analysis protocol provided that the cells were washed with 1 ml of PBS and fixed with a fixation buffer solution. The analysis of H2A.X phosphorylation was performed 5h and 24h after PAM treatment. After 20 min of ice-incubation, cells are permeabilized with a permeabilization buffer solution. A further incubation in ice for 20 minutes occurred and the anti-H2A.X antibody marked with FITC was applied to the cellular sample, then stored in dark environment for 30 minutes. After washing with 1ml of PBS, the cytofluorimetric analysis was performed. Etoposide was used as positive control.

2.3.2. Detection of Hydrogen Peroxides and Nitrites in Plasma-treated Medium

Since hydrogen peroxide and nitrites are the reactive species mainly involved in the induction of apoptotic signalling [64,65,72,73], the chemical analysis was focused on the measurement of concentrations of H₂O₂ and NO₂⁻ in 1 ml of PAM performed through the Amplex® Red Hydrogen

Peroxide Assay Kit (Thermo Fisher Scientific, Waltham, MA, USA) and Nitrate/Nitrite Colorimetric Assay (Roche, Basel, Switzerland) respectively. PAM was diluted 100-fold in PBS immediately after treatment to avoid any influence of pH on measurements, obtaining a solution with hydrogen peroxide concentration below 10 μ M. The absorbances were measured photometrically with a microplate reader (Rayto, Shenzhen, P.R. China).

2.4. Results

2.4.1. Cell viability

By means of flow cytometry, the PAM efficacy of induction of tumor cell death was evaluated and the cellular death mechanisms were discriminated after 24h and 48h. As shown in Fig.2.6, PAM treatment clearly showed cytotoxic properties, resulting in a relevant decrease of cell viability under all the tested CAP treatment conditions, proportionally to the applied voltage and to the plasma exposure time. As an example, after 48h of incubation, none viability recovery was observed for cells treated in condition A and B, that achieved a cell viability of 27,5% and 29% respectively. Although at 24h the cell population in necrotic state overcame the apoptotic one, after 48h apoptotic pathways were induced in the most of cells. In particular, for the conditions B and C, the apoptotic population reached approximately 50% with statistical significance in respect with the control.

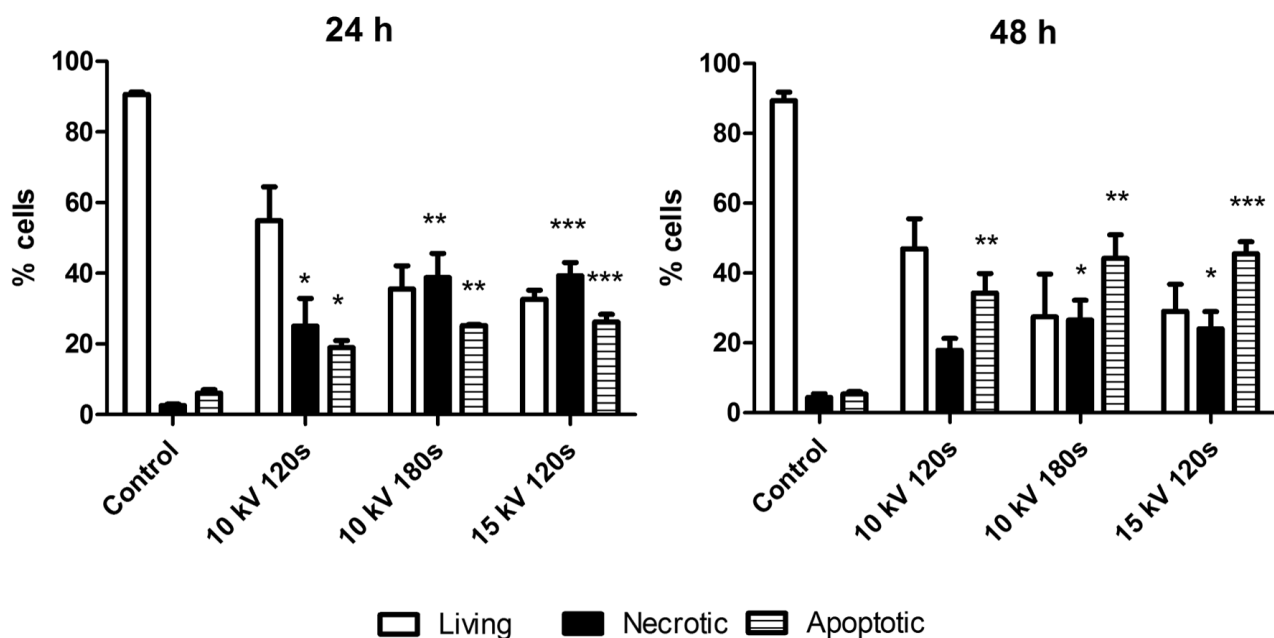


Fig. 2.6. % of living, apoptotic and necrotic cells 24 and 48 h after PAM treatment of Jurkat cells under A, B and C conditions

2.4.2. Analysis of cell cycle

By analyzing the fluorescence histograms of Guava Cell Cycle ® reagent, a nucleic acid dye, the treatment of Jurkat cells with PAM was demonstrated to inhibit cell-cycle progression and induce an accumulation of cells in the G2/M phase. The results are reported in Fig.2.7. In particular, the condition A induced death signalling mainly after the phase S of cell replication (27,3%), while conditions B and C led to arrest the cell cycle both in S and G2/M phases (B: 23% for S phase and 28% for G2/M phase; C: 24,2% for S phase and 26,2% for G2/M phase).

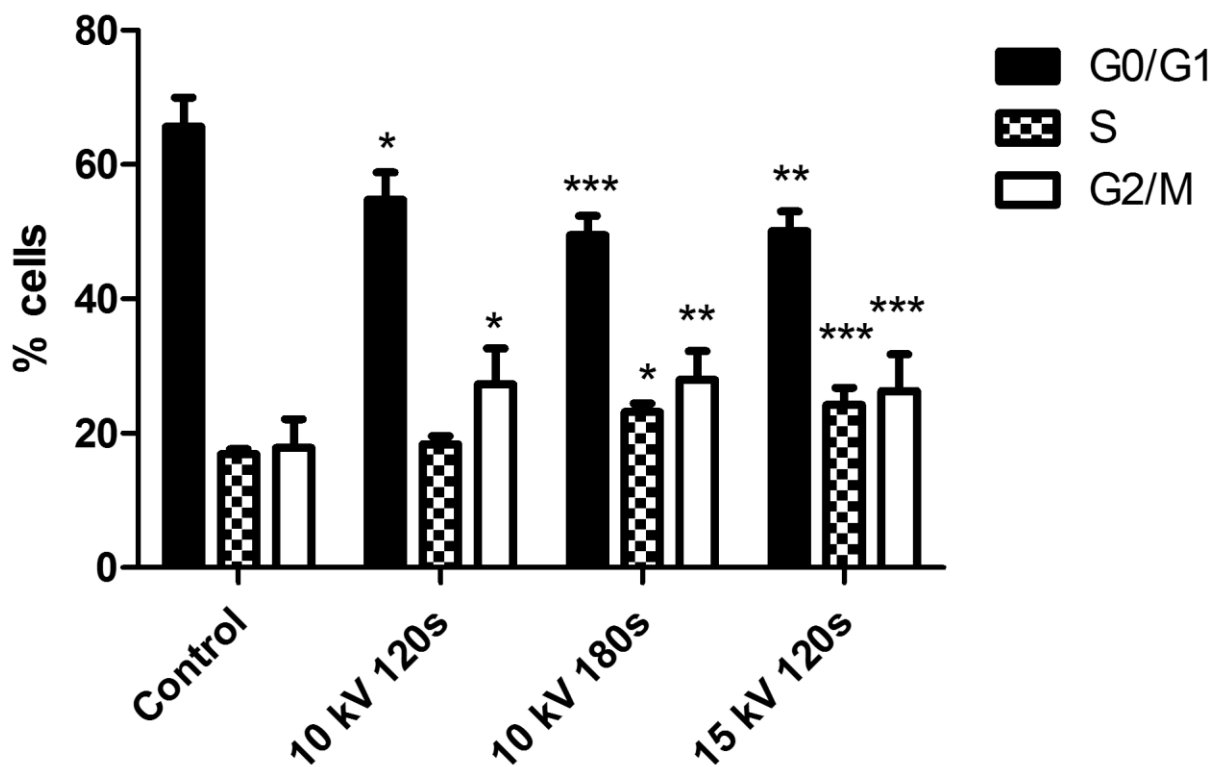


Fig. 2.7. Histograms of % of cells in different phase of cell cycle under A, B and C conditions.

2.4.3. Analysis of mitochondrial membrane potential

To explore the involvement of the intrinsic pathway in CAP-induced apoptosis, the perturbation of mitochondrial membrane potential was evaluated. The results, reported in Fig. 2.8, highlighted significant differences between the investigated cases. Though, as discussed in paragraph 2.1, the condition B and C resulted similar apoptotic effects, greater involvement of intrinsic pathway was related to the condition C with 48,3% of cells with decreased mitochondrial potential. However, also the conditions A and B showed to induce apoptosis through intrinsic pathway involving 17% (A) and 30% (B) of cells.

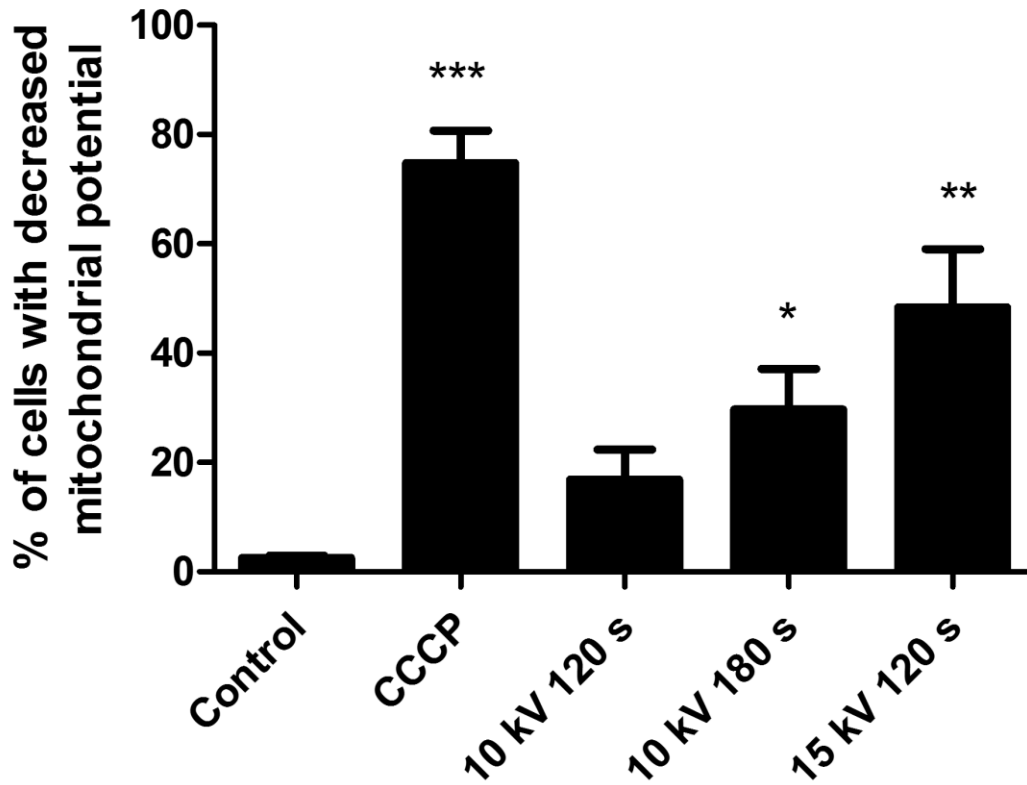


Fig. 2.8. % of cells with decreased mitochondrial potential 24h after PAM treatment of Jurkat cells under A, B and C conditions.

2.4.4. Analysis of γ -H2AX phosphorylation

Since PAM is characterized by the presence of RONS in liquid phase, its genotoxic potential should be carefully examined. For this reason, γ -H2AX phosphorylation test of genotoxicity was driven with the aim to investigate mutagenic effect directly related the DNA damage induced by CAP treatment; the results are shown in Fig.2.9. 5h after the contact with PAM, a 3-fold, 3,7-fold and 3,5-fold increase in p-H2A.X compared to the untreated cells was observed for the condition A, B and C, respectively. 24h after PAM treatment, the level of p-H2A.X was significant reduced reaching values comparable with the negative control, around 1,5-fold, highlighting a common DNA repair. Although a DNA damage was induced by PAM contact, no significant differences were observed between the investigated conditions.

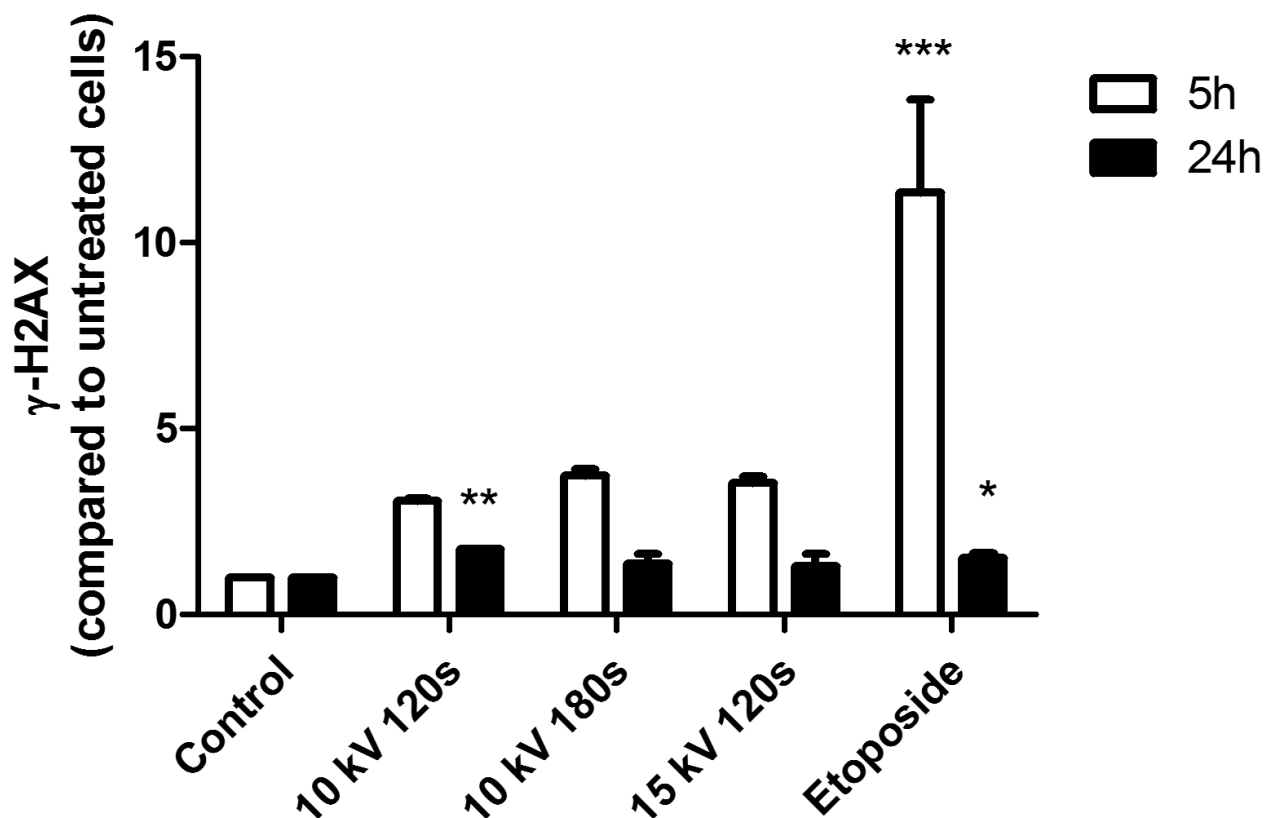


Fig. 2.9. Histograms of γ -H2AX phosphorylation in comparison to untreated cells 5h and 24h after PAM treatment under conditions A, B and C and for the positive control made with etoposide.

2.4.5. Measurement of RONS concentration in PAM

Since the cytotoxic effects of PAM on cancer cells seem to be mediated by reactive species, the concentrations of H_2O_2 and NO_2^- in medium produced by CAP treatment were quantitatively evaluated. In Fig. 2.10, the concentrations of hydrogen peroxides and nitrites in 1mL of PAM for the tested conditions. Hydrogen peroxides and nitrites are not present in the untreated medium. Both concentrations of H_2O_2 and NO_2^- appeared to be proportionally related to the plasma exposure time and to the applied voltage. The condition C was found to lead to the production of a PAM with the highest concentration of hydrogen peroxides ($\sim 80 \mu M$) and nitrites ($\sim 145 \mu M$) compared to the other operative conditions.

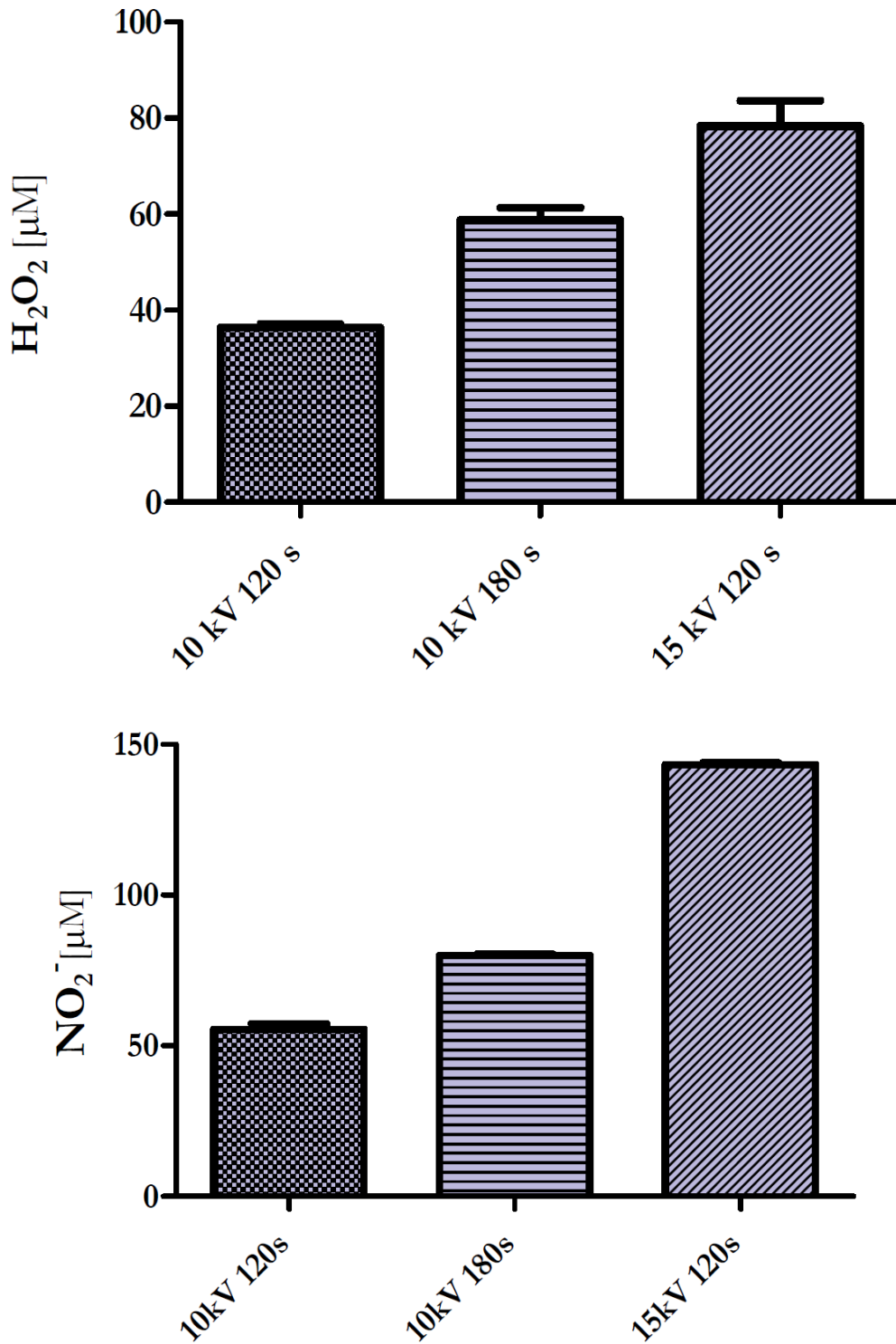


Fig. 2.10. Hydrogen peroxide and nitrite concentration in PAM, measured by specific colorimetric kits, under conditions A, B and C.

2.5. Discussion of results

The effects of PAM on cancer cells were observed in an *in vitro* leukemia model. Cell culture medium was treated by means of Plasma Gun source operating at different applied voltages and for different treatment times (conditions A, B and C). Quantitative measurements of hydrogen peroxides and nitrites highlighted how an increase of both applied voltage and plasma exposure time led to an increase of investigated species. Several studies showed the apoptotic induction effects of CAP in a dose-dependent manner [2,22–26,70][77] and related to the chemical composition of PAM [27,47,61,70,74–76]. A higher production of H₂O₂ and NO₂⁻ was observed in the case of an increase of +50% of applied voltage (A:10kV→C:15kV) with the respect of the same increment of treatment time (A:120s→B:180s). All the tested conditions caused the induction of Jurkat death as shown by cell viability analysis; 24h after PAM treatment necrotic cells overcame the apoptotic ones, while at 48h an inversion of cell death mechanism was observed shifting to apoptosis, while the percentage of survival cells maintained at same levels. Since the cell cycle of Jurkat cells takes around 24h, the analysis underlined how the PAM-induced apoptosis did not affect leukemia cells only in direct way but also inducing secondary apoptotic pathways involving also the replicated cells. Moreover, the direct action of PAM appeared to cause a too strong oxidative stress to cells resulting in necrosis, while the post-PAM contact effects were revealed to more promote a controlled cell death. This experimental evidence could be explained considering a bystander effect-like process evolving in time as proposed by Bauer et al. [3] and Graves [55,78]. Although the chemical composition of PAM was found to be different between conditions C or B, no significant differences of cell viability was observed. This consideration was also supported by the analysis of cell cycle where a similar accumulation of cells in phase S and G2/M was detected for both conditions. No single-phase accumulation was observed in the reproduction cell cycle; this result could be explained considering that PAM treatment causes the arrest of cell reproduction involving different mechanisms, that in synergy cooperate for the stop of mitosis cycle of malignant cells. The investigation regarding the perturbation of the mitochondrial membrane potential proved that intrinsic pathway is involved in PAM-induced apoptosis and its involvement is significantly related to the treatment conditions. 24h after PAM treatment, condition C induced the decrease of mitochondrial potential in 50% of cells. This means that mitochondrial membranes cannot avoid any more the release in cellular cytosol of cytochrome C and, thus, the free cytochrome C can cause the ignition of caspase cascade by the activation of caspase-9. The mitochondrial membrane potential could be affected by DNA alteration (p53 activation) but also by other different agents as reported in [79,80]. The results of phosphorylation of histone γ -H2AX at 5h after PAM treatment showed that conditions B and C cause similar DNA damages. Although DNA alterations were efficiently repaired after 24h, the PAM-

derived DNA damages were able to induce apoptosis through the intrinsic pathway that was found to self-sustain and self-amplifying until 48h after treatment. It is worth mentioning that the analysis of phosphorylation of histone γ -H2AX does not lead to a complete study on the DNA damage, but gives an information related to the activity of repairing system. These considerations regarding DNA damages and perturbation of mitochondrial membrane support the involvement of intrinsic pathway in PAM-induced apoptosis, whereas a direct correlation between the mentioned analysis cannot be run. As a matter of fact, tumor cells could counteract against intracellular oxidative stress and apoptosis inducing signaling through a cellular compensatory mechanisms, such as the post transcriptional regulation of SOD1, CAT, and GSR2 [70,81]. And, thus, the observed apoptotic cell population was the final product of a compensated induction of apoptosis.

A genetic analysis of DNA damages, combined with a study on p53 activation and mitochondrial pro-apoptotic proteins, such as BAX and BAK, could lead to a deeper knowledge of the fundamental mechanism involved in the PAM-induced apoptosis in leukemia cells. Moreover, using highly specific scavengers, the role of ROS and RNS could be experimentally investigated and discriminated. By the analysis of activity of cellular systems for oxidative compensatory, a measurement of level of intracellular oxidative stress could be obtained.

Then, as anticipated above, experiments on *ex vivo* leukemia cells, both malignant and non-malignant cells, will be carried out to verify the selectivity properties of PAM for cancer cells.

The presented results, providing a deeper understanding of PAM-leukemia cells interactions, support the progress of the project they are involved and pave the way for the development of a promising physic-pharmacologic strategy, based on CAP technology, for oncological applications.

2.6. Conclusions

The present activity regarded an essential step of the project “*Non-thermal plasma as an innovative anticancer strategy: in vitro and ex vivo studies in leukemia models*”, funded by a National SIR grant (RBSI14DBMB), focused on the study of the potentialities of a PAM treatment in the selective induction of apoptosis in leukemia cells. Plasma Gun was found to effectively activate cell culture medium producing H₂O₂ and NO₂⁻ in liquid phase, whose concentrations depend on the treatment operating conditions. By cytotoxicological analysis, the PAM-induced apoptosis on Jurkat cells was demonstrated mainly 48h after the treatment. Through the analysis of the perturbation of mitochondrial membrane potential and phosphorylation of histone γ -H2AX, the involvement of the intrinsic pathway was observed. Indeed, these promising results support the next experiments aimed at evaluating the selective effectiveness of PAM treatment on malignant and non-malignant *ex vivo* leukemia cells. The final goal of the project is to provide a consistent *in vitro* and *ex vivo* experimental study able to support a future transitioning of Plasma Gun treatment in real-life medical clinics.

2.7. Bibliography

- [1] Schlegel J, Köritzer J, Boxhammer V. Plasma in cancer treatment. *Clin Plasma Med* 2013;1:2–7.
- [2] Keidar M, Walk R, Shashurin a, Srinivasan P, Sandler a, Dasgupta S, et al. Cold plasma selectivity and the possibility of a paradigm shift in cancer therapy. *Br J Cancer* 2011;105:1295–301.
- [3] Bauer G, Graves DB. Mechanisms of Selective Antitumor Action of Cold Atmospheric Plasma-Derived Reactive Oxygen and Nitrogen Species. *Plasma Process Polym* 2016;13:1157–78.
- [4] Simon H-U, Haj-Yehia A, Levi-Schaffer F. Role of reactive oxygen species (ROS) in apoptosis induction. *Apoptosis* 2000;5:415–8.
- [5] Cohen GM. Caspases: the executioners of apoptosis. *Biochem J* 1997;326:1–16.
- [6] William C. Earnshaw, Luis M. Martins, Kaufmann SH. Mammalian Caspases: Structure, Activation, Substrates, and Functions During Apoptosis. *Annu Rev Biochem* 1999;68:383–424.
- [7] Thornberry NA, Lazebnik Y. Caspases: Enemies Within. *Science (80-)* 1998;281:1312–6.
- [8] Elmore S. Apoptosis : A Review of Programmed Cell Death. *Toxicol Pathol* 2007;35:495–516.
- [9] Fulda S, Debatin K-M. Extrinsic versus intrinsic apoptosis pathways in anticancer chemotherapy. *Oncogene* 2006;25:4798–811.
- [10] Deiss LP, Galinka H, Berissi H, Cohen O, Kimchi A. Cathepsin D protease mediates programmed cell death induced by interferon-gamma, Fas/APO-1 and TNF-alpha. *EMBO J* 1996;15:3861–70.
- [11] Abreu-Martin MT, Vidrich A, Lynch DH, Targan SR. Divergent induction of apoptosis and IL-8 secretion in HT-29 cells in response to TNF-alpha and ligation of Fas antigen. *J Immunol* 1995;155:4147–54.
- [12] Symonds H, Krall L, Remington L, Saenz-Robles M, Lowe S, Jacks T, et al. p53-Dependent apoptosis suppresses tumor growth and progression *in vivo*. *Cell* 1994;78:703–11.
- [13] Kluck RM, Bossy-Wetzel E, Green DR, Newmeyer DD. The Release of Cytochrome c from Mitochondria: A Primary Site for Bcl-2 Regulation of Apoptosis. *Science (80-)* 1997;275:1132–6.
- [14] Liu X, Kim CN, Yang J, Jemmerson R, Wang X. Induction of Apoptotic Program in Cell-Free Extracts: Requirement for dATP and Cytochrome c. *Cell* 1996;86:147–57.
- [15] Taylor RC, Cullen SP, Martin SJ. Apoptosis: controlled demolition at the cellular level. *Nat Rev Mol Cell Biol* 2008;9:231.
- [16] Stoffels E, Kieft IE, Sladek REJ, Bedem LJM van den, Laan EP van der, Steinbuch M. Plasma needle for *in vivo* medical treatment: recent developments and perspectives. *Plasma Sources Sci Technol* 2006;15:S169–80.
- [17] Kim C-H, Bahn JH, Lee S-H, Kim G-Y, Jun S-I, Lee K, et al. Induction of cell growth arrest by atmospheric non-thermal plasma in colorectal cancer cells. *J Biotechnol* 2010;150:530–8.
- [18] Lupu A-R, Georgescu N. Cold atmospheric plasma jet effects on V79-4 cells. *Roum Arch*

Microbiol Immunol 2010;69:67–74.

- [19] Kim C-H, Kwon S, Bahn JH, Lee K, Jun SI, Rack PD, et al. Effects of atmospheric nonthermal plasma on invasion of colorectal cancer cells. *Appl Phys Lett* 2010;96:243701.
- [20] Vandamme M, Robert E, Lerondel S, Sarron V, Ries D, Dozias S, et al. ROS implication in a new antitumor strategy based on non-thermal plasma. *Int J Cancer* 2012;130:2185–94.
- [21] Volotskova O, Hawley TS, Stepp MA, Keidar M. Targeting the cancer cell cycle by cold atmospheric plasma. *Sci Rep* 2012;2:636.
- [22] Kim JY, Ballato J, Foy P, Hawkins T, Wei Y, Li J, et al. Apoptosis of lung carcinoma cells induced by a flexible optical fiber-based cold microplasma. *Biosens Bioelectron* 2011;28:333–8.
- [23] Ahn HJ, Kim K II, Kim G, Moon E, Yang SS, Lee J-S. Atmospheric-pressure plasma jet induces apoptosis involving mitochondria via generation of free radicals. *PLoS One* 2011;6:e28154.
- [24] Thiagarajan M, Waldbeser L, Whitmill A. THP-1 leukemia cancer treatment using a portable plasma device. *Stud Health Technol Inform* 2012;173:515–7.
- [25] Barekzi N, Laroussi M. Dose-dependent killing of leukemia cells by low-temperature plasma. *J Phys D Appl Phys* 2012;45:422002.
- [26] Partecke LI, Evert K, Haugk J, Doering F, Normann L, Diedrich S, et al. Tissue Tolerable Plasma (TTP) induces apoptosis in pancreatic cancer cells *in vitro* and *in vivo*. *BMC Cancer* 2012;12:473.
- [27] Tanaka H, Mizuno M, Ishikawa K, Kondo H, Takeda K, Hashizume H, et al. Plasma with high electron density and plasma-activated medium for cancer treatment. *Clin Plasma Med* 2015;3:1–5.
- [28] Brullé L, Vandamme M, Riès D, Martel E, Robert E, Lerondel S, et al. Effects of a Non Thermal Plasma Treatment Alone or in Combination with Gemcitabine in a MIA PaCa2-luc Orthotopic Pancreatic Carcinoma Model. *PLoS One* 2012;7:1–10.
- [29] Walk RM, Snyder JA, Srinivasan P, Kirsch J, Diaz SO, Blanco FC, et al. Cold atmospheric plasma for the ablative treatment of neuroblastoma. *J Pediatr Surg* 2013;48:67–73.
- [30] Yan D, Talbot A, Nourmohammadi N, Sherman JH, Cheng X, Keidar M. Toward understanding the selective anticancer capacity of cold atmospheric plasma — A model based on aquaporins (Review) Toward understanding the selective anticancer capacity of cold atmospheric plasma — A model based on aquaporins (Review) 2015;40801.
- [31] Yan D, Xiao H, Zhu W, Nourmohammadi N, Zhang LG, Bian K, et al. The role of aquaporins in the anti-glioblastoma capacity of the cold plasma-stimulated medium. *J Phys D Appl Phys* 2017;50:55401.
- [32] Bauer G. The Antitumor Effect of Singlet Oxygen. *Anticancer Res* 2016;36:5649–64.
- [33] Kaushik NK, Kaushik N, Min B, Choi KH, Hong YJ, Miller V, et al. Cytotoxic macrophage-released tumour necrosis factor-alpha (TNF- α) as a killing mechanism for cancer cell death after cold plasma activation. *J Phys D Appl Phys* 2016;49:84001.
- [34] Miller V, Lin A, Fridman A. Why Target Immune Cells for Plasma Treatment of Cancer. *Plasma Chem Plasma Process* 2016;36:259–68.

- [35] Lin A, Truong B, Pappas A, Kirifides L, Oubarri A, Chen S, et al. Uniform Nanosecond Pulsed Dielectric Barrier Discharge Plasma Enhances Anti-Tumor Effects by Induction of Immunogenic Cell Death in Tumors and Stimulation of Macrophages. *Plasma Process Polym* 2015;12:1392–9.
- [36] Schumacker PT. Reactive oxygen species in cancer cells: Live by the sword, die by the sword. *Cancer Cell* 2006;10:175–6.
- [37] Raj L, Ide T, Gurkar AU, Foley M, Schenone M, Li X, et al. Selective killing of cancer cells by a small molecule targeting the stress response to ROS. *Nature* 2012;481:534–534.
- [38] Bauer G. Increasing the endogenous NO level causes catalase inactivation and reactivation of intercellular apoptosis signaling specifically in tumor cells. *Redox Biol* 2015;6:353–71.
- [39] Heigold S, Sers C, Bechtel W, Ivanovas B, Schafer R, Bauer G. Nitric oxide mediates apoptosis induction selectively in transformed fibroblasts compared to nontransformed fibroblasts. *Carcinogenesis* 2002;23:929–41.
- [40] Herdener M, Heigold S, Saran M, Bauer G. Target cell–derived superoxide anions cause efficiency and selectivity of intercellular induction of apoptosis. *Free Radic Biol Med* 2000;29:1260–71.
- [41] Bauer G. Central Signaling Elements of Intercellular Reactive Oxygen/Nitrogen Species-dependent Induction of Apoptosis in Malignant Cells. *Anticancer Res* 2017;37:499–513.
- [42] Bauer G, Bereswill S, Aichele P, Glocker E. *Helicobacter pylori* protects oncogenically transformed cells from reactive oxygen species-mediated intercellular induction of apoptosis. *Carcinogenesis* 2014;35:1582–91.
- [43] Scheit K, Bauer G. Direct and indirect inactivation of tumor cell protective catalase by salicylic acid and anthocyanidins reactivates intercellular ROS signaling and allows for synergistic effects. *Carcinogenesis* 2015;36:400–11.
- [44] Kroemer G, Galluzzi L, Brenner C. Mitochondrial membrane permeabilization in cell death. *Physiol Rev* 2007;87:99–163.
- [45] Bauer G. Tumor cell-protective catalase as a novel target for rational therapeutic approaches based on specific intercellular ROS signaling. *Anticancer Res* 2012;32:2599–624.
- [46] Bauer G. Targeting extracellular ROS signaling of tumor cells. *Anticancer Res* 2014;34:1467–82.
- [47] Yan D, Nourmohammadi N, Bian K, Murad F, Sherman JH, Keidar M. Stabilizing the cold plasma-stimulated medium by regulating medium’s composition. *Sci Rep* 2016;6:26016.
- [48] Graves DB. Reactive Species from Cold Atmospheric Plasma: Implications for Cancer Therapy. *Plasma Process Polym* 2014:1120–7.
- [49] Ratovitski EA, Cheng X, Yan D, Sherman JH, Canady J, Trink B, et al. Anti-cancer therapies of 21st century: Novel approach to treat human cancers using cold atmospheric plasma. *Plasma Process Polym* 2014;11:1128–37.
- [50] Bauer G. Targeting extracellular ROS signaling of tumor cells. *Anticancer Res* 2014;34:1467–82.
- [51] Bohm B, Heinzelmann S, Motz M, Bauer G. Extracellular localization of catalase is associated with the transformed state of malignant cells. *Biol Chem* 2015;396:1339–56.

- [52] Bechtel W, Bauer G. Catalase protects tumor cells from apoptosis induction by intercellular ROS signaling. *Anticancer Res* 2009;29:4541–57.
- [53] Heinzelmann S, Bauer G. Multiple protective functions of catalase against intercellular apoptosis-inducing ROS signaling of human tumor cells. *Biol Chem* 2010;391:675–93.
- [54] Gardner PR, Martin LA, Hall D, Gardner AM. Dioxygen-dependent metabolism of nitric oxide in mammalian cells. *Free Radic Biol Med* 2001;31:191–204.
- [55] Graves DB. Oxy-nitroso shielding burst model of cold atmospheric plasma therapeutics. *Clin Plasma Med* 2014;2:38–49.
- [56] Wende K, Williams P, Dalluge J, Van Gaens W, Aboubakr H, Bischof J, et al. Identification of the biologically active liquid chemistry induced by a nonthermal atmospheric pressure plasma jet. *Biointerphases* 2015;10:29518.
- [57] Pottgiesser SJ, Heinzelmann S, Bauer G. Intercellular HOCl-mediated Apoptosis Induction in Malignant Cells: Interplay Between NOX1-Dependent Superoxide Anion Generation and DUOX-related HOCl-generating Peroxidase Activity. *Anticancer Res* 2015;35:5927–43.
- [58] Bauer G. HOCl-dependent singlet oxygen and hydroxyl radical generation modulate and induce apoptosis of malignant cells. *Anticancer Res* 2013;33:3589–602.
- [59] Ivanovas B, Zerweck A, Bauer G. Selective and non-selective apoptosis induction in transformed and non-transformed fibroblasts by exogenous reactive oxygen and nitrogen species. *Anticancer Res* 2002;22:841–56.
- [60] Steinmann M, Moosmann N, Schimmel M, Gerhardus C, Bauer G. Differential role of extra- and intracellular superoxide anions for nitric oxide-mediated apoptosis induction. *In vivo* 2004;18:293–309.
- [61] Bauer G. Signal Amplification By Tumor Cells : Clue To The Understanding Of The Antitumor Effects Of Cold Atmospheric Plasma And Plasma-Activated Medium 2017;7311.
- [62] Miyamoto S, Ronsein GE, Correa TC, Martinez GR, Medeiros MHG, Di Mascio P. Direct evidence of singlet molecular oxygen generation from peroxyxynitrate, a decomposition product of peroxyxynitrite. *Dalton Trans* 2009:5720–9.
- [63] Riethmüller M, Burger N, Bauer G. Singlet oxygen treatment of tumor cells triggers extracellular singlet oxygen generation, catalase inactivation and reactivation of intercellular apoptosis-inducing signaling. *Redox Biol* 2015;6:157–68.
- [64] Girard P-M, Arbabian A, Fleury M, Bauville G, Puech V, Dutreix M, et al. Synergistic Effect of H₂O₂ and NO₂ in Cell Death Induced by Cold Atmospheric He Plasma. *Sci Rep* 2016;6:29098.
- [65] Kurake N, Tanaka H, Ishikawa K, Kondo T, Sekine M, Nakamura K, et al. Cell survival of glioblastoma grown in medium containing hydrogen peroxide and/or nitrite, or in plasma-activated medium. *Arch Biochem Biophys* 2016;605:102–8.
- [66] Riethmüller M, Burger N, Bauer G. Singlet oxygen treatment of tumor cells triggers extracellular singlet oxygen generation, catalase inactivation and reactivation of intercellular apoptosis-inducing signaling. *Redox Biol* 2015;6:157–68.
- [67] Engelmann I, Dormann S, Saran M, Bauer G. Transformed target cell-derived superoxide anions drive apoptosis induction by myeloperoxidase. *Redox Rep* 2000;5:207–14.
- [68] Held AM, Halko DJ, Hurst JK. Mechanisms of chlorine oxidation of hydrogen peroxide. *J*

Am Chem Soc 1978;100:5732–40.

- [69] Saran M, Beck-Speier I, Fellerhoff B, Bauer G. Phagocytic killing of microorganisms by radical processes: consequences of the reaction of hydroxyl radicals with chloride yielding chlorine atoms. *Free Radic Biol Med* 1999;26:482–90.
- [70] Turrini E, Gherardi M, Stancampiano A, Laurita R, Catanzaro E, Mater A, et al. Atmospheric non-equilibrium plasma induces apoptosis and oxidative stress pathway regulation in T-lymphoblastoid leukemia cells 2016;9:98652.
- [71] Gherardi M, Turrini E, Laurita R, De Gianni E, Ferruzzi L, Liguori A, et al. Atmospheric Non-Equilibrium Plasma Promotes Cell Death and Cell-Cycle Arrest in a Lymphoma Cell Line. *Plasma Process Polym* 2015:n/a-n/a.
- [72] Uchida G, Nakajima A, Ito T, Takenaka K, Kawasaki T, Koga K, et al. Effects of nonthermal plasma jet irradiation on the selective production of H₂O₂ and NO₂⁻ in liquid water. *J Appl Phys* 2016;120:203302.
- [73] Yan D, Talbot A, Nourmohammadi N, Cheng X, Canady J, Sherman J, et al. Principles of using Cold Atmospheric Plasma Stimulated Media for Cancer Treatment. *Sci Rep* 2016;5:18339.
- [74] Tanaka H, Mizuno M, Ishikawa K, Kondo H, Takeda K, Hashizume H, et al. Plasma with high electron density and plasma-activated medium for cancer treatment. *Clin Plasma Med* 2015;3:72–6.
- [75] Adachi T, Tanaka H, Nonomura S, Hara H, Kondo SI, Hori M. Plasma-activated medium induces A549 cell injury via a spiral apoptotic cascade involving the mitochondrial-nuclear network. *Free Radic Biol Med* 2015;79:28–44.
- [76] Tanaka H, Mizuno M, Ishikawa K, Nakamura K, Kajiyama H, Kano H, et al. Plasma-Activated Medium Selectively Kills Glioblastoma Brain Tumor Cells by Down-Regulating a Survival Signaling Molecule, AKT Kinase. *Plasma Med* 2011;1:265–77.
- [77] Norberg S a, Tian W, Johnsen E, Kushner MJ. Atmospheric pressure plasma jets interacting with liquid covered tissue: touching and not-touching the liquid. *J Phys D Appl Phys* 2014;47:475203.
- [78] Graves DB. Mechanisms of Plasma Medicine: Coupling Plasma Physics, Biochemistry, and Biology. *IEEE Trans Radiat Plasma Med Sci* 2017;1:281–92.
- [79] Chen LB. Mitochondrial membrane potential in living cells. *Annu Rev Cell Biol* 1988;4:155–81.
- [80] Ly JD, Grubb DR, Lawen a. The mitochondrial membrane potential in apoptosis; an update. *Apoptosis* 2003;8:115–28.
- [81] Liou M-Y, Storz P. Reactive oxygen species in cancer. *Free Radic Res* 2010;44.

3. Spectroscopy techniques for plasma processes characterization

3.1. Overview of literature and of experimental activities

3.1.1. Optical spectroscopy techniques for the characterization of plasma-assisted processes

Each component of the chemically active plasma, such as charged particles (electrons, negative and positive ions), excited (electronic, vibrational and rotational excitation) atoms and molecules, reactive atoms and radicals, and UV-photons, plays a specific and important role in plasma-assisted processes for industrial and biomedical applications [1]. Thus, a successful control of plasma chemical and physical parameters allows to tune the operating conditions of treatment resulting in an optimization of the (bio-)chemical process. An overview of all factors involved in a plasma process are schematically reported in Fig. 3.1.

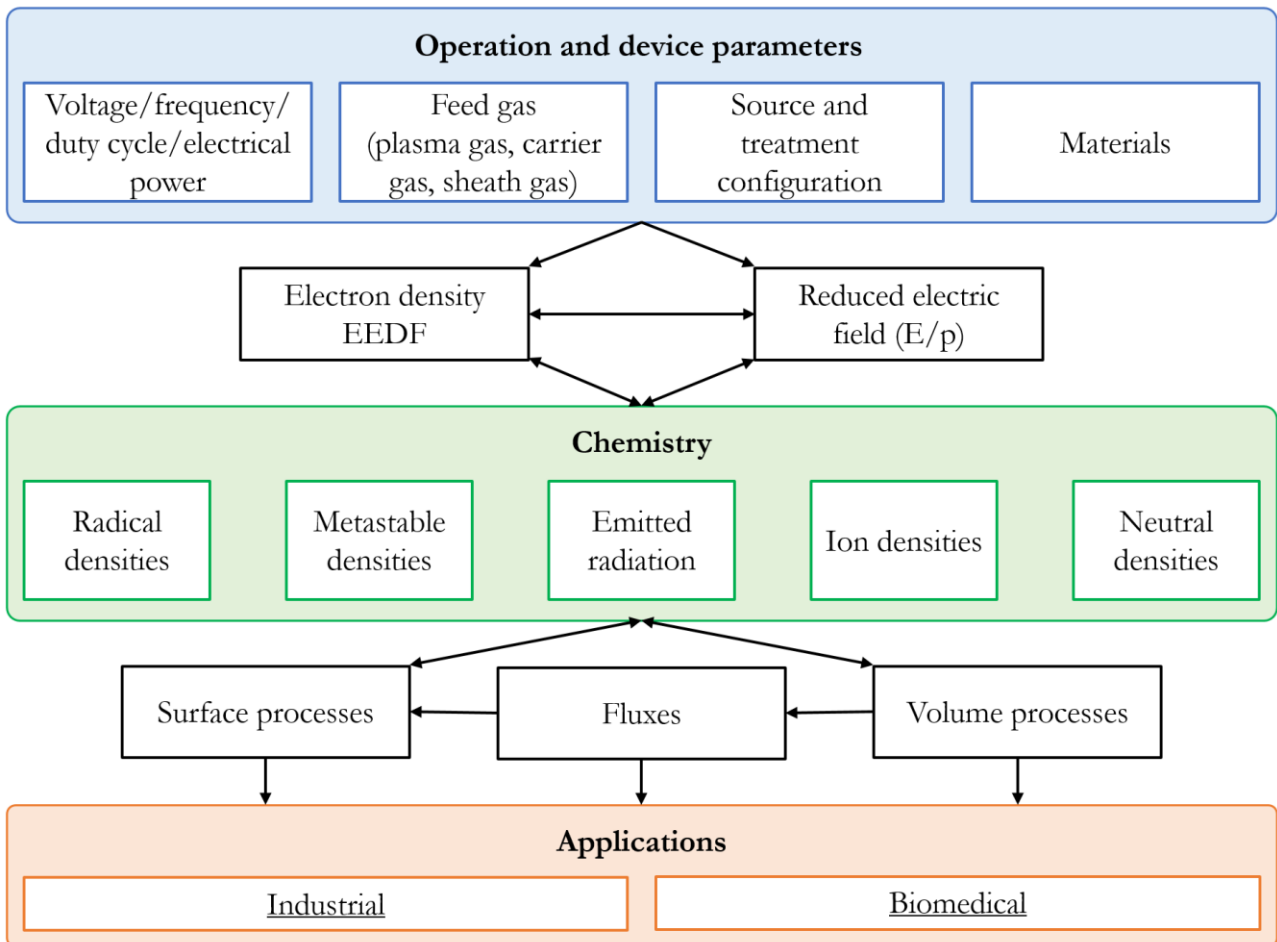


Fig. 3.1. Relation between device and operation parameters, plasma-induced physics and chemistry, and final applications of plasma processes [2].

In this context, the direct knowledge of the chemistry induced by plasma is a crucial step for the effectiveness of the process. Moreover, in the case of cold atmospheric pressure plasmas, the intrinsic

non equilibrium state leads a higher complexity of the system in which plasma fundamental theory (e.g. Maxwellian energy distribution) cannot always be verified and cannot fully support the experimental results [2]. Diagnostic techniques, able to give experimental information about the main features of plasma process, have been adopted since plasma was applied to the real industrial life: examples of traditional uses of plasma technology could be found in particularly for materials surface processing [3] such as etching [4], deposition of thin films [5] and modification of surface properties like hardness [6], corrosion resistance [7] or wettability [8].

The most used diagnostics for plasma processes could be divided in electrical measurements, optical and spectroscopic techniques.

Electrical characterization provides information regarding the energy deposited in the plasma system, and thus the power density used for the sustaining the discharge [2,9]. Different voltage waveforms, as well as pulsed, burst or continuous modes, can be adopted in view of the final application or energy costs. Fluid-dynamics of plasma discharges could be investigated through imaging techniques such as Shadowgraphy or Schlieren imaging [10–12].

Optical imaging diagnostics are widely used as non-intrusive technique, and are characterized by the detection of the whole radiation without any wavelength resolution. These diagnostics (such as CCD, iCCD, CMOS, Streak cameras imaging) offer the possibility to investigate the discharge morphology and its spatially and temporally resolved development [2,13–15].

When imaging is resolved in the field of wavelengths, diagnostics belong to the optical spectroscopy techniques. Being an optical diagnostic, spectroscopy maintains the advantages of being an in-situ, non-intrusive, spatially and temporally resolvable technique. The main feature of optical spectroscopy is related to obtain species-selective information [2,3,16]. Spectroscopic diagnostics can be divided in two main categories: passive, when the plasma emission is the only investigated radiation, and active, when an external light source interacts with plasma.

Optical Emission Spectroscopy (OES), the most important passive optical diagnostic, through the spectral and temporal analysis of plasma emission provides information relative to the electronically excited species like chemical composition of plasma gas phase, electronic vibrational and rotational temperatures, and electron density [2,16–21]. Although easily implemented and cost-effective, OES no information could be extrapolated about the ground state of species that represent the most abundant component in plasma and afterglow regions [3].

Active spectroscopy is based on the interaction of external radiation (generally produced by high intensity light source) with matter, in this case with the species involved in plasma, aim at obtaining direct measurements of species densities and temperature [2]. Absorption spectroscopy, optogalvanic spectroscopy, self-absorption, laser induced (or excited) atomic fluorescence (LIAF, LEAF), laser

induced (molecular) fluorescence (LIF), photofragmentation fluorescence, Rayleigh scattering, tunable diode laser absorption spectroscopy, tunable diode laser spectroscopy (TDLS), photo acoustic spectroscopy (PAS), light detection and ranging (LIDAR), differential absorption LIDAR (DIAL), cavity-ringdown spectroscopy (CRD), mask correlation spectroscopy, differential optical absorption spectroscopy (DOAS), Fourier Transform Infrared (FTIR) spectroscopy are examples of active spectroscopic techniques developed in different field of applications ranging from industrial to environmental [22–24].

In particular, optical absorption spectroscopy (OAS) provides a line-of-sight value of the absolute densities of species in their ground state [3] depending only on absorption coefficients and gas temperature [2]. Recently, Reuter et al. published a thorough review on the potentialities of absorption spectroscopy for the characterization of gas-phase chemistry produced by CAP sources [25]. They highlighted the method's simplicity and reliability in comparison with other spectroscopy techniques, such as LIF, mass spectroscopy or OES, because OAS is a non-invasive technique giving absolute densities, and is free of calibration procedures. Once known the main spectral properties (line strength, oscillator strength, or absorption cross-section), the absolute species concentration is trivially determined by solving the Beer–Lambert law. Moreover, OAS provides a direct knowledge on time-resolved species densities. In addition, the application of OAS method required the measurement of incident and transmitted intensities, resulting in a dimensional-less parameter, that simplifies considerably the data processing. As main drawbacks, OAS is characterized by line-of-sight averaged measurements and a lower sensitivity compared to laser-based techniques. By the way, the sensitivity drawback has been overcome by technical or methodical innovative solutions, comprising performant light sources and more sensitive detector technology. In case of axial symmetric *region of interest*, the line-integrated density can be converted in a space-resolved species distribution by means of the application of Abel inversion method or by the use of tomography technique [2,25].

The determination of reactive species average density and kinetics induced by CAP treatment is essential for the understanding of fundamental interactions in industrial and, even more, in medical applications involving the treatment of biological substrates [1,25].

OAS from UV to MIR radiation has been used for the detection of several species that play a key role in plasma processes such as $O_2(a^1\Delta_2)$, O_2 , O , N , O_3 , OH , N_2O_5 , H_2O_2 , $HONO$, $N_2(A)$, Ar^* , He^* , HNO_2 , HNO_3 , NO_2 , NO_3 as reviewed in [25] using appropriate experimental setup (light sources, monochromators, optical instrumentation, filter systems, photon detectors,...).

Recently, Monkhouse highlighted the necessity to develop on-line optical spectroscopy systems for species detection in industrial processes [23,24]. Optical spectroscopy provides a real-time fast

measuring system that collects and integrates signals in a non-intrusive and in-situ way [24]. These features can result not only in an improvement of industrial process monitoring but also can support the research in different scientific fields in which the knowledge of chemical kinetics is fundamental for a deeper understanding of investigated phenomena [23,24].

3.1.2. Overview of experimental activities

The knowledge of the chemistry induced in gas phase by CAP is a fundamental step for a more thorough understanding of CAP-derived effects on targeted substrates for any kind of final applications. As shown in previous chapters of this thesis, a Plasma Gun source was used to decontaminate root canal systems, to improve the bond strength adhesion between sealing materials and dentin, and finally to activate a liquid medium inducing pro-apoptotic properties. All these effects are directly and mainly affected by the amount and diversification of reactive species produced in gas phase and interacting with dentin surface or liquid medium as well. With the aim to optimize Plasma Gun treatments and better understand the mechanisms involved in the interaction of Plasma Gun with different substrates, great effort was given in the study of optical spectroscopy techniques for the gas phase characterization of a CAP treatment. Supported by two months of experience at Ghent University focused on emission and absorption spectroscopy under the supervision of Prof. Anton Nikiforov, an experimental setup for the detection of long-lived reactive species and for the measurement of plasma temperatures (electronic, vibrational and rotational) was first designed and then developed.

Since surface DBD are widely used in industrial and biological applications [26,27] for its ability to produce a highly reactive atmosphere independently from restrictive source parameters such as intra-electrode gap (for direct DBD or RBD) or gas flow rate (for APPJ), the kinetics of long-lived RONS produced by a surface DBD was investigated by means of spectroscopic techniques. The chemistry produced by a DBD operating in O₂/air is well established and studied because DBDs represents the technology mostly adopted for the industrial production of ozone [28–32]. In particular for air-fed ozonizers, or DBDs operating in air in general, the atmosphere generated by plasma sources is directly affected by the energy deposited in a cm³ of treated volume, or by the surface power density in case of stationary mode. At low power densities (<0,2 W/cm²), CAP treatment produces an ozone enriched atmosphere; while at high power conditions, the atmosphere shifts into a NO_x regime due to a so-called *ozone poisoning effect* [28–32,26,33–40]. The *ozone poisoning effect* is a time-dependent phenomenon [33] occurring at high power conditions, and thus it should affect the kinetics of NO_x (NO, NO₂, NO₃ and N₂O₅ molecules) concentrations in a time-dependent way as well. Although different studies demonstrated a direct correlation between the CAP-derived ozone concentration in

gas phase and the antimicrobial efficacy of CAP treatment [33–35], only few investigations were performed on the kinetics of both ROS and RNS densities [38,39].

Under these considerations, the *ozone poisoning effect* was studied through the measurements of the kinetics of O₃, NO₂ and NO₃ produced by a surface DBD working in air and stationary mode at different applied power densities. In order to perform high time-resolution acquisitions, the RONS kinetics were obtained by means of an absorption spectroscopy technique equipped with a Photo-Multiplier Tube (PMT) and fast oscilloscope. Electrical characterization of surface DBD was carried out to correctly evaluate the power density applied during the CAP treatment.

Moreover, since A. Fridman suggested that the *poisoning effect* is strictly affected by the vibrational excitation of the ground state of nitrogen molecules [26], the vibrational temperature of N₂ was determined by processing of OES measurements.

Finally, energy and cost management considerations, related to the obtained kinetics, were added in order to emphasize the potentialities of OAS techniques for industrial purposes.

It is worth mentioning that, although the activity was focused on the quantitative analysis of the chemistry produced by a surface DBD, OAS technique can be easily applied for the characterization of direct DBD and, in particular, atmospheric pressure Plasma Jet [25]. Indeed, further investigations based on OAS-OES techniques will be carried on with the scope of investigating the RONS kinetics promoted by a Plasma Gun source interacting with dental substrate and cell culture medium.

3.2. Material & Methods

3.2.1. Surface DBD plasma source

The CAP source adopted in this study is a surface DBD developed at the University of Bologna. A schematic of the plasma source is shown in Fig. 3.2. 2 mm of MICA layer is placed between the high voltage (HV) aluminium electrode and an AISI 316L mesh as grounded electrode in a DBD “sandwich” configuration. CAP is homogeneously produced on the surface of the mesh. The surface of the discharge is 6,75 cm². In order to confine the volume in which the plasma is generated, a closed chamber is designed with three quartz windows for optical spectroscopy analysis. The plasma source is driven by a micropulsed generator (AlmaPULSE, AlmaPlasma srl). The generator allows to apply high voltage in the range of 1-20 kV, with variable frequency (1-5 kHz, 10-20 kHz) and variable duty cycle (1-100%). To evaluate the power density dissipated by plasma source, voltage and current waveforms are recorded by means of voltage and current probes and oscilloscope (Tectronix).

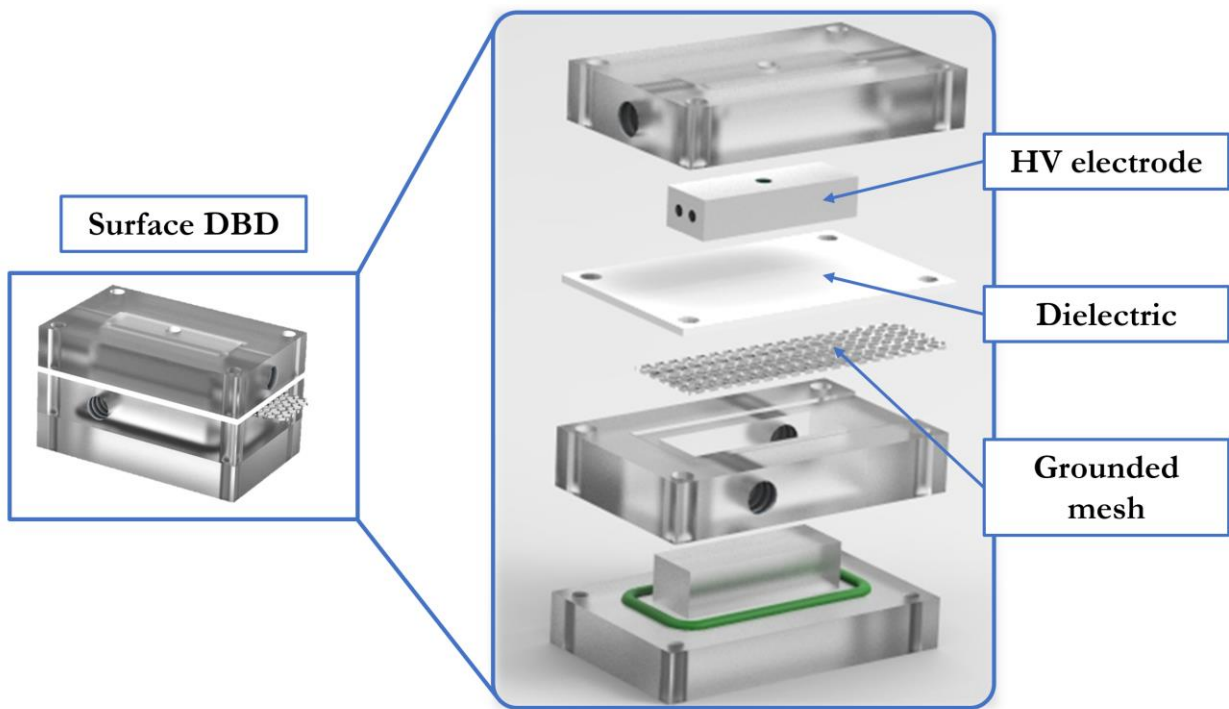


Fig. 3.2. 3D rendering of surface DBD plasma source used in the experimental activities.

3.2.2. Setup for optical absorption spectroscopy (OAS)

The setup for absorption spectroscopy is schematically represented in Fig. 3.3. A deuterium-halogen lamp, characterized by a broad band spectrum from UV to NIR radiation, is used as light source. The light beam is focused by means of optical fibres and fused silica lens (50 mm of focus length) to achieve a parallel beam passing through the plasma and then collected into the spectrometer. A 500 mm spectrometer (Acton SP2500i, Princeton Instruments) was used to collect and spectrally resolve the light beam in the UV, VIS and near infrared (NIR) regions. The width of the inlet slit is fixed at 15 μm for OAS acquisitions. The grating with a resolution of 1800 nm^{-1} is used. A photomultiplier tube (PMT - Princeton Instruments PD439) connected to a fast oscilloscope (Tecktronix) is used as detector to allow fast acquisitions and, then, to study the kinetics of investigating molecules with a time resolution of 0,04 sec. The outlet slit is kept open at 3 mm during OAS experiments. The PMT amplification factor is kept constant for all acquisitions. In order to ensure equal initial conditions, the discharge chamber is opened and flushed prior to every measurement.

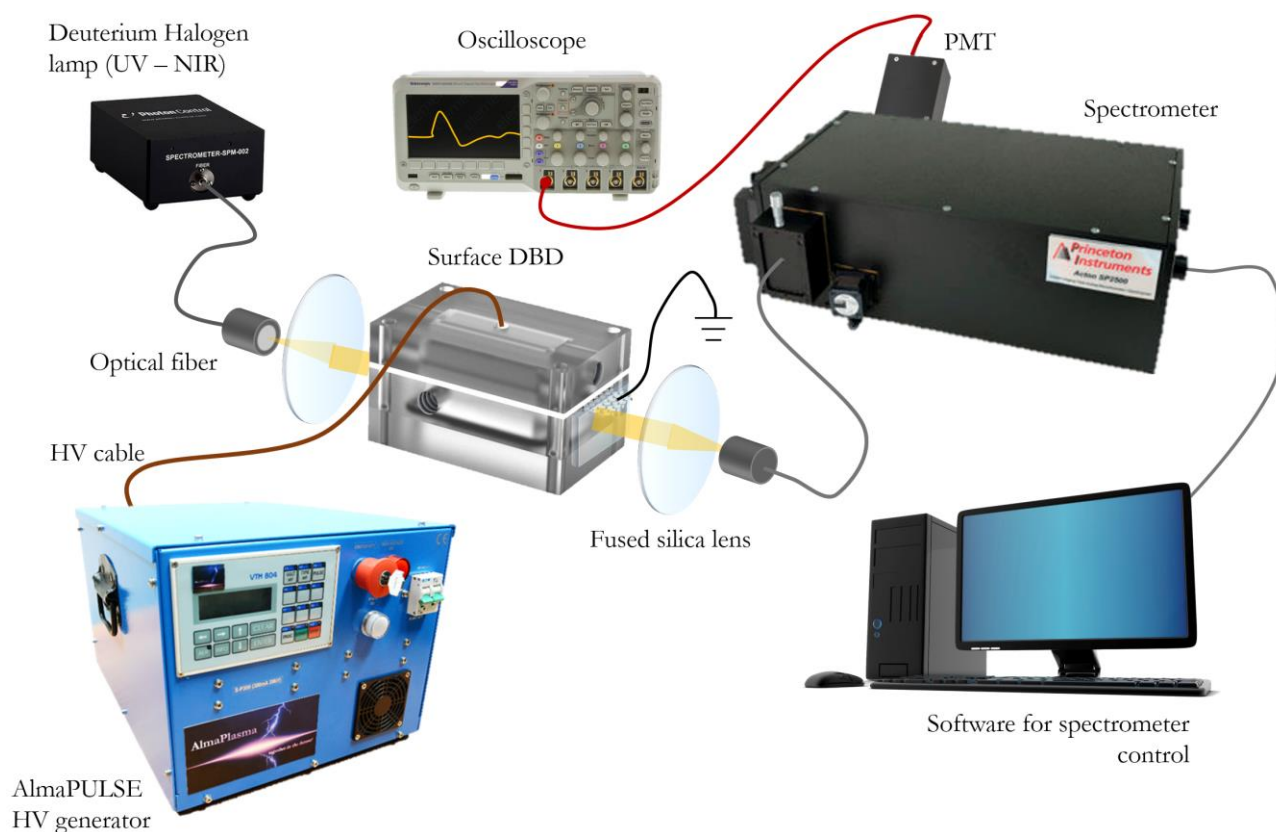


Fig. 3.3. Schematic of experimental setup for optical absorption spectroscopy.

3.2.3. Setup for optical emission spectroscopy (OES)

For OES setup (Fig. 3.4.), the plasma emission is directly collected through a quartz window in the back of source chamber (in front of the grounded mesh) by means of an optical fibre and collected with the same spectrometer used for OAS experiments. In order to achieve better resolved spectra, the inlet slit width is reduced to 7,5 μm . An Intensified CCD camera (iCCD – Princeton Instruments PIMAX 3) is preferred as detector. The acquisition parameters are tuned accordingly to the specific case (eg. for the cases with low plasma emission, the gain and the exposure time are consequently increased).

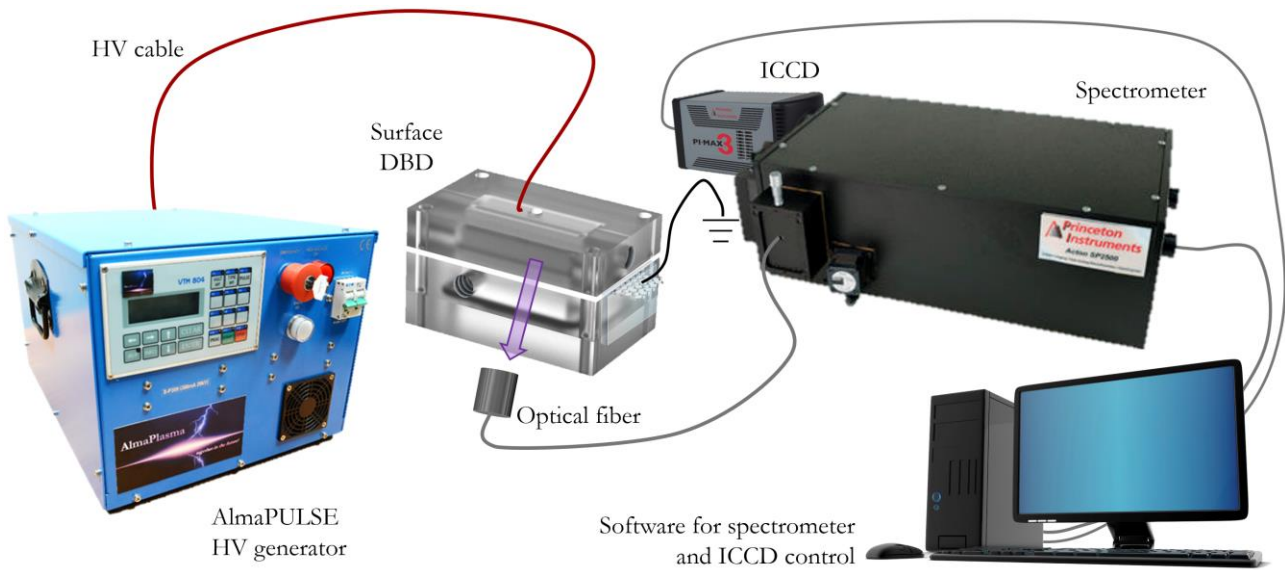


Fig. 3.4. Schematic of experimental setup for optical emission spectroscopy.

3.2.4. Data processing for OAS experiments

To quantitatively evaluate the species concentrations from absorption measurements, the Lambert-Beer law has to be taken into account, which describes the light absorption by a homogeneous medium as a function of the species density n in the medium as:

$$(1) \quad \frac{I}{I_0} = e^{(-L\sigma n)}$$

where I/I_0 is the ratio between the initial light intensity I and the light intensity remaining after an optical path length L through the medium I_0 . The probability of absorption is quantified by the absorption cross-section σ . The optical path length is equal to 4,5 cm in all experiments.

The wavelength range, specific for each investigated molecule (O_3 , NO_2 , NO_3), has been chosen according to Moiseev's studies [40] and integrated with the spectral resolution of the instrumentations used in this work (1,2 nm). Values for the absorption cross-sections are found by averaging data from

the MPI-Mainz UV/VIS Spectral Atlas database [41]. Tab. 3.1 presents the absorption cross-sections (in units of cm^2) for O_3 , NO_2 and NO_3 molecules:

Wavelength range	O_3 cross-section	NO_2 cross-section	NO_3 cross-section
$253 \pm 1,2$ nm	$(1,12 \pm 0,02)$ E-17	$(1,1 \pm 0,3)$ E-20	1 E-19*
$400 \pm 1,2$ nm	$(1,12 \pm 0,08)$ E-23	$(6,4 \pm 0,2)$ E-19	1 E-20*
$525 \pm 1,2$ nm	$(2,16 \pm 0,04)$ E-21	$(2,0 \pm 0,1)$ E-19	$(1,5 \pm 0,2)$ E-18

Tab. 3.1. Absorption cross-sections in cm^2 of the species of interest at each measurement wavelength. Values are obtained by averaging over a selection of studies from the MPI database, where for each study the average cross-section over the wavelength range was calculated. *: Values estimated by interpolation due to insufficient data to perform an averaging.

In order to correctly evaluate the light intensities, background and plasma emission radiations should be taken into account.

It is essential to consider a simultaneous contribution of different absorbing i -species ($i=1,2,\dots,N$) at a specific wavelength in the total absorption signal. In general, when N species can absorb at the same wavelength j , Lambert-Beer equation can be re-written as:

$$(3) \quad \frac{I}{I_0} = e^{(-L \sum_{i=1}^N \sigma_i n_i)} \text{ at } \lambda = \lambda_j$$

and solving it for the determination of the density n of specific species k :

$$(4) \quad n_k = -\frac{1}{L\sigma_k} \ln\left(\frac{I}{I_0}\right) - \sum_{i \neq k} \frac{\sigma_i}{\sigma_k} n_i$$

It shows that each secondary absorber n_i constitutes a weighted linear correction to the density of n_k , where the weight is equal to the ratio of the absorption cross-sections of the i -species with the k -species. Since the concentrations of species are unknown variables, a system of linear equations should be set, rewriting equation (4) in a more useful form:

$$(5) \quad \sigma_1 n_1 + \sigma_2 n_2 + \dots + \sigma_N n_N = -\frac{1}{L} \ln\left(\frac{I}{I_0}\right)$$

Since the equation presents N variables, N measurements of absorbance at N different wavelength have to be taken in order to close the linear system of equations, resulting in:

$$(6) \quad \begin{bmatrix} \sigma_{11} & \dots & \sigma_{1N} \\ \vdots & \ddots & \vdots \\ \sigma_{N1} & \dots & \sigma_{NN} \end{bmatrix} \begin{pmatrix} n_1 \\ \vdots \\ n_N \end{pmatrix} = \begin{pmatrix} b_1 \\ \vdots \\ b_N \end{pmatrix}$$

Where b_j with $j=1,2,\dots,N$ is the measured absorbance at the λ_j wavelength as:

$$(7) \quad b_j = -\frac{1}{L} \ln \left(\frac{I_j}{I_{0,j}} \right)$$

3.2.5. Data processing for OES experiments

Optical emission spectroscopy allows to characterize a plasma discharge starting from its spontaneous emission in a non-invasive way, with fast measurements and easy-to-implement instrumentation. In particular, the vibrational temperature T_{vib} can provide useful information on the chemical activity of the discharge, since the level of vibrational energy of heavy molecules is directly involved in many energy transfers and reactions. T_{vib} can be estimated from the relative intensity distribution of vibrational bands, belonging to a single electronic state but different vibrational quantum numbers.

Theoretically, intensity of an emission line can be expressed as [20,42,43]:

$$(8) \quad I_{v'v''} = h\nu_{v'v''} A_{v'v''} N_{v'}$$

where v', v'' refer to the vibrational quantum of upper (') and lower (') levels. $\nu_{v'v''}$ is the wave number of emission, $A_{v'v''}$ is the related Einstein's transition probability and $N_{v'}$ is the upper level density of molecule. Vibrational energy of a vibrational state v is:

$$(9) \quad E_v = w_e \left(v' + \frac{1}{2} \right) - w_e x_e \left(v' + \frac{1}{2} \right)^2 + w_e y_e \left(v' + \frac{1}{2} \right)^3 + \dots$$

where w_e , $w_e x_e$ and $w_e y_e$ are vibrational constant. Under the hypothesis of local thermal equilibrium (LTE), a Boltzmann distribution can describe the molecules population of the upper level molecules as:

$$(10) \quad N_{v'} = N_0 e^{-\frac{E'_v}{kT_{vib}}}$$

Where N_0 is atomic density and k is the Boltzmann constant.

The re-elaboration of the above-mentioned formulas results in the following equation:

$$(11) \quad \ln \left(\frac{I_{v'v''}}{\nu_{v'v''} A_{v'v''}} \right) = \ln(hcN_0) - \frac{E'_v}{kT_{vib}}$$

This equation shows a linear relationship between $\ln(I_{v'v''}/\nu_{v'v''} A_{v'v''})$ and E'_v and its data-representation leads to the use of Boltzmann's plot method, in which the T_{vib} is directly calculated from the slop of straight line.

Since the vibrational energy of N_2 is known to play a key role in the formation of NO molecule at low temperature (one of the most reactive quencher of ozone molecules) the relative intensity

distribution levels for the second positive system $N_2(C^3\Pi_u \rightarrow B^3\Pi_g)$ is investigated to determine T_{vib} of N_2 . The vibrational parameters of the system $N_2(C^3\Pi_u \rightarrow B^3\Pi_g)$ are reported in Tab. 3.2.

	w_e [cm^{-1}]	$w_e x_e$ [cm^{-1}]	$w_e y_e$ [cm^{-1}]
$N_2:C^3\Pi_u$	2047,18	28,45	2,0883
$N_2:B^3\Pi_g$	1733,39	14,12	-0,0569

Sequence $\Delta v = v' - v''$	Vibrational transition $v' - v''$	Wavelength λ [nm]	Transition probability $A_{v'v''} \cdot E6$ [s^{-1}]	E_v [eV]
+1	1-0	315,8	10,27	0,3721
	2-1	131,5	8,84	0,6139
	3-2	311,5	5,48	0,8526
-1	0-1	357,6	7,33	0,1255
	1-2	353,6	4,61	0,3721
	2-3	349,9	1,46	0,6139
-2	0-2	394,2	2,94	0,1255
	1-3	399,7	4,10	0,3721
	2-4	405,8	3,37	0,6139

Tab. 3.2. Vibrational parameters and transitions of $N_2(C^3\Pi_u \rightarrow B^3\Pi_g)$ for the determination of T_{vib} [42,43].

Finally, in order to evaluate the dissociation of N_2 molecules into N atoms, emission spectra are acquired in the wavelength range of 740-743,5 nm, in which a strong intensity N-line can be observed.

3.3. Results

3.3.1. Electrical characterization

The power density of the SDBD is recognized to be a key parameter for the production of RONS. The value of the power density dissipated in the plasma source was measured at voltages from 4 kV to 11 kV with 1 kV increments, with fixed frequency (10 kHz) and duty cycle (100%). The results, as shown in Fig. 3.5, are described by a quadratic polynomial (adj. R-square = 0.99955). The approximate relation between the applied voltage (in [kV]) and the power density (in [W/cm²]) is found to be:

$$(1) \quad P = 0,48 - 0,24V + 0,0336V^2$$

This quadratic behavior is in agreement with Dong et al [xxx], who proposed a relation of the form:

$$(2) \quad P = Af(V - V_0)^2$$

where A is proportional constant [W/(kHz·kV²·cm²)], f is the applied frequency [kHz] and V_0 is a parameter approximately equal to the voltage breakdown [kV].

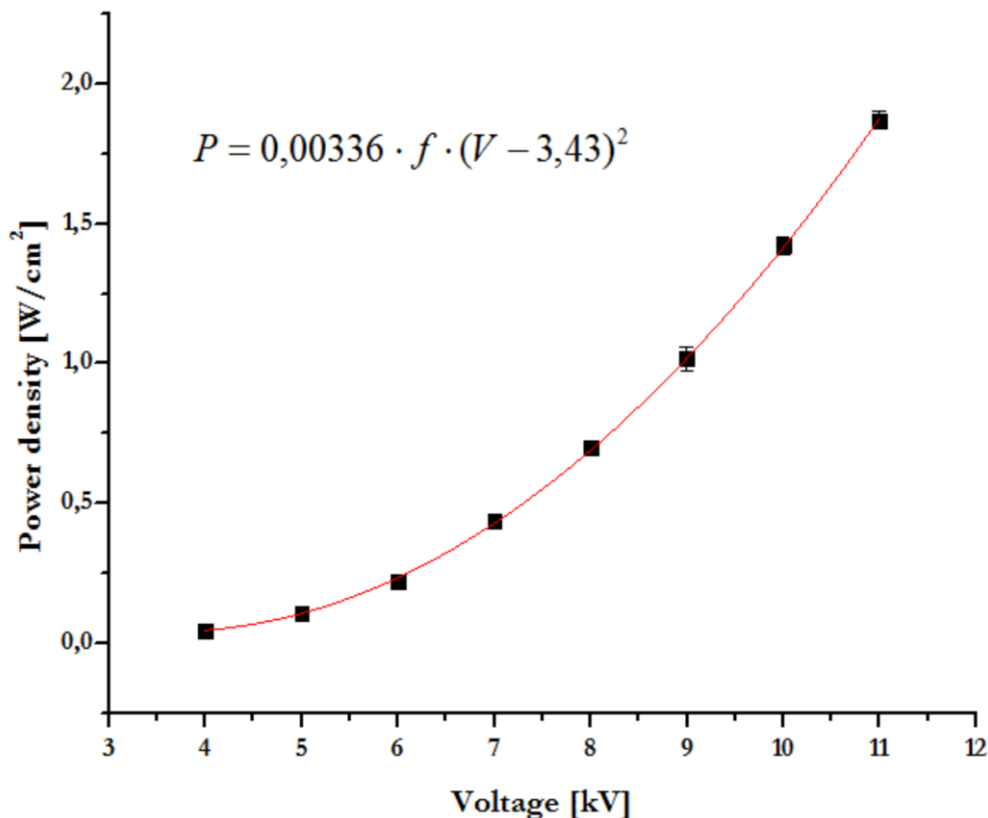


Fig. 3.5. Surface power density as a function of the applied voltage for 100% duty cycle and 10 kHz frequency of the SDBD ignition.

3.3.2. O₃ kinetics

The kinetics of ozone for the investigated power densities are shown in Fig. 3.6. At low power densities ($P \leq 0,011 \text{ W/cm}^2$), the ozone kinetics shows an increase of O₃ production with the increase of surface power density. After 90 sec of plasma treatment, the highest ozone density around 3500 ppm is achieved when the SDBD working at $0,11 \text{ W/cm}^2$. Once the value of power density overcomes $0,11 \text{ W/cm}^2$, the ozone kinetics changes: its concentration reaches the maximum and then starts to decrease, resulting in the ozone quenching phenomenon. The higher the power density the faster the ozone quenching is. Ozone density becomes undetectable within 30 sec of treatment by OAS experimental setup for $P > 0,70 \text{ W/cm}^2$. It must be noted that the initial ozone production rate remains proportional to the applied voltage for all tested power densities.

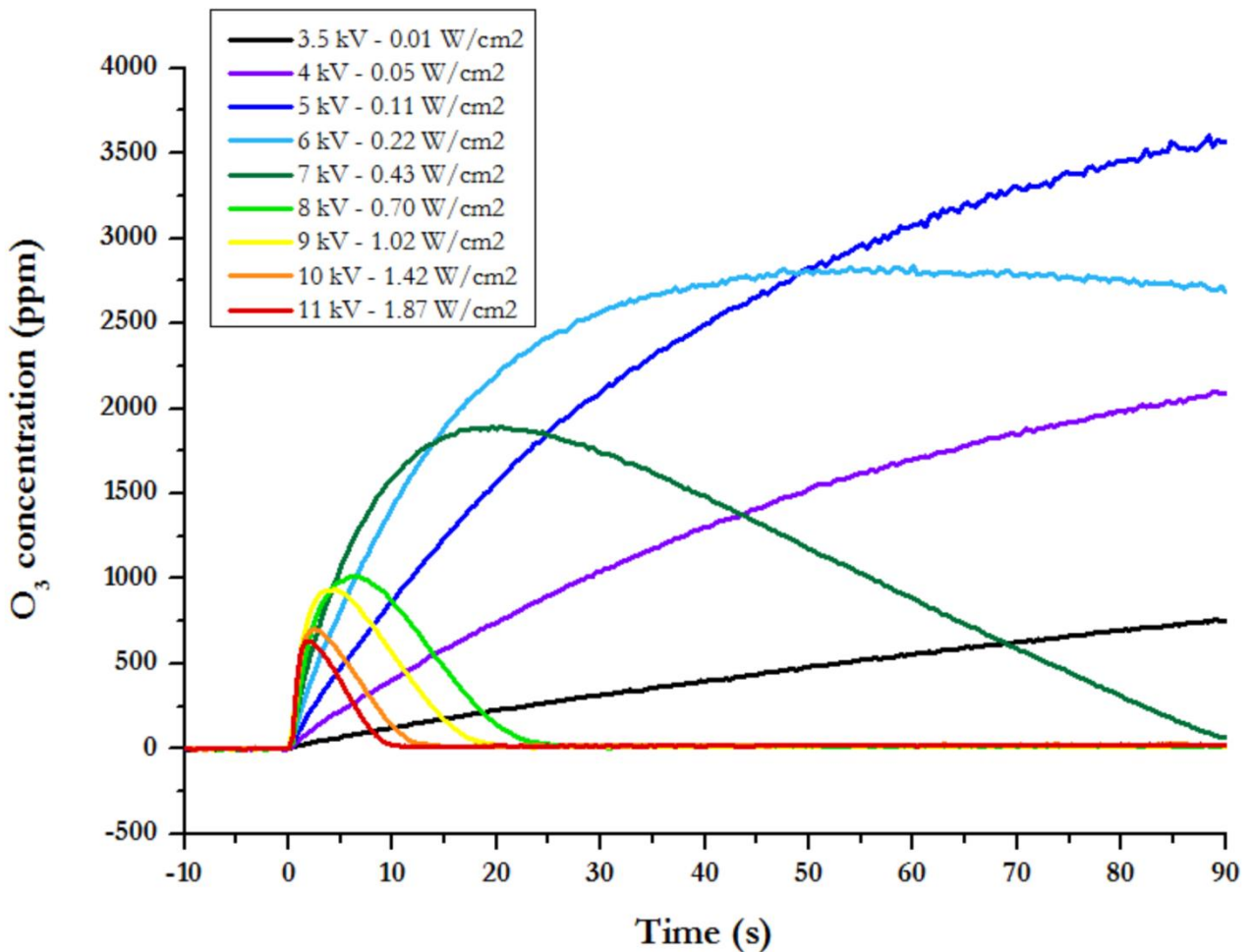


Fig. 3.6. Kinetics, for different surface power densities ($0,01 - 1,87 \text{ W/cm}^2$), of O₃ density produced during 90 sec of SDBD plasma treatment.

3.3.3. NO₃ kinetics

The kinetics of NO₃ depending on the power density in the range between 0,01 – 1,89 W/cm², is shown in Fig. 3.7. The results underline that the time behaviour of NO₃ concentration follow the ozone kinetics. In along with ozone kinetics, the density of NO₃ steadily increases for power densities lower than 0,11 W/cm² reaching higher values of concentration for higher values of power density. The maximum value of NO₃ density achieved within the 90 sec of plasma treatment is around 3500 ppm working at 0,1-0,2 W/cm². For P > 0,22 W/cm², NO₃ molecules start to be quenched with a rate proportional to the power density. As for the ozone studies, with P > 0,7 W/cm² the concentration of NO₃ is undetectable within 30 sec after discharge ignition.

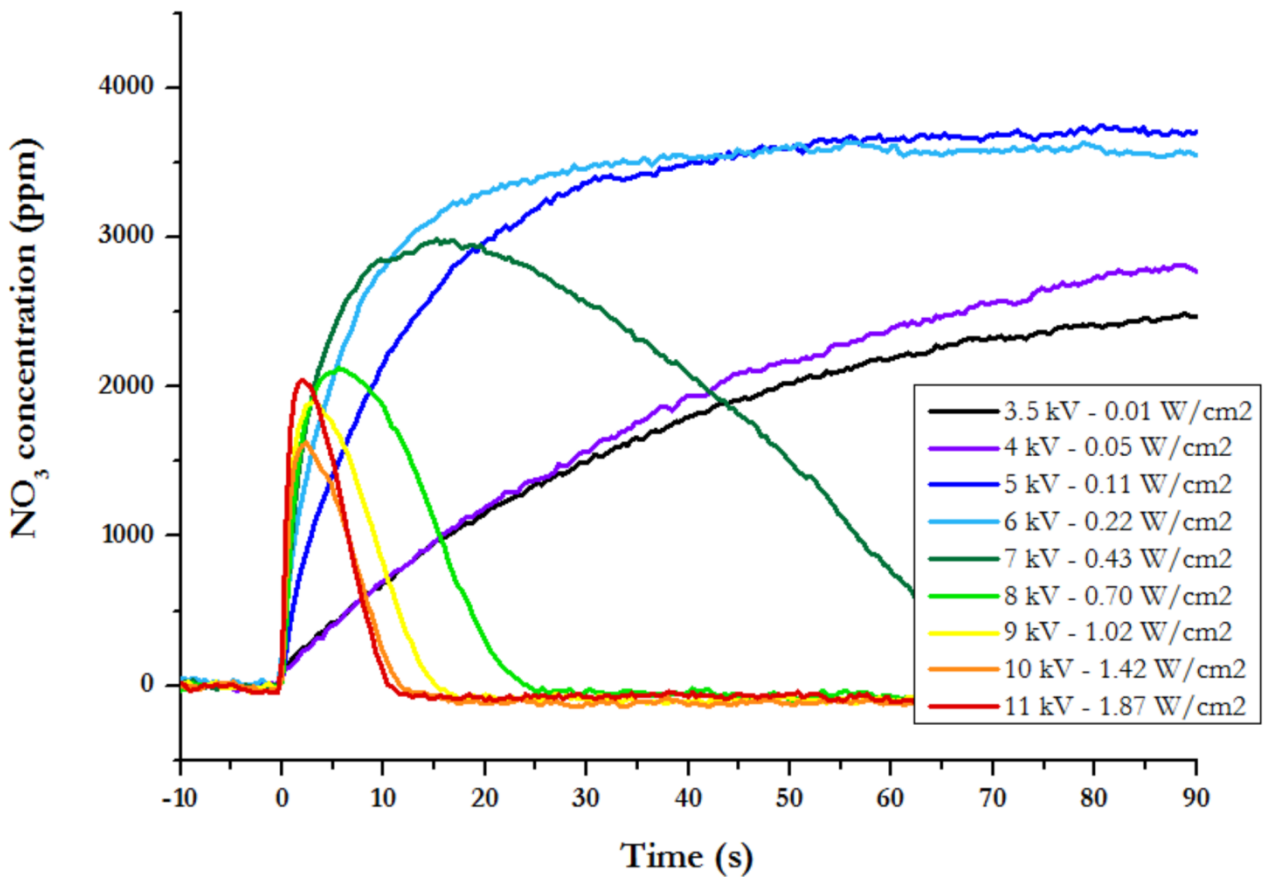


Fig. 3.7. Kinetics, for different surface power densities (0,01 – 1,87 W/cm²), of NO₃ density produced during 90 sec of SDBD plasma treatment.

3.3.4. NO₂ kinetics

The study of RONS has been accomplished by the measurements of kinetics of another stable product, NO₂. The measured NO₂ kinetics for different power densities (0,01 - 1,87 W/cm²) are presented in Fig. 3.8 considering 90 sec of plasma treatment time. Differently from O₃ and NO₃ concentration profiles, NO₂ molecules are detectable only working with power density higher than 0,22 W/cm², corresponding to the overcoming of the threshold for O₃ quenching. Within the first 30 sec, NO₂ production rate is proportional to the power density; on the other hand, after 30 sec higher is the applied power density lower is the NO₂ production rate. The highest concentration of NO₂, around 1400 ppm, is obtained after 90 sec working above the power density level of 0,7 W/cm².

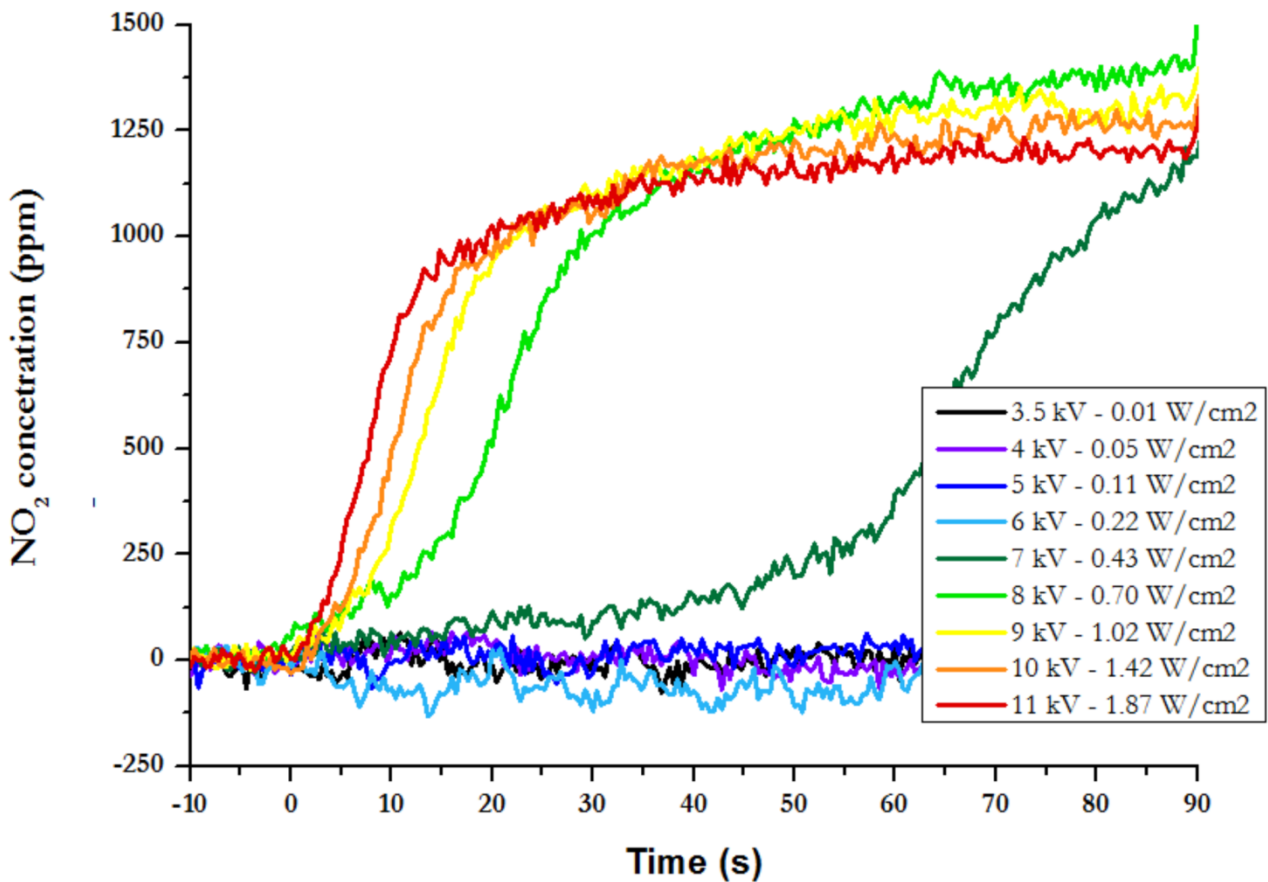


Fig. 3.8. Kinetics, for different surface power densities (0,01 – 1,87 W/cm²), of NO₂ density produced during 90 sec of SDBD plasma treatment.

3.3.5. Measurements of vibrational temperature of N₂

The values of T_{vib} of N₂ measured by means of OES technique are plotted in Fig. 3.9 as a function of applied voltage. The T_{vib} has a linear dependence on the voltage applied to SDBD. The results highlight the non-equilibrium state of the plasma in which vibrational temperature is higher than the gas temperature of 320 K.

As reported in [26], the NO production at low temperature stimulated by vibrational energy of N₂ increases significantly for T_{vib} of N₂ higher than 0,4 eV (around 4700 K). The experimental data obtained in this work show how this value can be overcome with applied voltage higher than 5 kV, corresponding to power densities higher than 0,11 W/cm². At these power densities, ozone quenching is experimentally observed, as previously described.

On the left side of Fig. 3.9, the emission spectrum of N atoms for each investigated condition is reported. The N emission is observable for power densities higher than 0,11 W/cm², and the intensity of the line is directly proportional to the applied power density.

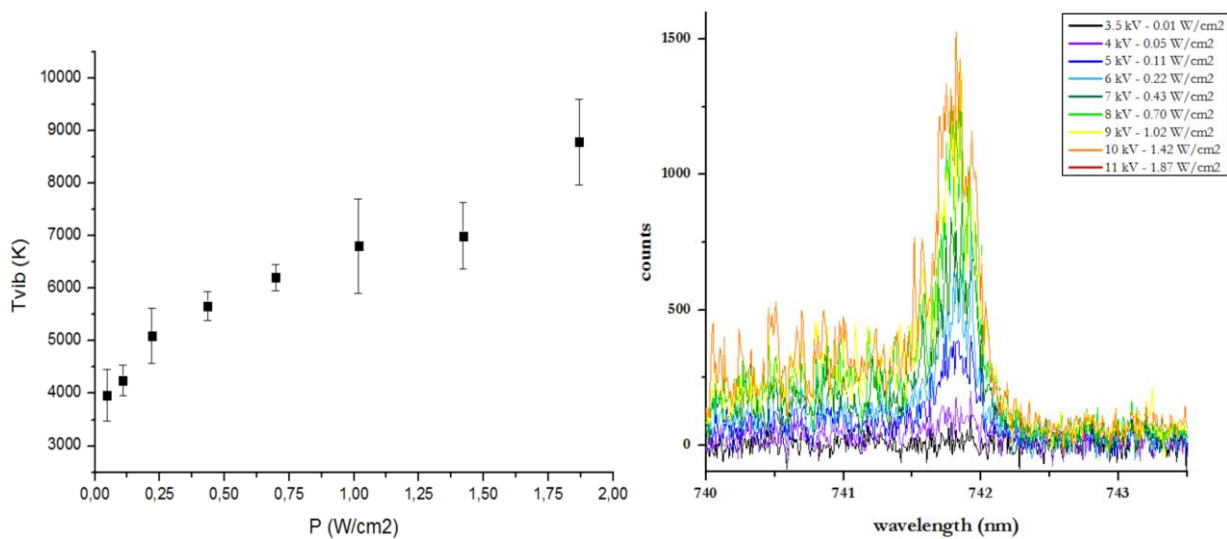


Fig. 3.9. Values of T_{vib} of N₂ (left) and the emission spectra related to N-line at 742 nm (right) measured for different power densities by means of OES technique. Frequency: 10 kHz, Duty Cycle: 100%. Gas is around ambient temperature (25°C).

3.4. Discussion of results

Differently from oxygen ozonisers, in air plasmas the production-destruction cycle of ozone is affected by the presence of nitrogen molecules and air humidity [28,29,31,26,33,34,37–39]. Several gas-phase reactions between charge, excited and neutral species run simultaneously in the plasma and in the afterglow region involving different RONS such as ozone (O₃), nitrogen oxides (NO, NO₂, NO₃, N₂O₃...) and nitric acids (HNO₂, HNO₃...). The main reaction pathways regarding O₃, NO₃ and NO₂ are reported in Tab. 3.3 highlighting the reactions involved in the production and in the destruction cycles. For a greater clarity, the reactions are divided into three different groups: *plasma*, reactions with radicals and highly-reactive species taking place mainly in the plasma region; *neutral*, reactions between neutral species that characterize the afterglow chemistry; *water-based*, reactions involving water-based molecules like OH, H₂O, HNO, HNO₂...

Plasma	Neutral	Water-based
O₃ production		
R1. O+O ₂ →O ₃ (10 ⁻²¹)		
O₃ destruction		
R2. O ₃ +e→O+O ₂ ⁻ (10 ⁻¹⁵)	R5. O ₃ +NO→NO ₂ +O ₂ (10 ⁻²⁰)	R8. O ₃ +H→OH+O ₂ (10 ⁻¹⁷)
R3. O ₃ +O→2O ₂ (10 ⁻²⁰)	R6. O ₃ +NO ₂ →NO ₃ +O ₂ (10 ⁻²³)	R9. O ₃ +OH→HO ₂ +O ₂ (10 ⁻¹⁹)
R4. O ₃ +N→NO+O ₂ (10 ⁻²¹)	R7. O ₃ +M→O ₂ +O (10 ⁻³²)	R10. O ₃ +HO ₂ →OH+2O ₂ (10 ⁻²¹)
NO₃ production		
R11. NO ₂ +O→NO ₃ (10 ⁻¹⁸)	R12. NO ₂ +O ₃ →NO ₃ +O ₂ (10 ⁻²⁵)	R14. OH+HNO ₃ →NO ₃ +H ₂ O (10 ⁻²¹)
	R13. N ₂ O ₅ →NO ₃ (10 ⁻²⁵)	
NO₃ destruction		
R15. NO ₃ +O→NO ₂ +O ₂ (10 ⁻¹⁷)	R17. NO ₃ +NO ₂ →N ₂ O ₅ (10 ⁻¹⁷)	R19. NO ₃ +OH→HO ₂ +NO ₂ (10 ⁻¹⁷)
R16. NO ₃ +NO→2NO ₂ (10 ⁻¹⁷)	R18. 2NO ₃ →NO ₂ +O ₂ (10 ⁻²²)	R20. NO ₃ +HO ₂ →HNO ₃ (10 ⁻¹⁸)
NO₂ production		
R21. NO ₃ +O→NO ₂ +O ₂ (10 ⁻¹⁷)	R26. O ₃ +NO→NO ₂ +O ₂ (10 ⁻²⁰)	R31. NO ₃ +OH→NO ₂ +HO ₂ (10 ⁻¹⁷)
R22. NO+NO ₃ →2NO ₂ (10 ⁻¹⁷)	R27. N ₂ O ₃ +HO ₂ →NO ₂ +NO (10 ⁻²⁰)	R32. OH+HNO ₂ →NO ₂ +H ₂ O (10 ⁻¹⁸)
R23. NO+HO ₂ →NO ₂ +OH (10 ⁻¹⁷)	R28. N ₂ O ₄ →2NO ₂ (10 ⁻²⁰)	R33. HNO+O ₂ →NO ₂ +OH (10 ⁻²¹)
R24. O+NO→NO ₂ (10 ⁻¹⁸)	R29. 2NO ₃ →2NO ₂ +O ₂ (10 ⁻²²)	R34. O+HNO ₂ →NO ₂ +OH (10 ⁻²¹)
R25. O ₃ +NO→NO ₂ +O ₂ (10 ⁻²⁰)	R30. N ₂ O ₅ →NO ₂ +NO ₃ (10 ⁻²⁵)	R35. HNO ₂ +HNO ₃ →2NO ₂ +H ₂ O (10 ⁻²³)
		R36. 2HNO ₂ →NO ₂ +NO+H ₂ O (10 ⁻²⁰)
NO₂ destruction		
R37. NO ₂ +N→N ₂ O+O (10 ⁻¹⁷)	R41. NO ₂ +NO ₃ →N ₂ O ₅ (10 ⁻¹⁷)	R45. NO ₂ +H→OH+NO (10 ⁻¹⁰)
R38. NO ₂ +O→NO ₃ (10 ⁻¹⁸)	R42. 2NO ₂ →N ₂ O ₄ (10 ⁻²⁰)	R46. NO ₂ +OH→HNO ₃ (10 ⁻¹⁸)
R39. NO ₂ +NO→N ₂ O ₃ (10 ⁻²¹)	R43. NO ₂ +NO→N ₂ O ₃ (10 ⁻²¹)	
R40. NO ₂ +O→NO+O ₂ (10 ⁻²¹)	R44. NO ₂ +O ₃ →O ₂ +NO ₃ (10 ⁻²³)	

Tab. 3.3. Main reaction pathways involving O₃, NO₃, NO₂, separated into plasma radical-dependent reactions, reactions between long-lived neutral species and water-dependent reactions which are enabled by air humidity. The reactions are ordered by descending reaction rate, indicated in brackets (). All reactions taken from [37].

Ozone is mainly formed by the reaction between oxygen atoms, formed by electron impact dissociation of O_2 , and oxygen molecules following the reaction R1. As Yagi and Tanaka [28] showed in their study on air-fed ozonisers, the formation rate of O atoms is directly proportional to the surface power density. This relation between the production of O and the power density supports the behaviour of ozone kinetics during the first seconds of plasma treatment in which the ozone rate production increases linearly with the power density.

On the other hand, different pathways (R2, R4) may cause the depletion of ozone also in an oxygen atmosphere and these reactions should be taken into account in the development and control of pure oxygen ozone generator. In the case of air plasma, such as for air-fed ozonisers, the main contribution in the destruction of ozone is given by NO_x molecules forming the catalytic cycle represented by R5 and R6 [28,31], which consume directly ozone and by R38 that reduces the O atoms density, reagent of O_3 formation reaction. Clearly the study of NO_x kinetics becomes essential to understand the O_3 kinetics as function on power density.

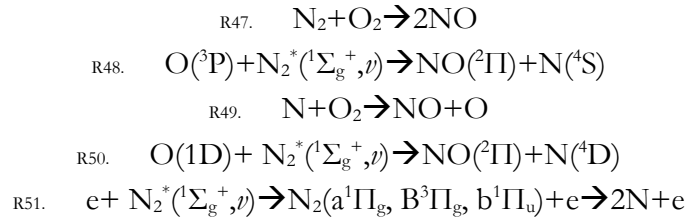
If a $P > 0,22 \text{ W/cm}^2$ is applied to the SDBD, a significant reduction of ozone concentration is observed. Several studies on air ozonisers [28,29,31] and on air micro-discharges [26] describe this phenomenon as the *ozone poisoning effect* and suggest that it is caused by an increase of nitrogen oxides as NO and NO_2 . When the concentration of NO- NO_2 exceeds the threshold value of about 0,1%, the reactions R24 and R40 become faster competitive with R1 and thus remove O atoms involving in the ozone formation.

As shown in the kinetics profiles obtained in the experiments, NO_2 becomes detectable when O_3 is going to be completely quenched. This behaviour supports the fact that firstly NO_2 reacts with O_3 and O following the reactions R44 and R40 and then, when the O_3 density drops, NO_2 may be stored and accumulated, resulting in an increase of its concentration. Higher the power density applied, faster the ignition of *ozone poisoning effect* and the NO_2 density build-up. On the other hand, after 30 seconds working at high power densities ($P > 1,4 \text{ W/cm}^2$) the NO_2 density tends to stabilize itself, showing an equilibrium among NO_2 formation-depletion reactions; while at the lower power densities of the poisoning regime ($0,22 \text{ W/cm}^2 < P < 1,4 \text{ W/cm}^2$) the NO_2 concentration increases continuously during the plasma treatment time due to the slower quenching of ozone, and thus shifting the equilibrium toward the NO_2 formation. Since the experiment were performed at ambient air with a relative humidity in the order of 20-40%, the NO_2 equilibrium may be described by the formation reactions (R24, R28) with high reactive species (O, NO, O_3) and depletion reactions based on HNO_x and OH (R31, R32, R33, R34, R35, R36), that can be considered as water-based molecules.

As far as the chemistry related to NO_3 is concerned, the molecule of NO_3 can be considered as the final step of the ozone depletion in humid atmosphere, where the reaction R17 can be neglected [31].

In the region of *ozone poisoning*, the total quenching of ozone leads to the decay of NO₃ concentration which is manifested by the appearance of NO₂, experimentally measured. The comparison of the kinetics of O₃, NO₂ and NO₃ shows that at low power densities NO₂ is completely consumed in the reactions with a relevant amount of ozone promoting the formation of NO₃. The *ozone poisoning effect* is noticeable as threshold phenomenon, associated to a fast increase of NO-NO₂ density. As a matter of fact, the NO molecule is generally recognized to be the major quencher of O₃ [26,33] because it can react with ozone to form NO₂. Different experimental and modelling studies analysed the NO production and loss reaction pathways [26,44–47]. In Tab. 3.4, the main mechanisms for the production of NO molecules are reported.

Mechanisms involved in the NO synthesis



Tab. 3.4. Main mechanisms of NO synthesis provided in non-thermal plasma [26].

The process of NO synthesis, expressed by the reaction R47, is limited by the breaking of the strong bond (10 eV) in the N₂ molecule. At high temperature, the chain propagation formed by the sum of R48 and R49, gives the total NO synthesis (R47), and this reactions chain is well known in chemical kinetics as Zeldovich mechanism. The reaction R51, taking place in air non-thermal plasmas, shows an alternative and more efficient mechanism for direct N₂ dissociation based on a stepwise electronic excitation sequence, resulting in an added production of N atoms for the NO synthesis reaction R49. Neutral molecules, low-excited by electron impact in non-equilibrium discharges, promote the formation of highly vibrationally excited N₂ molecules in air through vibrational-vibrational (VV) energy exchanges. The reaction R48 and R50, those can take place in non-equilibrium plasmas at low temperature, show other mechanisms, more efficient than the direct reaction R47, to synthesize NO stimulated by non-equilibrium vibrational excitation of nitrogen molecules. Moreover, R48 and R50 form free N atoms, reagents for the fast reaction R49, producing an extra amount of NO molecules. These considerations support the importance of a N₂ population vibrationally excited in non-equilibrium discharges in the process for the synthesis of NO and, thus, for the promotion of ozone quenching. Moreover, in respect to the NO synthesis at high temperature plasma, in which the energy is distributed over all degrees of freedom, including those non effective in the NO synthesis, in air non-equilibrium discharges most of energy is transferred from electrons to vibrational excitation of N₂ molecules [26].

In Fig. 3.10, A. Fridman showed the fast increase of energy efficiency of NO production in air plasma as a function of energy input comparing thermal with CAP-assisted NO-synthesis [26].

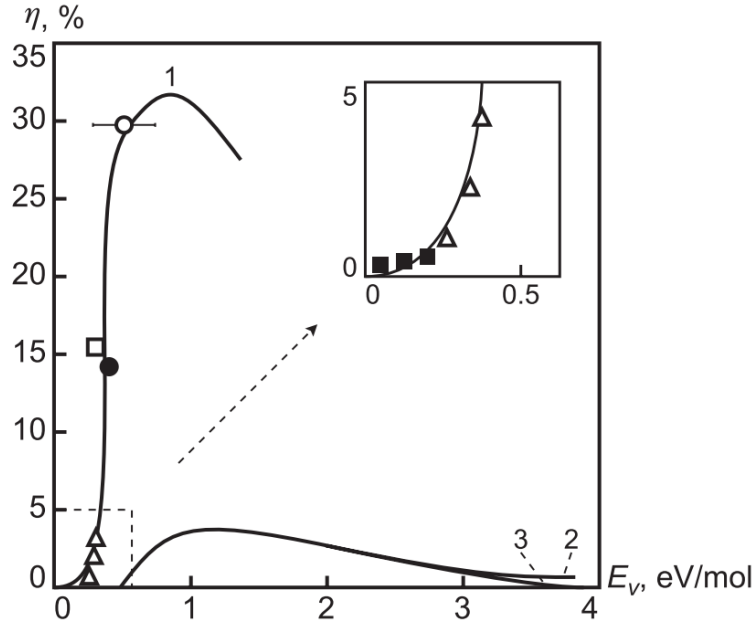


Fig. 3.10. Energy efficiency of NO synthesis in air plasma as a function of energy input: (1) non-equilibrium process stimulated by vibrational excitation; (2,3) thermal synthesis with (2) ideal and (3) absolute quenching [26].

In order to run chemical reactions by stimulation of vibrational excited N_2 molecules, the vibrational temperature (T_{vib}) of N_2 should be high enough to avoid the vibrational-translational (VT) relaxation. Fridman underlined how the temporal increasing evolution of vibrational temperature continues reaching a critical value for which the consumption of vibrational energy for NO synthesis stabilizes the growth of T_{vib} of N_2 [26]. Theoretically, NO synthesis is characterized by a critical value of $T_{vib}^{min}=0,20-0,25$ eV ($\sim 2300 - 2900$ K) and, to maintain a stable synthesis, a higher value of stationary vibrational temperature (T_{vib}^{St}) should be achieved in the plasma active zone [26]. Thus, the production of NO is strictly dependent on the T_{vib} of N_2 and becomes stable with a stationary vibrational temperature around 4000-5000 K; in these conditions, the VT relaxation can be neglected with respect to chemical reactions [26].

The measurements of T_{vib} highlight a proportional relation between T_{vib} and the applied power density. T_{vib} reaches values over 5000 K for $P > 0,22$ W/cm², where the quenching of ozone starts to be observable. The correlation between the T_{vib} and ozone kinetics seems to support the idea that, after a critical value of T_{vib} of N_2 , a stable production of NO molecules occurs resulting in the *ozone poisoning effect*. Moreover, the production of free N atoms, due to the N_2 vibrational excitation, at power densities higher than 0,11 W/cm² is experimentally proven by the emission on N-line at 742 nm as reported in Fig. 3.9.

Shimizu et al [33] developed a simple model (the chemical reactions involved are reported in Tab. 3.5), based on the idea that $N_2(v)$ (N_2 molecule vibrationally excited) is a key species to quench O_3 .

Shimizu's model reactions	
R52.	$O + O_2 + M \rightarrow O_3 + M$ (10^{-46})
R53.	$N_2(v) + O \rightarrow NO + N$ (10^{-17})
R54.	$O_3 + NO \rightarrow NO_2 + O_2$ (10^{-20})
R55.	$O + NO + M \rightarrow NO_2 + M$ (10^{-43})

Tab. 3.5. List of reactions used in Morfill's model with relative order of magnitude of the rate constant in brackets () [33].

The model shows that, in an example case of $P=0,3 \text{ W/cm}^2$, ozone is mainly quenched by NO generated by $N_2(v)$ and O atoms, and that the *poisoning effect* starts once T_{vib} of N_2 becomes stable around 4700 K. The stabilization of T_{vib} requires time and the overcoming of the critical value is dependent by the power density. These considerations lead to a better understanding of the characteristic timing of O_3 quenching: higher is the applied power density, higher is the T_{vib} of N_2 , greater the NO production, resulting in a faster ozone quenching.

The kinetics analysis of long-lived neutral species leads to consider the treatment time and surface power density as two key parameters for the control of afterglow chemistry. Similar value of ozone density (around 2000 ppm) can be achieved operating at $0,02 \text{ W/cm}^2$ for 90 seconds or at $0,41 \text{ W/cm}^2$ for only 20 seconds; on the other hand, considering the energy consumption (simply multiplying the power density for the plasma generating surface and the treatment time), the first plasma treatment, that consumes around 12,5 J, results to be cheaper than the short treatment at high power density, corresponding at a consumption of 55,4 J. These considerations can become interesting for the applications involved in the field of water treatments [48–51] or NO_x removal processes [26]. Differently, in order to quench completely the ozone and achieve a NO_x -enriched atmosphere, greatly demanding for chemical technologies of fertilizers and explosives [26], short treatment at high power density (energy consumption is around 101,3 J) is more convenient than a long plasma treatment at a power density close to the threshold values for discharge poisoning, that consumes around 249,5 J for the complete ozone depletion.

The experimental activity presented in this work supported the idea of using OAS technique as an on-line monitoring system for the control of plasma activated atmosphere. The possibility to monitor in real-time the kinetics of the most important reactive species can pave the way for the development of a retro-active system based on OAS diagnostic to implement in industrial (plasma-assisted) processes. Moreover, as discussed above, the characterization of gas phase by means of spectroscopy

techniques can gain a deeper understating of the CAP-effects in biological applications correlating the chemistry in gas phase with the chemistry induced in biological target or liquid substrates.

3.5. Conclusions

Optical absorption and emission spectroscopy was adopted in this experimental activity in order to investigate the *ozone poisoning effect*. Surface DBD can activate air promoting an ozone- or NO_x-enriched atmosphere operating at low or high applied power densities respectively. As reported in literature, the experimental results proved that the *ozone poisoning effect* behaves as a threshold phenomenon and it is observable for applied power densities higher than 0,11 W/cm². Moreover, the kinetics analysis highlighted the temporal dynamics of poisoning and how the chemical composition of the atmosphere changes in time. The measurements of vibrational temperature of nitrogen molecules supported A. Fridman's explanation regarding the ozone poisoning effect: once overcome a critical value of vibrational energy (~ 5000 K), NO synthesis becomes possible at low temperature and NO production rate increases significantly, resulting in the ignition of a strong ozone quenching. Kinetics study provided also important considerations about the energy costs for the production of active atmosphere with a specific chemical composition. Finally, the activity supported the idea to adopt and develop OAS diagnostic as on-line monitoring system for the control of plasma-assisted processes and optimization of plasma treatment for biomedical applications. Further investigations will be carried out to characterize the gas phase chemistry produced by a Plasma Gun source treating dental substrates and cell culture medium. The achievable information will gain a deeper understanding of the Plasma Gun-effects in the explored field of dentistry and oncology.

3.6. Bibliography

- [1] Fridman A, Friedman G. Plasma Medicine. 2013.
- [2] Bruggeman P, Brandenburg R. Atmospheric pressure discharge filaments and microplasmas: physics, chemistry and diagnostics. *J Phys D Appl Phys* 2013;46:464001.
- [3] Sadeghi N. Molecular Spectroscopy Techniques Applied for Processing Plasma Diagnostics. *J Plasma Fusion Res* 2004;80:767–76.
- [4] Detter X, Palla R, Thomas-Boutherin I, Pargon E, Cunge G, Joubert O, et al. Impact of chemistry on profile control of resist masked silicon gates etched in high density halogen-based plasmas. *J Vac Sci Technol B Microelectron Nanom Struct Process Meas Phenom* 2003;21:2174–83.
- [5] Shimizu T, Iizuka S, Kato K, Sato N. High quality diamond formation by electron temperature control in methane–hydrogen plasma. *Plasma Sources Sci Technol* 2003;12:S21.
- [6] Kaltofen R, Sebald T, Schulte J, Weise G. Plasma substrate interaction effects on composition and chemical structure of reactively rf magnetron sputtered carbon nitride films. *Thin Solid Films* 1999;347:31–8.
- [7] Camps E, Muhl S, Alvarez-Fregoso O, Juarez-Islas JA, Olea O, Romero S. Microwave plasma nitriding of pure iron. *J Vac Sci Technol A Vacuum, Surfaces, Film* 1999;17:2007–14.
- [8] Coulson SR, Woodward IS, Badyal JPS, Brewer SA, Willis C. Ultralow surface energy plasma polymer films. *Chem Mater* 2000;12:2031–8.
- [9] Staack D, Farouk B, Gutsol A, Fridman A. Characterization of a dc atmospheric pressure normal glow discharge. *Plasma Sources Sci Technol* 2005;14:700–11.
- [10] Settles GS, Hargather M. A review of recent developments in schlieren and shadowgraph techniques. *Meas Sci Technol* 2017.
- [11] Settles GS. *Schlieren and shadowgraph techniques: visualizing phenomena in transparent media*. Springer Science & Business Media; 2001.
- [12] Boselli M, Colombo V, Gherardi M, Laurita R, Liguori A, Sanibondi P, et al. Characterization of a Cold Atmospheric Pressure Plasma Jet Device Driven by Nanosecond Voltage Pulses 2014:1–13.
- [13] Kettlitz M, Höft H, Hoder T, Weltmann K-D, Brandenburg R. Comparison of sinusoidal and pulsed-operated dielectric barrier discharges in an O₂/N₂ mixture at atmospheric pressure. *Plasma Sources Sci Technol* 2013;22:25003.
- [14] Gerling T, Hoder T, Bussiahn R, Brandenburg R, Weltmann K-D. On the spatio-temporal dynamics of a self-pulsed nanosecond transient spark discharge: a spectroscopic and electrical analysis. *Plasma Sources Sci Technol* 2013;22:65012.
- [15] Gherardi M, Puač N, Marić D, Stancampiano A, Malović G, Colombo V, et al. Practical and theoretical considerations on the use of ICCD imaging for the characterization of non-equilibrium plasmas. *Plasma Sources Sci Technol* 2015;24:64004.
- [16] Ochkin VN. *Spectroscopy of low temperature plasma*. 2009.
- [17] Stancu GD, Kaddouri F, Lacoste D a, Laux CO. Atmospheric pressure plasma diagnostics by OES, CRDS and TALIF. *J Phys D Appl Phys* 2010;43:124002.

- [18] Laux CO, Spence TG, Kruger CH, Zare RN. Optical diagnostics of atmospheric pressure air plasmas. *Plasma Sources Sci Technol* 2003;12:125.
- [19] Lu XP, Leipold F, Laroussi M. Optical and electrical diagnostics of a non-equilibrium air plasma. *J Phys D Appl Phys* 2003;36:2662–6.
- [20] Herzberg G. *Molecular spectra and molecular structure*. vol. 1. Read Books Ltd; 2013.
- [21] Bruggeman PJ, Sadeghi N, Schram DC, Linss V. Gas temperature determination from rotational lines in non-equilibrium plasmas: a review. *Plasma Sources Sci Technol* 2014;23:23001.
- [22] Platt U, Stutz J. *Differential Optical Absorption Spectroscopy*. 2008.
- [23] Monkhouse P. On-line diagnostic methods for metal species in industrial process gas. *Prog Energy Combust Sci* 2002;28:331–81.
- [24] Monkhouse P. On-line spectroscopic and spectrometric methods for the determination of metal species in industrial processes. *Prog Energy Combust Sci* 2011;37:125–71.
- [25] Reuter S, Sousa JS, Stancu GD, Hubertus van Helden J-P. Review on VUV to MIR absorption spectroscopy of atmospheric pressure plasma jets. *Plasma Sources Sci Technol* 2015;24:41.
- [26] Fridman A. *Plasma Chemistry*. 2008.
- [27] Kogelschatz U. Dielectric-Barrier Discharges: Their History, Discharge Physics, and Industrial Applications. *Plasma Chem Plasma Process* 2003;23:1–46.
- [28] Yagi S, Tanaka M. Mechanism of ozone generation in air-fed ozonisers. *J Phys D Appl Phys* 1979;12:1509–20.
- [29] Kogelschatz U, Eliasson B, Hirth M. Ozone generation from oxygen and air Discharge physics and reaction mechanisms. *Ozone Sci Eng* 1988;10:12.
- [30] Kogelschatz U. Atmospheric-pressure plasma technology. *Plasma Phys Control Fusion* 2004;46:B63–75.
- [31] Kogelschatz U, Baessler P. Determination of Nitrous Oxide and Dinitrogen Pentoxide Concentrations in the Output of Air-Fed Ozone Generators of High Power Density. *Ozone Sci Eng* 1987;9:195–206.
- [32] Kogelschatz U. Dielectric-barrier Discharges : Their History, Discharge Physics, and Industrial Applications. *Plasma Chem Plasma Process* 2003;23:1–46.
- [33] Shimizu T, Sakiyama Y, Graves DB, Zimmermann JL, Morfill GE. The dynamics of ozone generation and mode transition in air surface micro-discharge plasma at atmospheric pressure. *New J Phys* 2012;14.
- [34] Pavlovich MJ, Chang H-W, Sakiyama Y, Clark DS, Graves DB. Ozone correlates with antibacterial effects from indirect air dielectric barrier discharge treatment of water. *J Phys D Appl Phys* 2013;46:145202.
- [35] Shimizu T, Zimmermann JL, Binder S, Li Y, Cantzler M, Weilemann H, et al. Surface micro-discharge plasma for disinfection 2016;115012:145202.
- [36] Pavlovich MJ, Clark DS, Graves DB. Quantification of air plasma chemistry for surface disinfection. *Plasma Sources Sci Technol* 2014;23.

- [37] Sakiyama Y, Graves DB, Chang H-W, Shimizu T, Morfill GE. Plasma chemistry model of surface microdischarge in humid air and dynamics of reactive neutral species. *J Phys D Appl Phys* 2012;45:425201.
- [38] Vinogradov IP, Wiesemann K. Classical absorption and emission spectroscopy barrier discharges in N₂/NO and O₂/NO_x mixtures. *Plasma Sources Sci Technol* 1997;6:307–16.
- [39] Graham RA, Johnston HS. The Photochemistry of NO₃ and the Kinetics of the N₂O₅ - O₃ System. *J Phys Chem* 1978;82:254–68.
- [40] Moiseev T, Misra NN, Patil S, Cullen PJ, Bourke P, Keener KM, et al. Post-discharge gas composition of a large-gap DBD in humid air by UV–Vis absorption spectroscopy. *Plasma Sources Sci Technol* 2014;23:65033.
- [41] Keller-Rudek H, Moortgat GK, Sander R, Sorensen R. MPI-Mainz UV/VIS Spectral Atlas of Gaseous Molecules of Atmospheric Interest n.d.
- [42] Xiaolong Deng. Atmospheric Pressure Plasma Jet for the Deposition of Nanocomposite Antibacterial Coatings 2015:135–7.
- [43] Shemansky DE, Broadfoot AL. Excitation of N₂ and N₂⁺ systems by electrons—I. Absolute transition probabilities. *J Quant Spectrosc Radiat Transf* 1971;11:1385–400.
- [44] Gaens W Van, Bogaerts a. Reaction pathways of biomedically active species in an Ar plasma jet. *Plasma Sources Sci Technol* 2014;23:35015.
- [45] Tanaka H, Ishikawa K, Mizuno M, Toyokuni S, Kajiyama H, Kikkawa F, et al. State of the art in medical applications using non-thermal atmospheric pressure plasma. *Rev Mod Plasma Phys* 2017;1:3.
- [46] Lu X, Naidis G V., Laroussi M, Reuter S, Graves DB, Ostrikov K. Reactive species in non-equilibrium atmospheric-pressure plasmas: Generation, transport, and biological effects. *Phys Rep* 2016;630:1–84.
- [47] Uddi M, Jiang N, Adamovich I V., Lempert WR. Nitric oxide density measurements in air and air/fuel nanosecond pulse discharges by laser induced fluorescence. *J Phys D Appl Phys* 2009;42.
- [48] Pavlovich MJ, Sakiyama Y, Clark DS, Graves DB, Machala Z, Tarabova B, et al. Non-thermal plasmas in and in contact with liquids. *J Phys D Appl Phys* 2016;10:53001.
- [49] Locke BR, Sato M, Sunka P, Hoffmann MR, Chang JS. Electrohydraulic Discharge and Nonthermal Plasma for Water Treatment. *Ind Eng Chem Res* 2006;45:882–905.
- [50] Locke BR. Environmental Applications of Electrical Discharge Plasma with Liquid Water -A Mini Review. *Int J Plasma Environ Sci Technol* 2012;6:194–203.
- [51] Foster JE. Plasma-based water purification : Challenges and prospects for the future Plasma-based water purification : Challenges and prospects for the future. *Phys Plasmas* 2017;24.

4. Development of Plasma Gun source

4.1. Introduction

The application of cold atmospheric pressure plasmas in the medical research field has been growing rapidly in the last years. Promising studies regarding the positive effects of CAP treatment in dermatology, in microbiology and in oncology, have prompted the scientific community to address the common effort towards the development of innovative medical therapies assisted by CAP technology [1–7]. Among other limiting factors of this growth, the wide variety of different plasma sources and biological systems investigated, that avoid a direct comparison of scientific data [8]. Since a plasma treatment is characterized by a great complexity and variability of effective plasma parameters, an accurate definition of “plasma dose” has not been yet fully developed and accepted [1]. Furthermore, the majority of the studies was performed on *in vitro* or *ex vivo* biological samples, and in many fields of application only few clinical trial studies were carried out. These evidences caused a limited introduction of plasma technology in the medicine field, and as a matter of fact, only few plasma-based medical devices were fully developed and marketed. First approach of plasma in medical application could be found in the 1970s with the development of innovative scalpels for electrosurgical procedures able to promote a fast coagulation induced by a thermal argon plasma [1,9–12]. Firstly, two different plasma devices, the Plazon system [1,13–16] and the microwave plasma torch MicroPlaSter [17–22], developed for wound healing and skin regeneration applications, were designed to produce an atmosphere enriched with biophysical active species and, after the performing of different *in vivo* tests assessing their effectiveness and safety, were commercialized. DBD sources were introduced as potential plasma medical device by the Fridman’s research group of Drexel University, Philadelphia (USA), that worked on the development of a Floating Electrode Dielectric Barrier Discharge (FE-DBD) operating with the biological tissue as counter electrode. Different studies were run aim at evaluating the FEDBD performances varying from coagulation to immune system stimulation [2,23–29]. Based on DBD configuration, in Germany clinical trials to investigate the safety, efficacy and applicability of DBD plasma source, called PlasmaDerm (CINOGY GmbH Duderstadt, Germany), for the treatment of chronic wounds, was conducted and revealed promising results that support the registration of CE marking for medical devices in 2013 [30–36]. Concerning atmospheric pressure plasma jets, the kINPen jet source developed by the INP Greifswald, Germany, has been comprehensively investigated with regard to estimate the biological effects, to characterize physical and chemical plasma characteristics, and to perform a risk assessment [37–43]; and under responsibility of Neoplas tools GmbH, Greifswald, Germany, which fulfills the technical requirements of a medical device, an optimized version named kINPen MED was developed [1,8,44–

46]. An images collection of the described CAP devices for medical application is reported in Fig. 4.1.

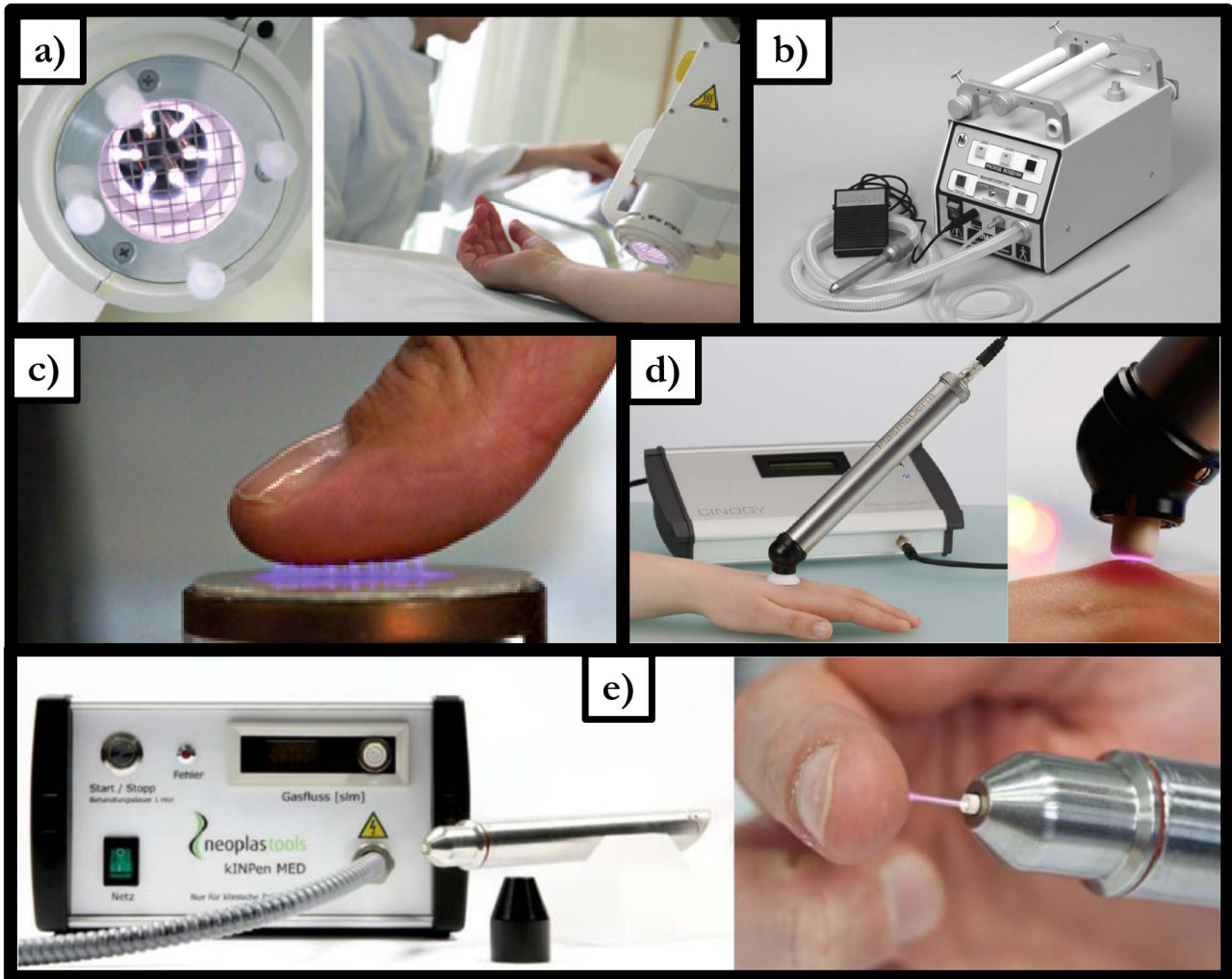


Fig. 4.1. Plasma devices for medical applications: a) plasma torch “MicroPlaSter” [47], b) air plasma unit “Plazon” [14], c) Floating Electrode DBD “FE-DBD” [27], d) DBD plasma source “PlasmaDerm” [1], e) atmospheric pressure argon plasma jet “kINPen MED” [1].

For a common development of plasma technologies for medicine, the involvement of medical expertise and stakeholders is crucial. Moreover, in order to estimate the benefits and potential side effects of CAP-assisted therapies, the definition of basic criteria for the performance characterization of CAP devices represents a fundamental step [8]. Firstly, in Germany general requirements for basic safety and essential performances were hypothesized and DIN-SPEC 91315 with the title “General requirements for medical plasma sources” was drafted as a complement to the existing standards and rules for medical devices [8]. This document should be considered as a first attempt to regularize the development of CAP-based medical devices, based on a common consensus between the all stakeholders involved and aimed at the benefit of the society as a whole [8].

On the other hand, the application of DIN-SPEC 91315 can support the development of a CAP device for medical application, but for the real exploitation in medical world and for the achievement of the certification as medical device, *in vivo* clinical trials should be carried to fulfill the high expectations of patients and ensure the functionality and safety of medical plasma sources [8].

4.2. Development of a medical device prototype based on Plasma Gun configuration

In light of the promising results obtained in the field of dental and cancer applications, a thorough design and development of a source based on the Plasma Gun concept was conducted. With the aim to ensure a high level of reliability and safety, both for user and for patient, a risk assessment based on standard IEC 14971 [48] was performed on the laboratory prototype of Plasma Gun, resulting in the individuation of the most hazardous issues. After the evaluation of risk factors, through the indications provided by standard IEC 60601 [49], a new plasma device was designed based on the solutions found for the electrical and structural issues.

To receive a CE marking as medical device, general requirements have to be satisfied. The directive 2007/47/EC concerning medical devices states that the devices have to be designed and manufactured considering the clinical benefit/ risk profile and that their use don't compromise the clinical status and safety of patients, the safety and health of users [50].

As suggested by standard ISO 4971 "Medical devices - Application of risk management to medical devices" [48], the risk assessment was performed identifying firstly the risks associated to the Plasma Gun source, analysing and evaluating the risk factors and, finally, implementing technical solutions aiming at reducing the risks.

The risk assessment comprises a phase of risk analysis in which the intended use, the main characteristics to the safety of the medical device, and the associated hazards are identified and the risks for each hazardous situation are estimated, and a phase of risk evaluation, considering the risk severity, the risk probability and the benefits/risk ratio.

The risk management continues with a risk control phase through which a risk control option analysis is carried out with the aim to design and implement new solutions for the reduction of associated risks. A residual risk evaluation should be performed and, thus, a new risk/benefit analysis can be run. The final step of risk management is the evaluation of overall residual risk acceptability.

The design and the development of a new Plasma Gun source were run focusing the attention on the structural and electrical hazards. After the risk assessment, new solutions regarding the electrical connections, the gas connections, the conductive and grounded external case of the plasma source, the dielectric internal structure, were considered during the design of the prototype. In particular, the adopted solutions were aimed at reducing the ignition of undesired discharges, at avoiding the

transition to arc plasma, at decreasing the overheating of the source for operating times greater than 5 minutes, at simplifying the operations of assembly and disassembly of the source and substitution of a single component.

Moreover, a gas supply system and a specific pulse generator were implemented to move towards the development of a table-top stand-alone device.

In Fig. 4.2., a schematic evolution of Plasma Gun is reported highlighting the development of the source towards the realization of a prototype of medical device based on Plasma Gun configuration.



Fig. 4.2. Development of Plasma Gun source.

Finally, a compact CAP device to be exploited in *in-vivo* medical procedures was designed and developed. As shown in Fig. 4.3, the CAP system is composed by the Plasma Gun source that can be hand-heldable, a dedicated pulse generator, a compact gas supply system, with a user-friendly interface. The micropulsed He DBD plasma can propagate through a dielectric capillary and a

touchable plasma plume is formed at the outlet of the device, due to the mixing of He plasma with the surrounding ambient air. The terminal part of the glass tube is removable and autoclavable, ensuring a high level of safety and sterility in clinics. The device is electrically insulated, in order to guarantee safe handling for the users. The working gas (Helium) is supplied from a small disposable tank, designed to last for several treatments at relatively low flow rates (0.5-3 slpm) and easily replaceable when empty. The CAP system features a high versatility in various applications: as given an example, for instance, both a thin plume for endodontic practice and a larger plume for surface treatment can be generated, coupling disposable tips of various shapes with the terminal part of the glass tube.

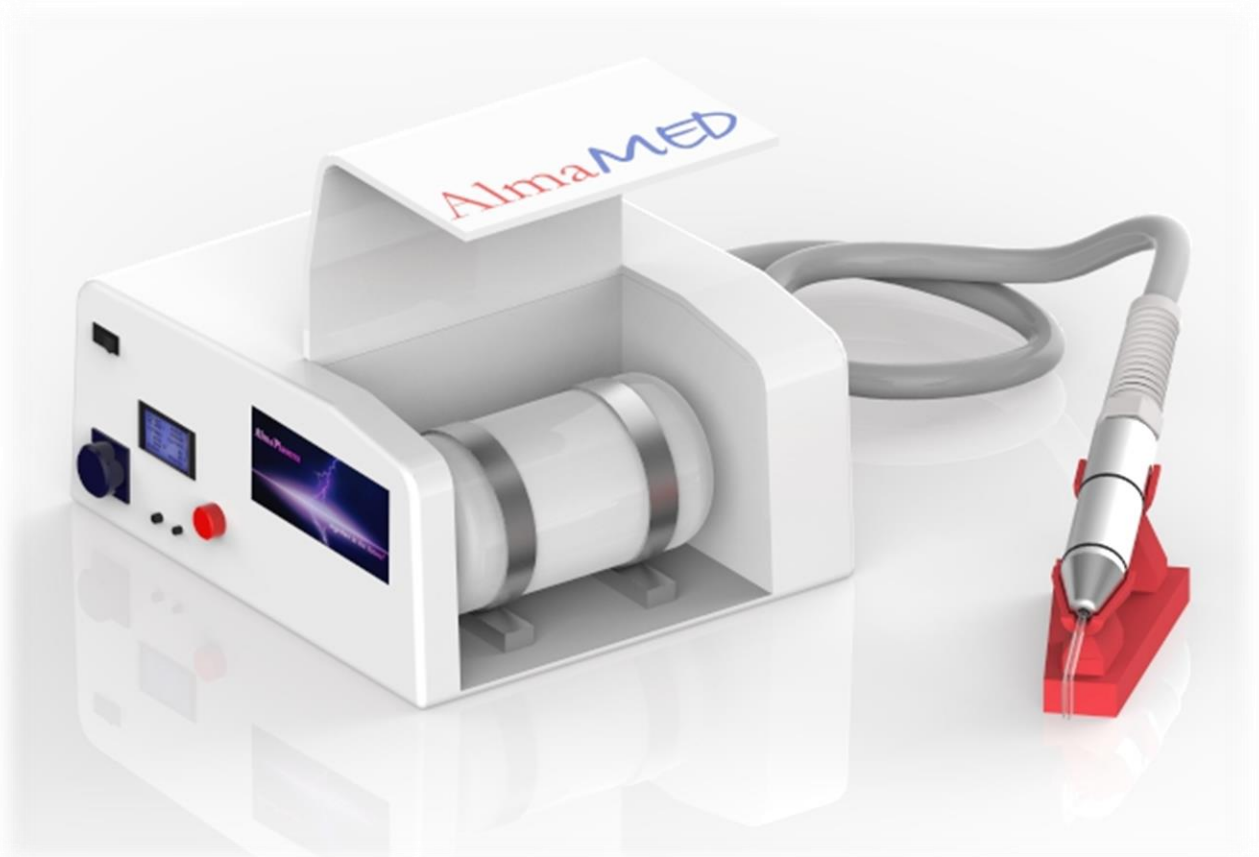


Fig. 4.3. Rendering of table-top stand-alone CAP system for biomedical applications.

The study resulted effectively in the development of a CAP system based on Plasma Gun configuration producing a painless plasma plume (Fig. 4.4), exploitable in real clinical procedure.



Fig.4.4. Photos of plasma plume produced by the CAP system [51,52].

It is worth mentioning that, in order to achieve the CE marking as medical device, further analyses should be carried out. In particular, as required by standard ISO 10993 [53], whose primary aim is the protection of humans from potential biological risks arising from the use of medical devices, biological tests and investigations such as:

- ▶ Tests for genotoxicity, carcinogenicity and reproductive toxicity
- ▶ Tests for interactions with blood
- ▶ Tests for *in vitro* cytotoxicity
- ▶ Tests for local effects after implantation
- ▶ Ethylene oxide sterilization residuals
- ▶ Framework for identification and quantification of potential degradation products
- ▶ Tests for irritation and skin sensitization
- ▶ Tests for systemic toxicity
- ▶ Sample preparation and reference materials
- ▶ Identification and quantification of degradation products from polymeric medical devices
- ▶ Identification and quantification of degradation products from ceramics
- ▶ Identification and quantification of degradation products from metals and alloys
- ▶ Animal welfare requirements
- ▶ Toxicokinetic study design for degradation products and leachables
- ▶ Establishment of allowable limits for leachable substances
- ▶ Chemical characterization of materials
- ▶ Physico-chemical, morphological and topographical characterization of materials
- ▶ Principles and methods for immunotoxicology testing of medical devices

are suggested depending on the intended use for a thorough biological evaluation of a generic medical device.

Furthermore, as discussed above, no international standard exists regarding medical devices based on atmospheric pressure non thermal plasmas; the DIN-SPE 91315 recommends to perform further tests that can allow to control and compare the effects induced by a CAP system, designed for biomedical applications [8]. Biological test procedures (inactivation of microorganisms in-vitro, cytotoxicity, and detection of chemical species in liquids) and physical test methods (temperature, thermal capacity, optical emission spectrometry, UV-irradiance, gas emission, and leakage current) are provided in the mentioned specification to obtain basic information about performance characteristics as well as effectiveness and safety of a medical CAP system.

The presented work, supported by promising results in the endodontic and cancer fields, paved the way towards the realization and development of a prototype of medical device based on Plasma Gun configuration.

4.3. Bibliography

- [1] Von Woedtke T, Metelmann HR, Weltmann KD. Clinical Plasma Medicine: State and Perspectives of in Vivo Application of Cold Atmospheric Plasma. *Contrib to Plasma Phys* 2014;54:104–17.
- [2] Fridman G, Friedman G, Gutsol A, Shekhter AB, Vasilets VN, Fridman A. Applied plasma medicine. *Plasma Process Polym* 2008;5:503–33.
- [3] Adamovich I, Baalrud SD, Bogaerts A, Bruggeman PJ, Cappelli M, Colombo V, et al. The 2017 Plasma Roadmap: Low temperature plasma science and technology. *J Phys D Appl Phys* 2017;50:323001.
- [4] Tanaka H, Ishikawa K, Mizuno M, Toyokuni S, Kajiyama H, Kikkawa F, et al. State of the art in medical applications using non-thermal atmospheric pressure plasma. *Rev Mod Plasma Phys* 2017;1:3.
- [5] Schlegel J, Köritzer J, Boxhammer V. Plasma in cancer treatment. *Clin Plasma Med* 2013;1:2–7.
- [6] Laroussi M. Low-temperature plasmas for medicine? *IEEE Trans Plasma Sci* 2009;37:714–25.
- [7] Keidar M. Plasma application for cancer therapy 2015:31–3.
- [8] Mann MS, Tiede R, Gavenis K, Daeschlein G, Bussiahn R, Weltmann KD, et al. Introduction to DIN-specification 91315 based on the characterization of the plasma jet kINPen® MED. *Clin Plasma Med* 2016;4:35–45.
- [9] Stalder KR, McMillen DF, Woloszko J. Electrosurgical plasmas. *J Phys D Appl Phys* 2005;38:1728–38.
- [10] Raiser J, Zenker M. Argon plasma coagulation for open surgical and endoscopic applications: State of the art. *J Phys D Appl Phys* 2006;39:3520–3.
- [11] Lloyd G, Friedman G, Jafri S, Schultz G, Fridman A, Harding K. Gas plasma: Medical uses and developments in wound care. *Plasma Process Polym* 2010;7:194–211.
- [12] Zenker M. Argon plasma coagulation. *GMS Krankenhhyg Interdiszip* 2008;3:Doc 15.
- [13] Shekhter A, Kabisov R, Pekshev A, Kozlov N, Perov YL. Experimental and clinical validation of plasmadynamic therapy of wounds with nitric oxide. *Bull Exp Biol Med* 1998;126:829–834.
- [14] Shekhter AB, Serezhenkov VA, Rudenko TG, Pekshev A V., Vanin AF. Beneficial effect of gaseous nitric oxide on the healing of skin wounds. *Nitric Oxide - Biol Chem* 2005;12:210–9.
- [15] Bogle MA, Arndt KA, Dover JS. Evaluation of Plasma Skin Regeneration Technology in Low-Energy Full-Facial Rejuvenation. *Arch Dermatol* 2007;143.
- [16] Vasilets VN, Shekhter AB, Guller AE, Pekshev A V. Air plasma-generated nitric oxide in treatment of skin scars and articular musculoskeletal disorders: Preliminary review of observations. *Clin Plasma Med* 2015;3:32–9.
- [17] Shimizu T, Steffes B, Pompl R, Jamitzky F, Bunk W, Ramrath K, et al. Characterization of microwave plasma torch for decontamination. *Plasma Process Polym* 2008;5:577–82.

- [18] Isbary G, Heinlin J, Shimizu T, Zimmermann JL, Morfill G, Schmidt HU, et al. Successful and safe use of 2 min cold atmospheric argon plasma in chronic wounds: Results of a randomized controlled trial. *Br J Dermatol* 2012;167:404–10.
- [19] Ermolaeva SA, Varfolomeev AF, Chernukha MY, Yurov DS, Vasiliev MM, Kaminskaya AA, et al. Bactericidal effects of non-thermal argon plasma in vitro, in biofilms and in the animal model of infected wounds. *J Med Microbiol* 2011;60:75–83.
- [20] Isbary G, Morfill G, Schmidt HU, Georgi M, Ramrath K, Heinlin J, et al. A first prospective randomized controlled trial to decrease bacterial load using cold atmospheric argon plasma on chronic wounds in patients. *Br J Dermatol* 2010;163:78–82.
- [21] Isbary G, Shimizu T, Zimmermann JL, Thomas HM, Morfill GE, Stolz W. Cold atmospheric plasma for local infection control and subsequent pain reduction in a patient with chronic post-operative ear infection. *New Microbes New Infect* 2013;1:41–3.
- [22] Heinlin J, Isbary G, Stolz W, Morfill G, Landthaler M, Shimizu T, et al. Plasma applications in medicine with a special focus on dermatology. *J Eur Acad Dermatology Venereol* 2011;25:1–11.
- [23] Jung JM, Yang Y, Lee DH, Fridman G, Fridman A, Cho YI. Effect of dielectric barrier discharge treatment of blood plasma to improve rheological properties of blood. *Plasma Chem Plasma Process* 2012;32:165–76.
- [24] Kalghatgi S, Fridman G, Nagaraj G, Cooper M, Peddinghaus M, Balasubramanian M, et al. Mechanism of blood coagulation by non-thermal atmospheric pressure dielectric barrier discharge. *PPPS-2007 - Pulsed Power Plasma Sci* 2007;2:1058–63.
- [25] Dobrynin D, Fridman G, Friedman G, Fridman A. Physical and biological mechanisms of direct plasma interaction with living tissue. *New J Phys* 2009;11.
- [26] Dobrynin D, Wasko K, Friedman G, Fridman A., Fridman G. Fast Blood Coagulation of Capillary Vessels by Cold Plasma: A Rat Ear Bleeding Model. *Plasma Med* 2011;1:241–7.
- [27] Fridman G, Peddinghaus M, Ayan H, Fridman A, Balasubramanian M, Gutsol A, et al. Blood coagulation and living tissue sterilization by floating-electrode dielectric barrier discharge in air. *Plasma Chem Plasma Process* 2006;26:425–42.
- [28] Lin A, Truong B, Pappas A, Kirifides L, Oubarri A, Chen S, et al. Uniform Nanosecond Pulsed Dielectric Barrier Discharge Plasma Enhances Anti-Tumor Effects by Induction of Immunogenic Cell Death in Tumors and Stimulation of Macrophages. *Plasma Process Polym* 2015;12:1392–9.
- [29] Kaushik NK, Kaushik N, Min B, Choi KH, Hong YJ, Miller V, et al. Cytotoxic macrophage-released tumour necrosis factor-alpha (TNF- α) as a killing mechanism for cancer cell death after cold plasma activation. *J Phys D Appl Phys* 2016;49:84001.
- [30] Kuchenbecker M, Bibinov N, Kaemling A, Wandke D, Awakowicz P, Viöl W. Characterization of DBD plasma source for biomedical applications. *J Phys D Appl Phys* 2009;42.
- [31] Kaemling C, Kaemling A, Tümmel S, Viöl W. Plasma treatment on finger nails prior to coating with a varnish. *Surf Coatings Technol* 2005;200:668–71.
- [32] Rehn P, Wolkenhauer A, Bente M, Förster S, Viöl W. Wood surface modification in dielectric barrier discharges at atmospheric pressure. *Surf Coatings Technol* 2003;174–175:515–8.

- [33] Rajasekaran P, Opländer C, Hoffmeister D, Bibinov N, Suschek CV, Wandke D, et al. Characterization of dielectric barrier discharge (DBD) on mouse and histological evaluation of the plasma-treated tissue. *Plasma Process Polym* 2011;8:246–55.
- [34] Daeschlein G, Scholz S, Ahmed R, Majumdar A, von Woedtke T, Haase H, et al. Cold plasma is well-tolerated and does not disturb skin barrier or reduce skin moisture. *J Dtsch Dermatol Ges* 2012;10:509–15.
- [35] Daeschlein G, Scholz S, Ahmed R, Von Woedtke T, Haase H, Niggemeier M, et al. Skin decontamination by low-temperature atmospheric pressure plasma jet and dielectric barrier discharge plasma. *J Hosp Infect* 2012;81:177–83.
- [36] Emmert S, Brehmer F, Hanßle H, Helmke A, Mertens N, Ahmed R, et al. Atmospheric pressure plasma in dermatology: Ulcus treatment and much more. *Clin Plasma Med* 2013;1:24–9.
- [37] Lademann J, Richter H, Schanzer S, Patzelt A, Thiede G, Kramer A, et al. Comparison of the antiseptic efficacy of tissue-tolerable plasma and an octenidine hydrochloride-based wound antiseptic on human skin. *Skin Pharmacol Physiol* 2012;25:100–6.
- [38] Bender C, Partecke L-I, Kindel E, Döring F, Lademann J, Heidecke C-D, et al. The modified HET-CAM as a model for the assessment of the inflammatory response to tissue tolerable plasma. *Toxicol Vitr* 2011;25:530–7.
- [39] Fluhr JW, Sassning S, Lademann O, Darvin ME, Schanzer S, Kramer A, et al. In vivo skin treatment with tissue-tolerable plasma influences skin physiology and antioxidant profile in human stratum corneum. *Exp Dermatol* 2012;21:130–4.
- [40] Bender C, Matthes R, Kindel E, Kramer A, Lademann J, Weltmann K, et al. The Irritation Potential of Nonthermal Atmospheric Pressure Plasma in the HET-CAM. *Plasma Process Polym* 2010;7:318–26.
- [41] Kramer A, Lademann J, Bender C, Sckell A, Hartmann B, Münch S, et al. Suitability of tissue tolerable plasmas (TTP) for the management of chronic wounds. *Clin Plasma Med* 2013;1:11–8.
- [42] Weltmann K, Kindel E, Brandenburg R, Meyer C, Bussiahn R, Wilke C, et al. Atmospheric pressure plasma jet for medical therapy: plasma parameters and risk estimation. *Contrib to Plasma Phys* 2009;49:631–40.
- [43] Lademann J, Ulrich C, Patzelt A, Richter H, Kluschke F, Klebes M, et al. Risk assessment of the application of tissue-tolerable plasma on human skin. *Clin Plasma Med* 2013;1:5–10.
- [44] Bekeschus S, Schmidt A, Weltmann K-D, von Woedtke T. The plasma jet kINPen–A powerful tool for wound healing. *Clin Plasma Med* 2016;4:19–28.
- [45] Wende K, Bekeschus S, Schmidt A, Jatsch L, Hasse S, Weltmann KD, et al. Risk assessment of a cold argon plasma jet in respect to its mutagenicity. *Mutat Res Toxicol Environ Mutagen* 2016;798:48–54.
- [46] Metelmann H-R, von Woedtke T, Bussiahn R, Weltmann K-D, Rieck M, Khalili R, et al. Experimental recovery of CO₂-laser skin lesions by plasma stimulation. *Am J Cosmet Surg* 2012;29:52–6.
- [47] Heinlin J, Isbary G, Stolz W, Zeman F, Landthaler M, Morfill G, et al. A randomized two-sided placebo-controlled study on the efficacy and safety of atmospheric non-thermal argon plasma for pruritus. *J Eur Acad Dermatology Venereol* 2013;27:324–31.

- [48] ISO 14971: Medical devices - Application of risk management to medical devices. 2007.
- [49] IEC 60601-1: Medical electrical equipment_1 General requirements for basic safety and essential performance. 2005.
- [50] European Parliament and the Council. Directive 2007/47/EC concerning active implantable medical devices, medical devices and placing of biocidal products on the market. Off J Eur Union 2007:35.
- [51] Gherardi M, Tonini R, Colombo V. Plasma in Dentistry: Brief History and Current Status. Trends Biotechnol 2017;xx:1–3.
- [52] Stancampiano A. Design and diagnostic of non-equilibrium atmospheric plasma sources for cell treatment and bacterial decontamination. Alma Mater Studiorum - University of Bologna, 2016.
- [53] BS EN ISO 10993-1: Biological evaluation of medical devices_1 Evaluation and testing within a risk management process. 2009.

Acknowledgment

I would like that the fulfillment of my PhD is considered a common goal because, as Micheal Jordan suggested, *talent wins games, but teamwork and intelligence win championships*. Thus, I would like to express my sincere gratitude to my advisor Prof. Vittorio Colombo who firstly transposed my wish to actively explore the mysterious world of plasma research. Thank you, Prof, for giving me the possibility to do research, to carry it around the world, to have taught to feel myself as a member of an international scientific community walking next to me with common goals.

Matteo Gherardi, thank you for the *words* you donate to each member of this group. You are for me an example of maturity, profoundness and consistency.

Enrico, thanks because you have been for me the best fellow traveler I could image.

I want to especially thank Tommaso and Filo because you have been always sun rays in cloudy days.

Many thanks go to relevant people met during these year Dr. Tonini, Dr.ssa Turrini, Prof. Nikiforov, for the immense knowledge they shared with and for me; many thanks to my fellow labmates Augusto, Marco, Anna L., Anna M., Alina for all the experiments, all the discussions on plasma physics and random stuff, all travels and all the fun.

Federica and Romolo... you are the most important discovery of all my research. Thanks.

Then, I want to write “thank you” to all the people who have been walking with me towards this achievement during these years.

A “thank” to Giordano, to Cocchi, to Narciso and to my Clan Trencadis. What we are building, what we believe in, what for which we are freely spending time and energies, is tremendously important. All of you have been fresh strength and joy for me every time.

Sara, Cesare, Pier, Paola, Taglia, Sofi & Fiore, Fra & Nicola, thank you all because you were next to me when I needed you.

To Nicola, alias zio Cuscione, you were, you are, and you will be for me a never-ending friendship. You can't image what it means for me. Thank you.

To Nicole... the present is messed up, the future is full of hopes, but the past is simply the past. And it was great. I'll thank you forever.

To my family, to my mother especially... no tears, no threads, no diseases will ever waver the love you give me, and I hope to give you all.

